Force Transfer Mechanism of Concrete Plug Connections in Steel Pipe Piles without Mechanical Connections

Master Thesis Report

N.L. van Dam

TU Delft

Force Transfer Mechanism of Concrete Plug Connections in Steel Pipe Piles without Mechanical Connections

Master Thesis Report

by

N.L. van Dam

to obtain the degree of Master of Science

at the Delft University of Technology,

to be defended publicly on Thursday August 22, 2024 at 2:45 PM.

Student number:	5653096	
Project duration:	February, 2024 – August, 2024	
Thesis committee:	Dr. ir. Y. Yang,	TU Delft, chairman
	Dr. ir. M. Poliotti,	TU Delft, supervisor
	Dr. ir. F. Kavoura,	TU Delft, supervisor
	ir. W.A. van der Mersch,	Iv-Infra b.v., external supervisor

An electronic version of this thesis is available at http://repository.tudelft.nl/.

TU Delft

Preface

This thesis is the result of my graduation internship at Iv-Infra b.v. as final part to obtain the degree of Master of Science, with a specialisation in Structural Engineering at the Delft University of Technology. This work could not have been possible without the support of many people.

First of all, I would like to thank my supervisors Yuguang Yang, Mauro Poliotti and Florentia Kavoura from TU Delft. Their expertise, guidance and motivation have made a great contribution to the project. I would also like to thank Wilco van der Mersch for his daily guidance and support on the project and also for his input on the practical side of the subject.

In addition, I would also like to thank Iv-Infra for their interest, support and giving me the opportunity to work on this project at their company. I would also like to thank all colleagues who were interested in the subject and provided me with valuable information for the project.

Last but not least, I would also like to thank my family and friends for their support and understanding over the past period, but also during the rest of my time at TU Delft. This has helped me a lot during my study time.

N.L. van Dam
Delft, August 2024

Abstract

This thesis investigates the force transfer mechanisms between concrete substructures and steel pipe piles, specifically focusing on connections made using a concrete plug within the steel pipe pile. This thesis explores the mechanisms of force transfer in concrete plug connections within open-ended steel pipe piles, focusing on the viability of frictional (bond) transfer versus mechanical connections. The primary research objective was to determine the extent to which forces—both normal forces and bending moments—can be transferred through a concrete plug without the use of mechanical connections and to compare this with scenarios where mechanical connections, such as shear rings, are employed.

A comprehensive literature review revealed significant gaps in existing design codes and recommendations, which inadequately address concrete plug connections in steel pipe piles. Notably, regulations such as Rijkswaterstaat's ROK V2.0 restrict the extent of force transfer through friction without clear justification. Existing standards like Eurocode 4 and the British Standard (BSI) offer bond strength values that vary widely and do not consider key parameters such as connection geometry and concrete shrinkage, potentially leading to inaccurate strength estimations. Although some models for grouted sleeve connections might be applicable, their validation for concrete plug connections remains uncertain.

To address these gaps, a new analytical model was proposed to estimate the bond strength between concrete and steel in plugged connections. The model incorporates factors including connection geometry, material properties, concrete shrinkage, surface irregularities, and the Coulomb friction coefficient. Push-out test results were used to update and validate the model, resulting in conservative bond strength values. Key parameters identified were the value for the surface and the Coulomb friction coefficient. The model's predictions showed a Mean Average Error (MAE) of 0.589 MPa, primarily due to high variability in some test sets. However, the error was smaller for less variable data.

The findings indicate that connection geometry, particularly the diameter of the steel pipe pile, significantly affects bond strength. Smaller diameters exhibit higher bond strength due to better confinement and reduced concrete shrinkage effects. For larger diameter piles, where friction is insufficient to transfer normal forces, mechanical connections such as shear rings are recommended. These connections were evaluated using Eurocode 4 and CUR Recommendation 77 and found to provide substantially higher normal force resistance, enabling effective utilization of the geotechnical load-bearing capacity.

Regarding the transfer of bending moments, the study found that the wrenching mechanism between the concrete plug and steel pipe pile can manage the transfer through contact stresses. This stress distribution is linear along the plug height and sinusoidal around its circumference, provided it remains within allowable concrete compressive stress limits. The plug's length should be designed to ensure these stresses do not exceed permissible values. A model for the interaction between bending moment and normal force was also developed, indicating that additional normal force resistance can be achieved under a certain bending moment, though this requires careful stress distribution verification.

In conclusion, while friction can achieve normal force transfer in concrete plug connections, it is often insufficient for larger piles. Mechanical connections such as shear rings offer a more effective solution, providing significantly higher normal force resistance and enabling efficient design. The wrenching mechanism can be used to transfer bending moments, but the ultimate bending moment resistance is governed by the concrete plug's cross-sectional resistance. This is because the resistance of the concrete plug's cross-section is lower than the wrenching resistance. This research provides a comprehensive framework for understanding and optimizing force transfer mechanisms in concrete plug connections within steel pipe piles, highlighting the importance of mechanical connections for effective and practical design.

Contents

1

Introduction

This chapter describes the context of the research and its main objectives. This also includes the research questions that this thesis attempted to answer.

1.1. Research context

In practice, the foundation of many civil engineering structures is constructed using steel pipe piles. Variants are possible for these foundations, including closed-ended steel pipe piles or open-ended steel pipe piles. It must be ensured that the force transfer from the superstructure to the ground is properly taken care of. To guarantee this force transfer, the detailing between the steel pipe pile and the concrete cap is crucial. Figure 1.1 shows typical designs that require a force transfer between a concrete element and a steel pipe pile.

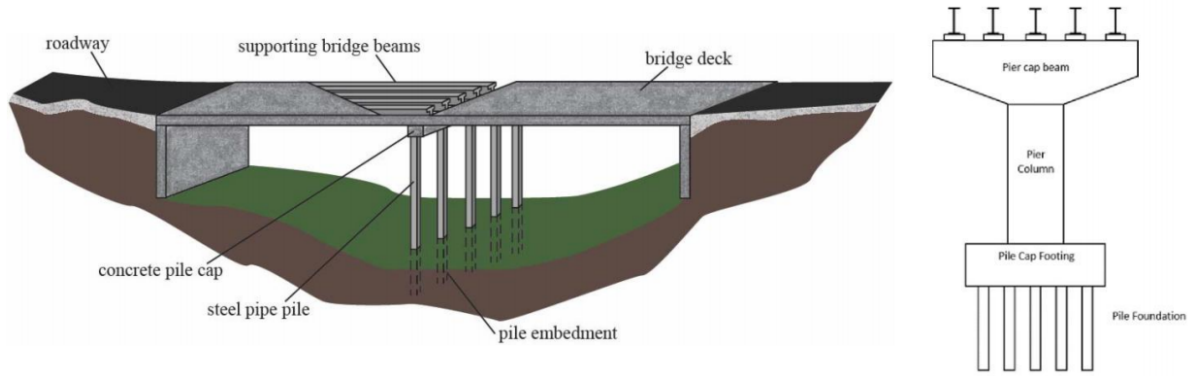

Figure 1.1: Typical designs in which a connection must be realized between the steel pipe pile and the concrete pile cap (Kidwell et al. 2018).

1.2. Research problem

For the detailing between the steel pipe pile and the concrete of the substructure, many clients in the Netherlands use the requirements of the ROK V2.0 (Richtlijnen Ontwerp Kunstwerken / Guidelines for the Design of Civil Engineering Works), a document drawn up by Rijkswaterstaat GPO in the context of the safe and sustainable design and implementation of Rijkswaterstaat's structures. The ROK contains additions to the Eurocodes designated in the 2012 Building Decree and the associated European and Dutch standards. This requirement (ROK-0626) states that if forces have to be transferred from the concrete part in the pile to the steel pipe pile, a connection between the concrete and steel must be

realized, which is at all times able to guarantee the force transfer. The same requirement also states that it is not permitted to fully realize the transfer of force through friction between the concrete and steel, which often requires mechanical connections, such as shear rings, to realize the transfer of force. In practice, however, this leads to a lot of discussion between the parties involved in a project, partly because the application of these mechanical connections often entails many additional costs and intensive construction work. In addition to this fact, it is often difficult for the engineer to substantiate why such an mechanical connections is required, because the requirements provide little clarification as to why the connection may not be realized through friction. The requirement also does not describe what share of the friction may be included in the calculation, which means that there is a lot of discussion about the significance in which these mechanical connections should be applied.

One of the alternatives to these mechanical connections, that can be applied to comply with the additional requirements, is the installation of shear rings on the inside of the steel pipe pile, as shown in Figure 1.2, among other options. The figure also shows why these mechanical connections entail a lot of costs and intensive work, because the application of these types of mechanical connections often requires a lot of intensive welding work on the inside of the steel pipe pile.

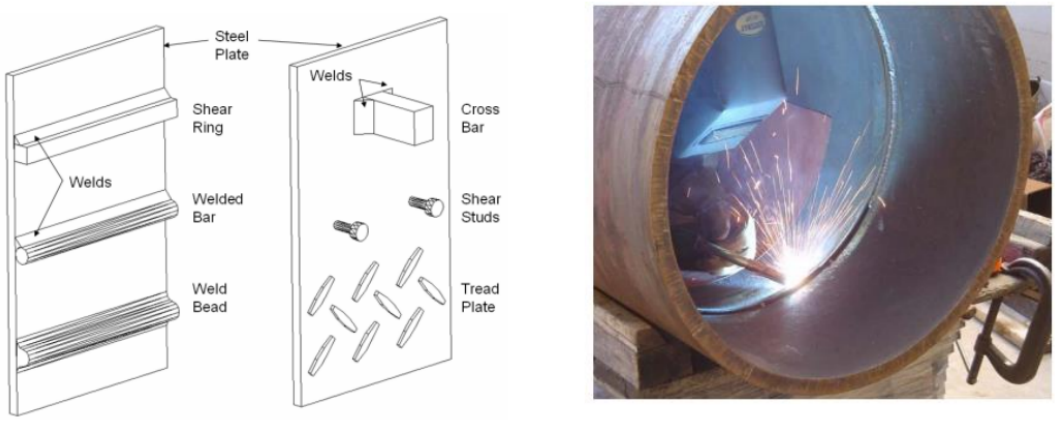

Figure 1.2: Alternatives for the mechanical connections and the realization of one of these connections (Gebman et al. 2006).

1.3. Research objectives

The main objective of this research is to investigate how the forces acting on the substructure can be transferred from the concrete part in the pile to the steel pile, so that they can be transferred to the ground. The end product sought is a standard solution method or a selection of a number of solutions, from which a substantiated and supported connection detail can be chosen that can be applied to the given situation. To investigate this, research will be conducted into various components.

One of the objectives of this research is to provide insight and substantiation for when and in which situations mechanical connections are required in the connection to transfer the forces between the concrete and steel part. A distinction can be made between the forces acting on the pile, such as normal force and bending moment.

The second objective of the research is to gain more insight into the transfer of force through friction. The ROK (ROK-0626) states that the force transfer cannot be fully realized through friction, but does not provide clarity about the extent to which this mechanism may be included in the force transfer and how it can be determined.

When mechanical connections are required in the connection between the concrete and steel, these mechanical connections also needs to be verified. The third goal of this research is to investigate how this mechanical connections can be verified.

1.4. Research scope

In practice, both steel pipe piles with a closed end and with an open end are used for the foundation piles. This research will specifically focus on a steel pipe pile with an open end, whereby the steel pipe pile is not completely filled with concrete, but only partly at the top of the pile. This was chosen because the detailing for the transfer of force between the steel and concrete is even more important with this alternative, because the concrete cannot transfer part of the force to the bottom of the pile. It was also decided not to include the pile in the concrete construction further than 30 mm in the study. Incorporating the pile further into the concrete has practical disadvantages on the overlying concrete structure, and in particular for the application of the reinforcement.

Many variations are also possible for the forces acting on the pile. This study will assume a predominant compressive normal force in combination with a bending moment. The reason why a predominant compressive normal force is assumed is because, in contrast to a predominant axial tensile load, there is more uncertainty in this case regarding the application of mechanical connections. In practice, for a predominant tensile load, in most cases the application of mechanical connections for transferring the loads is already chosen.

A final demarcation in the scope is the exclusion of integral bridges. Instead, it was decided to only treat ”ordinary” bridges in this study. With ”ordinary” bridges, the road deck lies on supports and there is a joint between the bridge deck and the substructure, in contrast to the integral bridge where the road deck is monolithically connected to the underlying structure. This was chosen so that fatigue is not part of the scope, because this requires a more specific approach to the research.

1.5. Research questions and methodology

The main research question central to this study is as follows:

“To what extent can the force transfer in concrete plug connections within open-ended steel pipe piles be achieved without mechanical connections, and how does this compare to a situation with mechanical connections?”

The main goal of this research is to investigate how the forces acting on the substructure can be transferred from the concrete part in the pile to the steel pile, so that they can be transferred to the ground. To investigate this, research will be conducted into various components. To answer the main question, a number of sub-questions are also used to guide the research and identify important aspects for the research. These sub-questions are as follows:

1. **What factors influence the amount of force that can be transferred through friction?**
   For this sub-question, research will be conducted into the various influencing factors for determining the amount of force to be transmitted through friction. To answer this sub-question, literature research will be carried out into various standards, guidelines and papers that describe something about the determination of force transfer through friction. The aim of this research is to identify the various influencing factors, so that at a later stage of the research the exact influence of these factors on the determination of the force transfer through friction can be examined.

2. **To what extent can the load transfer be achieved by means of friction between the steel pipe pile and the concrete plug?**
   For this sub-question, further research is being conducted into the amount of force that can be transferred through friction. As mentioned earlier, this is an important part of the research because the ROK-0626 requirement states that the force transfer cannot be fully realized by friction, but does not describe what part of the forces can be transferred by friction. However, it is important to determine what part of the forces can be transferred via friction, because this has a major influence on the amount and significance of the mechanical connections that must be applied to the connection. If the mechanical connections can be limited, because a large part of the force can be transferred via friction, this will save both application costs and intensive work on the construction site. The aim of answering this sub-question is therefore whether part or possibly,

contrary to what the ROK prescribes, the entire force transfer can be guaranteed by means of friction. To answer this sub-question, a new model will be set up to investigate how much force can be transferred through friction. The model will also be used to determine the influence of the various identified factors from sub-question 2. To set up this model, research will have to be conducted into the various parameters of the model, including, for example, the boundary and interface conditions. The model will also have to be validated. This can be done on the basis of test results obtained from literature research. The aim of the research is to establish a method that can demonstrate which part of the force transfer can be transferred through friction.

3. **In which situations do mechanical connections need to be taken in the connection between the concrete part of the substructure and the steel pipe pile to realize the transfer of force?** To answer this sub-question, the results of the previous sub-questions will be used to determine in which situations mechanical connections are required to transfer the forces between the concrete part of the substructure and the steel pipe pile. By varying the different parameters, it will be investigated which scenarios lead to a situation in which mechanical connections are or are not required.

4. **How should the forces be transferred when mechanical connections needs to be applied?** The previous sub-question ultimately leads to a answer for when mechanical connections needs to be applied. For these mechanical connections, insight must also be gained into the transfer of force. This will be done through research into the existing analytical methods for determining the force transfer of the mechanical connections. This method will then be used, to provide a calculation method for the force transfer of the entire connection.

2

Background

This chapter describes the concrete plug connection, which is used to connect the concrete substructure to steel pipe piles in applications such as bridge foundations. It outlines the typical design and all load combinations considered for the connection in this thesis. A description is also given of the embedment of the pile in the concrete cap and its influence on the transfer of forces in the connection. And finally, the differences between a closed-ended and open-ended pile are given. This provides an understanding of the factors influencing the design and performance of these connections.

2.1. Typical design concrete plug connection

In this thesis the concrete plug connection between a concrete pile cap and a steel pipe pile in standard bridge applications is considered. Integral bridges are therefore not taken into account. With standard bridges, the concrete plug often serves as a connection between the pile cap of a bridge pier and the underlying steel pipe piles. The concrete plug connections must transfer the normal force and bending moment originating from the bridge pier to the steel pipe piles. Figure 2.1 shows a typical design of a bridge pier with the location of the pile cap footing and the foundation piles indicated.

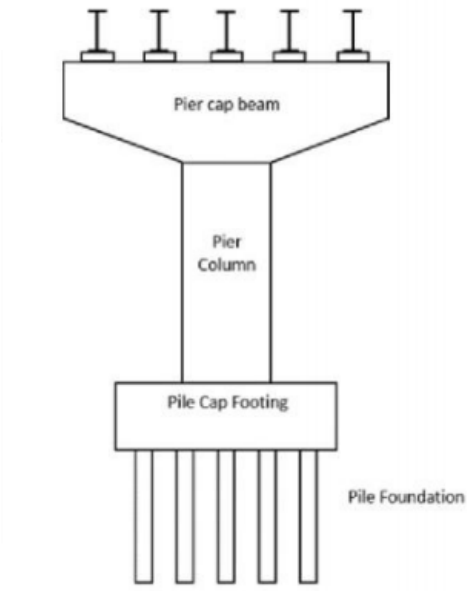

Figure 2.1: Concrete bridge pier (Kidwell et al. 2018).

The connection between the concrete pile cap and the steel pipe pile is shown in more detail in Figure 2.2. The figure shows how connection is provided by means of a concrete plug that is poured into the open-ended steel pipe pile. This concrete plug can be poured to the desired level by removing the soil on the inside of the open-ended steel pipe pile up to that level. The remaining soil then provides a kind of formwork during the pouring of the plug.

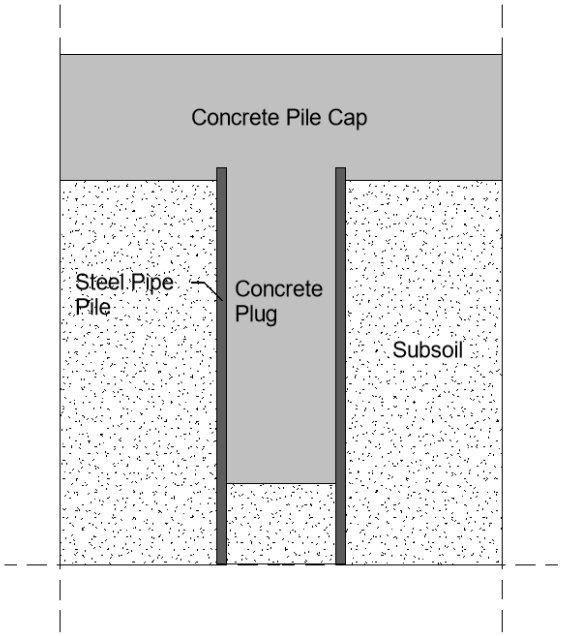

Figure 2.2: Typical concrete plug design.

2.2. Considered structural load combinations

This thesis considers two specific load combinations that are often regarded as governing in practice. The first load combination consists of only a compressive normal force and the second load combination consists of a compressive normal force in combination with a bending moment. These two load cases are shown in Figure 2.3.

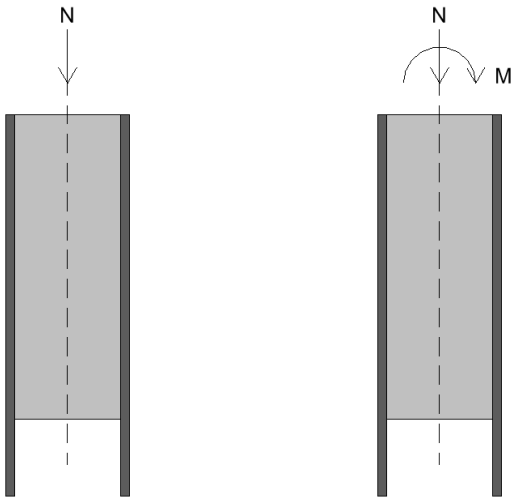

Figure 2.3: Considered structural load combinations.

The first load combination discussed involves a situation where only a compressive normal force acts on the connection. In practice, this situation often occurs when only permanent loads act on the structure. Permanent loads include the weight of the bridge itself, any superimposed dead loads such as roadways or barriers, and any other permanent fixtures. This load combination must be verified to determine whether the connection has sufficient strength to bear the constant permanent load.

The second situation is one in which both a compressive normal force and a bending moment act on the connection. This situation occurs in practice when both permanent loads and variable loads act on the structure. Variable loads include traffic loads, wind loads, thermal effects, and any other loads that can vary over time. In the bridge pier application, this is for example when a vehicle brakes on top of the bridge. Then the bridge pier, if it is designed to carry the horizontal load, must carry both the variable vertical load and the additional bending moment in the foundation as a result of the horizontal load. Verifying this load combination is important to determine whether the connection has sufficient strength to transfer the variable load in combination with the self-weight of the structure.

2.2.1. Load capacity due to friction between the steel and concrete

With this type of connection it is preferable to transfer the load through friction, also referred to as a bond. This is because the application of a mechanical connection such as shear rings or studs, also referred to as mechanical connections, is often both cost and labor intensive. In order for loads to be transferred by friction, the stress around the interface must be verified. The stress that arises around the interface of the concrete plug as a result of the normal force can be determined as follows:

$$f_N = \frac{N}{\pi \cdot D_c \cdot L} \tag{Eq. 2.1}$$

where:

N = normal force acting on the concrete plug (N)
D_c = outer diameter of the concrete plug (mm)
L = length of the concrete plug (mm)

The maximum stress caused by the the bending moment acting on the connection can be determined using the following formula:

$$f_M = \frac{M}{\pi \cdot D_c^2 \cdot L} \tag{Eq. 2.2}$$

where:

M = bending moment acting on the connection (Nmm)
D_c = outer diameter of the concrete plug (mm)
L = length of the concrete plug (mm)

The two stress components caused by the normal force and the bending moment respectively must be equal to or less than the bond strength, as given by:

$$f_N + f_M \leq f_{ba} \tag{Eq. 2.3}$$

where:

f_{ba} = bond strength (MPa)

However, in practice there is much uncertainty about the applicability of the value for the bond strength, f_{ba}, and its share in the force transfer. Many design regulations prescribe different values and differ in the complexity of their determination. Some design regulations, such as the ROK V2.0 (Guidelines for the Design of Civil Engineering Works), a document drawn up by Rijkswaterstaat GPO in the context of the safe and sustainable design and implementation of Rijkswaterstaat's structures, even go a step further and describe that the transfer of force may not be fully realized through this friction. The ROK explains this by describing that the concrete plug can detach from the steel pipe pile as a result of shrinkage, making the transfer of force through friction uncertain. As a result, in many cases mechanical connections are required to guarantee the force transfer between the concrete part in the pile and the steel pipe pile.

These mechanical connections are in most cases steel elements that are welded around the inside of the steel pipe pile, such as shear rings or shear studs. These serve to form a mechanical connection between the concrete of the plug and the steel pipe pile for the purpose of transferring the forces. These alternatives for mechanical connections are shown in Figure 2.4.

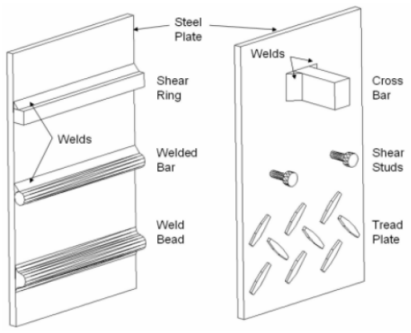

Figure 2.4: Alternatives for the mechanical connections (Gebman et al. 2006).

2.3. Pile embedment

Another point of attention in the design is the embedment of the pipe pile in the concrete of the pile cap. This affects the transfer of force of the connection. If this pile is not embedded in the pile cap, no force can be transferred directly from the pile cap to the pipe pile and all force must be introduced into the steel pipe pile via the concrete of the concrete plug so $N = N_c$, as shown in Figure 2.5.

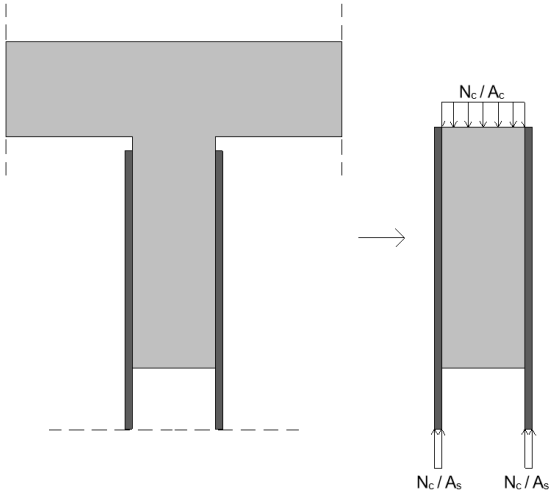

Figure 2.5: Non-embedded pipe pile.

When the steel pipe pile is embedded in the concrete of the pile cap, force can be transferred directly from the pile cap to the steel pipe pile, so that the force in the steel pipe pile is introduced by both the concrete of the pile cap and the concrete of the concrete plug. Then $N = N_c + N_s$, as shown in the Figure 2.6.

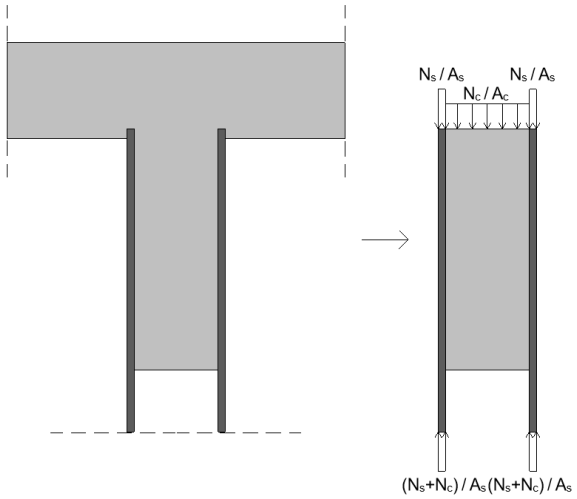

Figure 2.6: Embedded pipe pile.

This thesis will use a situation in which the steel pipe pile is embedded for 30 mm in the pile cap. This situation is generally applied more often in practice for practical reasons. These practical reasons are mainly that if the pile is not deeply embedded in the cap, it does not obstacle the realization of the bending reinforcement at the bottom of the concrete cap. This ensures that no additional reinforcement needs to be added. The force that can be introduced directly from the concrete of the pile cap into the steel of the pipe pile can be described as a function depending on the maximum compressive strength of the concrete, so that the durability aspect of the pile cap is taken into account, whereby no concrete should be crushed. The function can therefore be given as:

$$N_s = \frac{(D_p^2 - D_c^2) \cdot \pi \cdot f_{cd}}{4} \qquad \text{(Eq. 2.4)}$$

where:

D_p = outer diameter of the the steel tube (mm)
D_c = outer diamter of the concrete plug (mm) = $D_p - 2 \cdot t_p$
t_p = thickness of the steel tube (mm)
f_{cd} = design compressive strength of concrete (MPa)

2.4. Closed-ended and open-ended vibrated steel pipe piles

This research considers open-ended vibrated steel pipe piles for the foundation piles under the pile cap. These are types of piles that, unlike close-ended pipe piles, have an open end. Both types are shown in Figure 2.7. With this type of pile, the open end results in that the soil on the inside of the pile will hardly subside during the vibration of the pile. After the pile pile has been completely driven, soil will remain on the inside of the pile to almost the same level as before applying the pile.

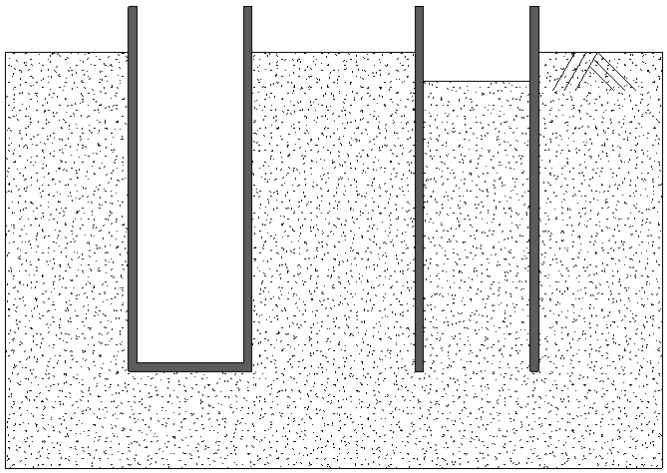

Figure 2.7: Closed-ended and Open-ended pipe pile.

Applying open-ended pipe piles compared to closed-ended pipe piles has several advantages. A first advantage is that they are often easier to drive-in due to vibration because they have less resistance at the tip of the pile. This is because the ground can come in while driving the pile, which reduces resistance. Because the piles are easier to drive in, this can save a lot of construction time during the execution of the foundation. Another advantage of the lower resistance during installation of the pile is that the loads acting on the pile during installation can also potentially be lower.

Another advantage is that the pile does not have to be completely filled with concrete because soil remains in the inside of the pipe pile. After the pile has been driven in, the remaining soil is removed to the level at which the concrete plug must be placed, after which the concrete can be poured. In some cases, this concrete of the plug is poured at the same time as the concrete of the pile cap. The fact that the pile does not have to be completely filled with concrete therefore results in an amount of concrete that can be saved, especially when the piles need to be placed deep in the ground.

A disadvantage of the open-ended pile is that the loads from the concrete plug must be fully transferred to the steel pipe pile so that they can be transferred to the ground. This is because the layer on which the concrete plug is applied is in many cases is non load-bearing. With closed-ended piles, where the concrete is fully applied up to the tip of the pile, part of the forces are also transferred directly via the concrete to the tip of the pile and can be transferred here via the tip resistance.

In this study, it was decided to discuss an open-ended pile application, because the force here must be fully transferred from the concrete of the plug to the steel pipe pile. This makes the transfer of forces in this case even more critical than in the case of the closed-ended pipe pile.

3

Literature study

The first step in this research was to conduct a literature study on load transfer through friction. In this study, a parameter study was first conducted into the influencing factors that, according to literature, influence the bond strength between steel and concrete at concrete plug connections. Subsequently, research was also conducted into various existing code provisions and recommendations that could possibly be applied to determine the transferable load due to friction. For this purpose, code provisions and recommendations have been analysed for concrete plug connections and for comparable types of connections. The purpose of this is also to investigate which parameters are used in existing methods for determining bond strength.

3.1. Parameter study

The first step of the literature study was therefore to conduct a parameter study. In this parameter study it was analysed which factors could possibly influence the bond strength between steel and concrete in concrete plug connections. Sources such as test results from push-out tests were used for this. What exactly a push-out test entails and how it is performed is described in Appendix A. This appendix also includes all test samples and results shown in this chapter.

3.1.1. Shrinkage

First, research was done into the shrinkage of the concrete. According to ROK V2.0 (Guidelines for the Design of Civil Engineering Works), a document drawn up by Rijkswaterstaat, the shrinkage of the concrete can cause the concrete plug to detach from the steel pipe pile, making the transfer of force through friction uncertain. This is in line with the conclusion of Nezamain et al. (2003) who stated that shrinkage of the concrete reduces the mechanical interlocking of the concrete of the plug with the steel of the pile, making the bond strength uncertain. Research by Nezamian et al. (2003) states that three different states can arise between the interface as a result of shrinkage of the concrete:

- State A: $\Delta_{tube} - \Delta_{rugosity} < \Delta_{concrete} - \Delta_{shrinkage}$
- State B: $\Delta_{tube} - \Delta_{rugosity} = \Delta_{concrete} - \Delta_{shrinkage}$
- State C: $\Delta_{tube} - \Delta_{rugosity} > \Delta_{concrete} - \Delta_{shrinkage}$

Where $\Delta_{rugosity}$ is the amplitude of the rugosity of the interior of the tube, Δ_{tube} the radial deflection of the tube, $\Delta_{concrete}$ the radial deflection of the concrete plug and $\Delta_{shrinkage}$ the radial reduction of the concrete plug due to shrinkage. The radial deflection of both the tub and the concrete plug is caused as a result of the compression or tension of the normal force.

The shrinkage of the concrete can be determined, using the following formula:

$$\Delta_{shrinkage} = (-c \cdot d)/2 \quad \text{(Eq. 3.1)}$$

where:

c = linear shrinkage strain of concrete (-)
d = diameter (mm)

According to Roeder et al. (1999), the tube displacement can be found using the following formula:

$$\Delta_{tube} = \frac{p \cdot d^2}{4 \cdot E_s \cdot t} \quad \text{(Eq. 3.2)}$$

where:

p = pressure of the concrete plug against the steel tube (MPa)
d = diameter (mm)
E_s = elasticity modulus of steel (MPa)
t = wall thickness (mm)

In state A, the concrete continues to exert pressure on the interface after shrinkage has occurred, and initial bond strength is provided by the chemical adhesion between the steel and the concrete. As the load increases on the connection, this chemical adhesion will break down due to the shear, after which the resistance will depend more on the mechanical characteristics at the interface. Here are two features: the resistance created by the interface contact pressure and the friction coefficient (micro-friction) and the resistance resulting from the mechanical interlock between the steel and the concrete (macro-friction). State B is an intermediate state where chemical adhesion decreases, and also mechanical resistance decreases in an unpredictable manner as state C is reached. In state C there is relatively no bond strength left and the two materials behave separately from each other.

3.1.2. Surface roughness and shape variations

According to research by Virdi and Dowling et al. (1975), the surface roughness and the variations of shape of the cross-section of the steel tube are also influencing factors in determining the maximum allowable normal force transfer stress. In this study, the push-out resistance of the concrete plug in a steel pipe pile was investigated by varying various parameters. The conclusion of the research was that the push-out resistance of the concrete plug was mainly based on two types of imperfections of the steel pipe pile. These two imperfections were the roughness of the surface of the steel pipe pile and the variations in shape of the cross section over the height of the pile. These imperfections ensure micro locking and macro locking of the concrete in the pipe pile respectively. The bond caused by micro locking breaks when the concrete interface reaches a local strain of 0.0035, which is equal to the crushing strain of the concrete. Macro locking is related to a later stage of the load deflection graph, being more related to the friction mechanism.

In another study, Virdi and Dowling et al. (1980) also used push-out tests to further investigate the influence of the surface roughness of the steel pile on the bond strength between the concrete and steel. They used three different groups of test specimens. Three specimens from the first group (Group ST) had the inner surface of the tubular steel pile machined with a smooth finish, so that the surface was less rough. The three specimens of the second group (Group PH) had the inner surface provided with a lubricant (Phebcur) treatment so that the roughness was intermediate between the first group and the piles used in practice. The last specimens of group CS had a normal surface without surface treatment, which is comparable to the treatment of steel pipe piles in practice.

The results of the study, shown in Figure 3.1, show that, as expected, bond strength increases as the roughness of the inner surface of the steel pipe pile increases. This is also in line with, for example, the regulations of the Eurocode, which describe that the bond strength they prescribe may only be used when the surface of the steel pipe pile has been cleared of oil, grease and loose mill scale or rust.

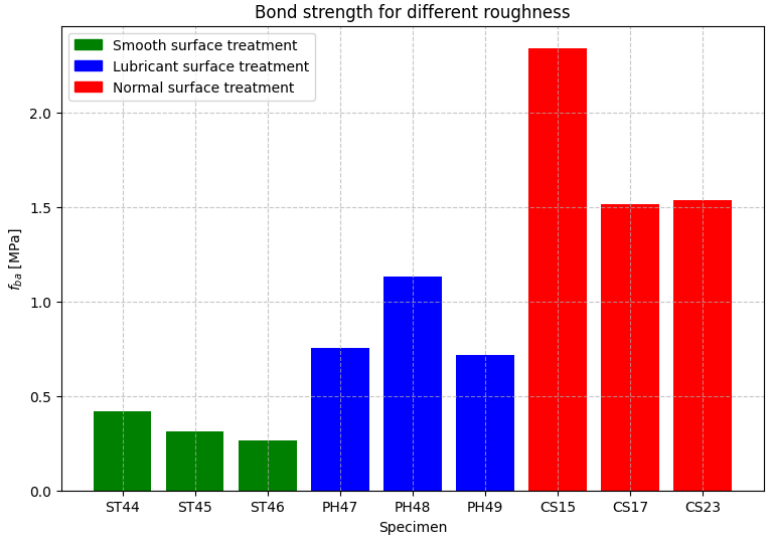

Figure 3.1: Bond strength versus different levels of surface roughness of the steel pile.

3.1.3. Diameter and thickness of the pile

According to research by Nezamian et al. (2003), shrinkage of concrete is an important factor for the bond strength, which is influenced, among other factors, by the diameter of the concrete plug in the steel tubular pile. Virdi and Dowling et al. (1980) therefore also investigated the influence of different diameters on the bond strength on the bond strength of the connection. Results of this study are shown in Figure 3.2. It can indeed be cautiously concluded that as the diameter increases, the bond strength between the concrete and steel decreases.

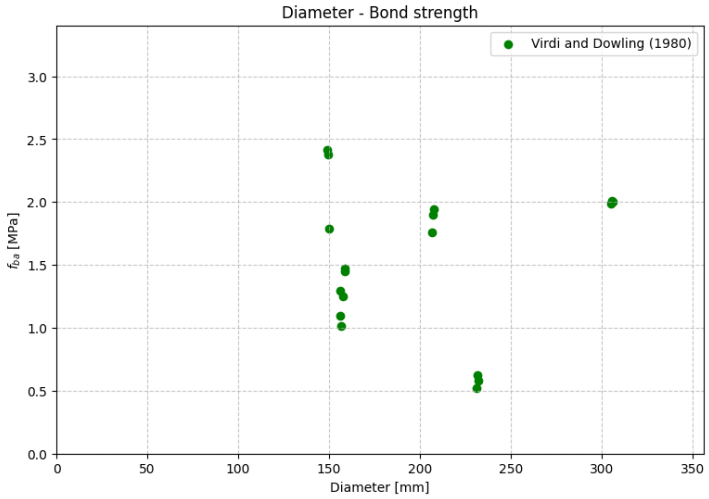

Figure 3.2: bond strength versus different diameters of the steel pile.

According to the study by Roeder et al. (1999), the bond strength between the concrete and steel also decreases as the diameter to thickness (D/t) ratio of the pile increases. This was explained by the fact that with a higher D/t ratio the stiffness of the steel pipe pile decreases, causing the concrete plug to benefit less from the irregularities in the cross section of the pipe pile. In other words, the confinement that the steel pipe offers to the concrete plug decreases. When this statement was compared with the test results from the Virdi and Dowling (1980) study, shown in Figure 3.3, Roeder's conjecture is consistent with the results of the tests.

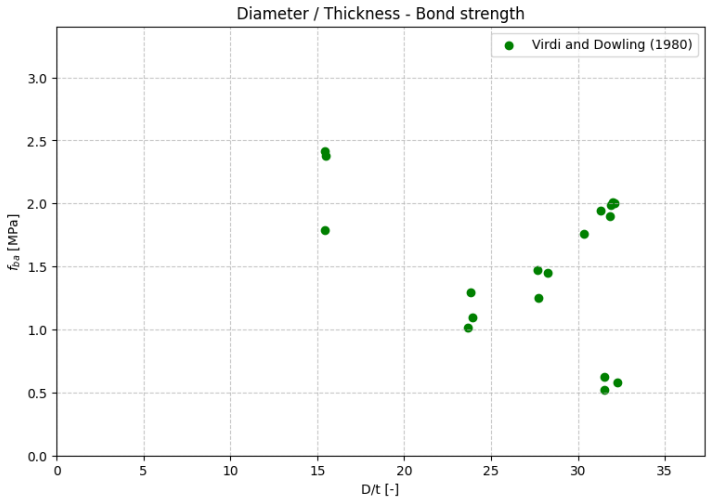

Figure 3.3: Bond strength versus different D/t ratios of the steel pile.

3.1.4. Interface length / diameter ratio

Several studies, in which push-out tests have been carried out, suspected that the bond strength is influenced by the length of the interface between the concrete and steel in the connection. Figure 3.4 shows these test results from the studies by Virdi and Dowling et al. (1980), Roeder et al. (1999), Nezamian et al. (2002) and Shakir-Kahlil et al. (1993). The results do not leave a one-sided answer about the influence of the L/D ratio on the bond strength due to the large degree of scatter in the plot. Virdi and Dowling's conclusion about their own research was that the L/D ratio has no significant influence on bond strength, while Nezamian's conclusion about their research was that as the L/D ratio increases, bond strength decreases.

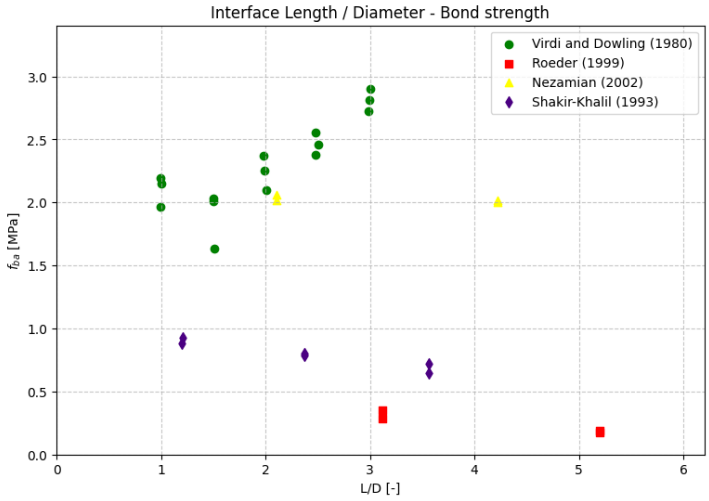

Figure 3.4: Bond strength versus different L/D ratios of the steel pile.

3.1.5. Concrete compressive strength

The influence of the concrete compressive strength on the bond strength has also been investigated in studies by Virdi and Dowling et al. (1980) and Aly et al. (2009). Results of these studies are shown in the Figure 3.5. From the research by Virdi and Dowling it can be concluded that the compressive strength has no significant influence on the bond strength of the concrete. This was also their own conclusion after the research. On the other hand, the results of Aly's research suggest that as the compressive strength increases, the bond strength decreases.

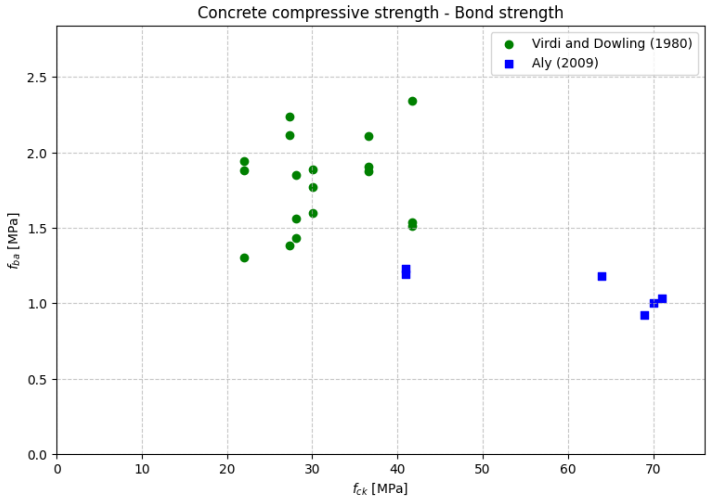

Figure 3.5: Bond strength versus different compressive strengths of the concrete.

3.1.6. Concrete compaction

Research by Virdi and Dowling et al. (1980) also showed that the higher the level of compaction of the concrete plug in the steel pipe pile, the better the micro-friction between the concrete and the steel pipe pile. This could be explained by the fact that the concrete is pressed better into the irregularities of the cross section of the steel pipe pile due to better compaction, resulting in a better bond.

To reach this conclusion, Virdi and Dowling conducted their research on specimens using six different levels of compaction to perform push-out tests. These six different levels are as follows, from better compaction to lesser compaction:

- Level 1: Aggregate/cement ratio 5.0, dry cured, well compacted with poker vibrator
- Level 2: Aggregate/cement ratio 5.0, wet cured, well compacted with poker vibrator
- Level 3: Aggregate/cement ratio 5.5, wet cured, well compacted with poker vibrator
- Level 4: Aggregate/cement ratio 5.5, wet cured, lightly compacted with poker vibrator
- Level 5: Aggregate/cement ratio 5.5, wet cured, well compacted by hand
- Level 6: Aggregate/cement ratio 5.5, wet cured, lightly compacted by hand

Figure 3.6 below shows the results of the push-out tests of Virdi and Dowling. From this figure it can be clearly concluded that, as expected, better compaction of the concrete leads to a higher bond strength.

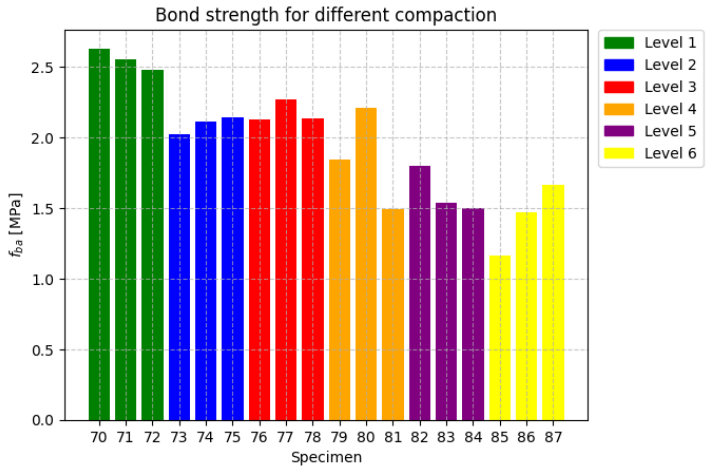

Figure 3.6: Bond strength versus level of compaction of the concrete of the plug.

3.1.7. Cyclic loading

Research by Nezamian et al. (2003) also shows that dynamic loading of the connection, using a concrete plug in a steel tubular pile, affects the bond strength of the concrete and steel. This has been tested by cyclic loading various test species using both pull-out tests and push-out tests. This research shows that cyclical loading of the connection reduces the bond strength in almost all cases. This can be explained by the fact that the slip increases with each load cycle and therefore the connection between the concrete and steel decreases. The research also states that a reduction factor can be assumed for this bond strength, whereby the static bond strength can be multiplied by this factor so that a dynamic bond strength can be obtained. According to the research, this factor appears to depend on several factors of the connection, including the rate of loading, number of load cycles, the properties and shrinkage of the concrete, the imperfections of the steel pipe, the length of the concrete plug and the presence of reinforcement in the plug. However, no analytical approach has been determined for this relationship, but rather an average reduction factor for these different scenarios. This average cyclic reduction factor for the bond strength is set at 0.74 with a standard deviation of 1.90.

3.2. Current code provisions and recommendations

The second step in the literature study is to examine existing code provisions and recommendations. An analysis was carried out into the code provisions of concrete plug connections and into comparable code provisions for, for example, grouted sleeve connections. The aim of this research is to analyse the current provisions which describe something about the part of forces that can be transferred by friction between steel and concrete and what influencing factors may be important for this.

3.2.1. Allowable bond strength for concrete plug connections

To determine the design of composite columns, there are currently a number of codes that provide recommendations on the determination of the maximum allowable bond strength. However, these recommendations differ from each other when further analysed in various aspects such as prescribed values, complexity and area of application. For example, the Eurocode and The British Standard (BSI) prescribe a value that can be used for the allowable bond strength in concrete-filled pipe profiles.

With the maximum allowable bond strength, the maximum value for the allowable normal load force transfer can then be determined using the following formula:

$$N_{Rd} = f_{ba} \cdot \pi \cdot D_c \cdot L \qquad \text{(Eq. 3.3)}$$

where:

N_{Rd} = allowable value for normal force transfer
f_{ba} = bond strength (MPa)
D_c = outside diameter of the concrete plug (mm)
L = lenght of connection (mm)

3.2.1.1. Eurocode 4

The Eurocode prescribes that mechanical connections must be applied in the force introduction areas and areas where the cross-section changes, if the design value of the shear strength is exceeded at the connection surface between steel and concrete. The value for the design shear strength of concrete-filled round tube profiles, f_{ba}, which is prescribed in the Eurocode is 0,55 MPa. This value may be retained provided that the surface of the steel profile adjacent to the concrete is unpainted and free of oil, grease and loose mill scale or rust. The shear forces must be determined on the basis of the change in cross-sectional forces in the steel profile or the cross-section of reinforced concrete within the lead-in length. If the loads are only introduced in the concrete cross-section, the value resulting from an elastic calculation, in which creep and shrinkage are taken into account, should be used. In other cases, the forces on the connecting surface should be determined according to the elasticity theory or the plasticity theory to determine the governing situation.

3.2.1.2. The British Standard (BSI)

The code provisions of the British standard BS5400, Steel, concrete and composite bridges, just like the Eurocode, prescribe that when the design value for the shear strength is exceeded, mechanical connections must be applied at the places where the forces must be introduced. The difference with the Eurocode is that the BSI prescribes a lower design value for the shear strength, f_{ba}, namely a value of 0,4 MPa. This value is based on the results of experimental work by Shakir-Khalil.

3.2.1.3. Roeder et al. (1999)

Roeder et al. (1999) recommended a bond strength model for both the ultimate and serviceability design stages, which is shown in Figure 3.7.

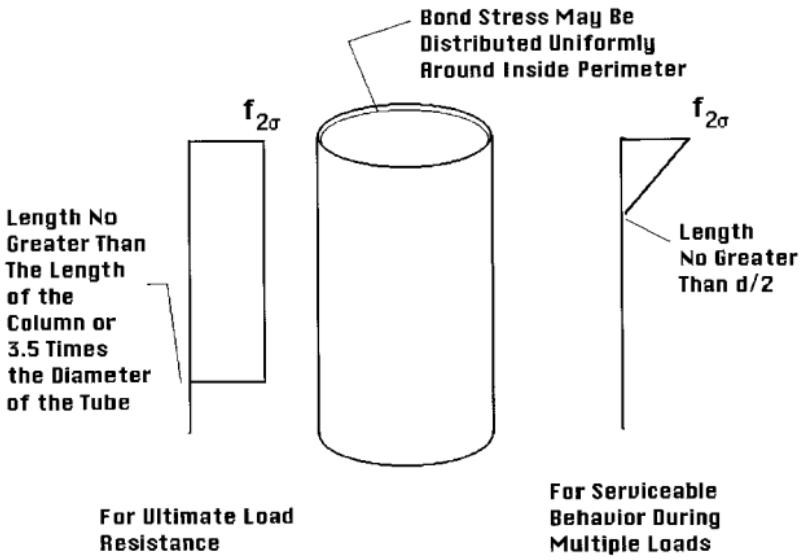

Figure 3.7: Proposed bond strength evaluation models (Roeder, 1999).

The study stated that the diameter, D, and the thickness of the steel pile, t, the most important parameters were for the determination of the bond strength. This led to a formula for determining the bond strength, which was drawn up using a linear regression analysis on bond strength data versus D / t ratio. The resulting formula has been drawn up in such a way that 97.5% of the specimens contain a greater maximum average bond strength than follows from the following formula:

$$f_{2\sigma} = 2.109 - 0.026 \cdot (\frac{D}{t}) \quad \text{(Eq. 3.4)}$$

where:

D = diameter of the pipe pile (mm)
t = thickness of the pipe pile (mm)

The formula states that there is no reliable bond strength capacity when the D / t ratio is greater than 80. The stress, $f_{2\sigma}$, is two standard deviations above the mean. The average stress, f_{mean} , is given by:

$$f_{mean} = 2.314 - 0.0195 \cdot (\frac{D}{t}) \quad \text{(Eq. 3.5)}$$

where:

D = diameter of the pipe pile (mm)
t = thickness of the pipe pile (mm)

3.2.2. Allowable bond strength for grouted connections

Recommendations have also been found for methods that can be used to determine the strength of a grouted connection between a steel pipe pile and an internal set or shell (sleeve) with or without shear rings, shown in Figure 3.8 These recommendations for a grouted connection have been found in codes of the American Petroleum Institute (API), the United Kingdom Department of Energy (UK DEO), the Det Norske Veritas (DNV) and the Norsok. These recommendations have also been presented because they have been applied in the past in the design of tube profiles filled with concrete.

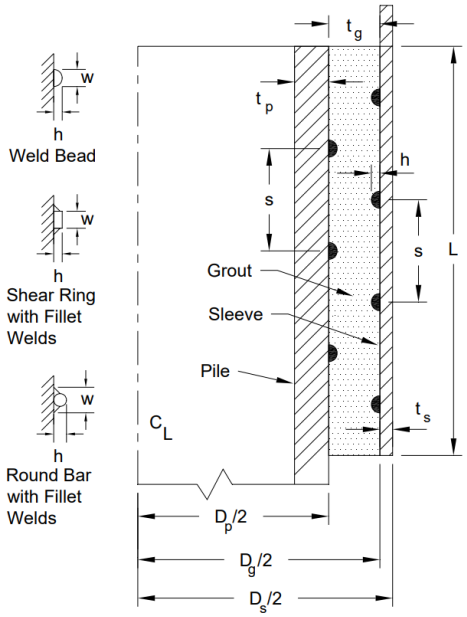

Figure 3.8: Steel Shell Pile to Steel Sleeve Connections Detail (Gebman, 2016).

3.2.2.1. American Petroleum Institute (API) - Working Stress Design

The API code recommends a method for determining the normal force transfer for both working stress design and load resistance factor design (LRFD). In this section, the load working stress design method is analysed. This method is described in the American Petroleum Institute Code (API, 2002). The formula for determining the ultimate strength of the connection is based on test observation in which mainly two different failure mechanisms occurred: first a slippage between the steel and the grout and second the crushing of the grout against the shear keys. Such a connection normally fails in a ductile manner, so the ultimate strength of the connection can be assumed to be the sum of the two different sources of strength. This gives rise to the following formula:

$$f_{ba} = 0.138 + 0.5 \cdot f_{cu} \cdot (\frac{h}{s}) \qquad \text{(Eq. 3.6)}$$

where:

f_{cu} = unconfined grout compressive strength (MPa)
h = height of shear connector (mm)
s = spacing of the shear connectors (mm)

The formula therefore consists of two different components, including the capacity of the friction between the grout and the steel pipe pile and the capacity of the shear keys. If it is therefore chosen not to use shear keys in the design, a residual value of 0.138 MPa remains for the friction between the steel and the grout.

The method from the API code also has limitations in how far it may be applied with certain parameters. These limitations are as follows:

1. Unconfined compressive strength: 17.25 MPa $\leq f_{cu} \leq$ 110 MPa
2. Sleeve geometry: $\frac{D_s}{t_s} \leq 80$
3. Pile geometry: $\frac{D_p}{t_p} \leq 40$
4. Grout annulus geometry: 7 $\leq \frac{D_g}{t_g} \leq$ 45
5. Mechanism spacing ratio: 2.5 $\leq \frac{D_p}{t_s} \leq$ 8
6. Mechanism ratio: $\frac{h}{s} \leq 0.10$
7. Mechanism shape factor 1.5 $\leq \frac{w}{h} \leq$ 3
8. Product of f_{cu} and $\frac{h}{s}$: $f_{cu} \cdot (\frac{h}{s}) \leq$ 5.5 MPa

3.2.2.2. American Petroleum Institute (API) - LRFD

In the load and resistance factor design (LRFD) method (API, 1993), the bond strength is determined in a comparable way to the method from the working stress design and the method also has the same limitations. The formula of the method is as follows:

$$f_{ba} = 0.248 + 0.9 \cdot f_{cu} \cdot (\frac{h}{s}) \quad \text{(Eq. 3.7)}$$

where:

f_{cu} = unconfined grout compressive strength (MPa)
h = height of shear connector (mm)
s = spacing of the shear connectors (mm)

When this method is applied without applying shear keys, the value for the bond strength results in 0.248 MPa, however, when no shear keys are applied, a reduction factor must be applied for this value. This formula with reduction factor is shown below:

$$f_{b,max} = \phi_{ba} \cdot f_{ba} \quad \text{(Eq. 3.8)}$$

where:

$f_{b,max}$ = maximum bond strength (MPa)
ϕ_{ba} = reduction factor of 0.9

3.2.2.3. United Kingdom Department of Energy Code

Recommendations for determining the strength of a grouted connection between a steel pipe pile and steel sleeve are also found in the United Kingdom Department of Energy Code. The code describes a formula in which the characteristic bond strength, f_{buc}, is determined in the contact surface between the steel pipe pile and the grout. This formula was drawn up using approximately 450 test results for steel pipe pils grouted to a steel sleeve (Billington and Tebbett, 1980). The following formula is given in the code:

$$f_{buc} = K \cdot C_L \cdot (9 \cdot C_s + 1100 \cdot \frac{h}{s}) \cdot (f_{cu})^{\frac{1}{2}} \quad \text{(Eq. 3.9)}$$

The formula can be applied for both connections with and without mechanical connections. In the formula, K is a dimensionless factor that can be determined with the following formula:

$$K = \frac{1}{m} \cdot (\frac{D}{t})_g^{-1} + [(\frac{D}{t})_p + (\frac{D}{t})_s)]^{-1} \quad \text{(Eq. 3.10)}$$

The formula for k is therefore composed of three different components, which are indicated with three different scripts: g, p and s. These represent the grout, pile and sleeve respectively. The other variables from the formula are as follows:

C_L = coefficient for grouted length to pile diameter ratio
C_S = surface condition factor
D_p = external diameter (mm)
f_{cu} = unconfined grout compressive strength (MPa)
h = height of shear connector (mm)
m = modular ratio of steel to grout
s = spacing of the shear connectors (mm)
t = wall thickness (mm)

A number of these coefficients are specific to this formula and the UK DEO recommends values for these coefficients in the code. For example, a conservative value of 18 can be used for m when no other data is available. For the length coefficient, C_L, values of 1.0, 0.9, 0.8 and 0.7 can be used for ratios of the grouted connection length to pile diameter of 2, 4, 8 and 12 or higher, respectively. The surface condition factor, C_s can be taken as 1.0 when mechanical connections are used and when the h / $s \geq$ 0.005. When h / $s \leq$ 0.005 or when no mechanical connections are applied, a value of 0.6 should be used for C_s.

To obtain the allowable bond strength, f_{ba}, the characteristic bond strength, f_{buc}, must be divided by a safety factor, FS, as shown below:

$$f_{ba} = \frac{1}{FS} \cdot f_{buc} \quad \text{(Eq. 3.11)}$$

where:

FS = factor of safety

The safety factor, FS, depends on the conditions under which the grout is applied to the connection. When the grout is applied in a way that displaces water, FS should be set to values of 4.5 and 6.0 for the extreme loading condition and the operating loading condition, respectively. If the grout is loaded in a manner that displaces drilling mud or a similar material, a value of 6.0 and 8.0 can be used for FS for the extreme loading condition and the operating loading condition, respectively.

The formula for determining f_{buc} can only be used when the following requirements are met:

1. Sleeve geometry: $50 \leq \frac{D_s}{t_s} \leq 140$
2. Pile geometry: $24 \leq \frac{D_p}{t_p} \leq 40$
3. Grout annulus geometry: $10 \leq \frac{D_g}{t_g} \leq 45$
4. Grouted connection length to pile diameter ratio: $2 \leq \frac{L}{D_p}$
5. Mechanism height ratio: $0 \leq \frac{h}{D_p} \leq 0.006$
6. Mechanism spacing ratio: $0 \leq \frac{D_p}{s} \leq 8$

7. Mechanism ratio: $0 \leq \frac{h}{s} \leq 0.04$

8. Mechanism shape factor: $1.5 \leq \frac{h}{s} \leq 3$

3.2.2.4. Det Norske Veritas (DNV)

The DNV also has a method for predicting the ultimate capacity of vertically loaded grouted tubular connections. This method can be used when the connection does not need to transfer significant bending moments. The bending moments are designated as significant when they lead to a stress exceeding 50 $\%$ or more of the stress caused by normal loading. The formula of the method for the allowable shear stress consists of two components; the interface shear strength due to fricton and the interface shear strength due to shear keys. Only the shear strength due to shear keys interface may be used to transfer the normal load. The interface shear strength due to friction is only used in this method to transfer the shear stress caused by the torsional moment acting on the connection.

The formula for the shear strength due to friction is as follows:

$$f_{kf} = \frac{\mu \cdot E}{F} \cdot [\frac{\delta}{D_p}] \quad \text{(Eq. 3.12)}$$

The formula for the shear strength due to shear keys is as follows:

$$f_{ks} = \frac{\mu \cdot E}{F} \cdot [\frac{h}{21 \cdot s} \cdot {f_{ck}}^{0.4} \cdot \sqrt{\frac{t_p}{D_p}}] \cdot \frac{s}{L_g} \cdot N \quad \text{(Eq. 3.13)}$$

where:

f_{kf} = characteristic interface shear strength due to friction (MPa)
f_{ks} = characteristic interface shear strength due to shear keys (MPa)
μ = grout to steel interface coefficient of friction to be taken as 0.4
δ = height of surface irregularities to be taken as 0.07 mm for rolled steel surfaces (mm)
N = number of shear keys
E = modulus of elasticity for steel (MPa)
E_g = modulus of elasticity for grout (MPa)
s = shear key spacing (mm)
D_p = pile outer radius (mm)
D_s = sleeve outer radius (mm)
L_g = length of the grout connection (mm)
t_p = wall thickness of pile (mm)
f_{ck} = characteristic compressive cube strenght of the grout (MPa)
F = flexibility factor = $\frac{D_p}{t_p} + \frac{E \cdot t_g}{E_g \cdot D_p} + \frac{D_s}{t_s}$

To obtain the allowable shear strengths, the characteristic bond strengths, must be divided by a safety factor, γ_M = 3.0 in ULS.

The above equations have been proven valid within the following limits:

1. Unconfined compressive strength: $f_{ck} \leq 80$ MPa

2. Pile annulus geometry: $5 \leq \frac{D_p}{t_p} \leq 30$

3. Sleeve annulus geometry: $9 \leq \frac{D_s}{t_s} \leq 70$

4. Mechanism ratio: $\frac{h}{s} \leq 0.1$

5. Mechanism spacing ratio: $\sqrt{D_p \cdot t_p} \leq s$

3.2.2.5. Norsok

The Norsok also describes a method that can be used to determine the capacity of vertically loaded grouted connections. This formula for the characteristic bond strength, f_{bks}, is as follows:

$$f_{bks} = (\frac{800}{D_p} + 140 \cdot (\frac{h}{s})^{0.8}) \cdot C_s^{0.6} \cdot f_{ck}^{0.3} \quad \text{(Eq. 3.14)}$$

where:

D_p = outer diameter of pile (mm)
D_s = outer diameter of pile sleeve (mm)
D_g = outer diameter of grout annulus (mm)
f_{ck} = unconfined grout compressive strength (MPa)
h = height of shear connector (mm)
s = spacing of the shear connectors (mm)
t_p = wall thickness of pile (mm)
t_s = wall thickness of pile sleeve (mm)
t_g = thickness of grout annulus (mm)
m = steel-grout elastic modular ratio (to be taken as 18 in lieu of actual data)
C_s = radial stiffness factor = $[\frac{D_p}{t_p} + \frac{D_s}{t_s}]^{-1} + \frac{1}{m} \cdot (\frac{D_g}{t_g})^{-1}$

To obtain the allowable bond strength, f_{ba}, the characteristic bond strength, f_{bks}, must be divided by a safety factor, γ_M, as shown below:

$$f_{ba} = \frac{f_{bks}}{\gamma_M} \quad \text{(Eq. 3.15)}$$

where:

γ_M = factor of safety (2.0 for ULS and 1.5 for ALS)

The formula can be used for a situation where no shear keys are used as well as a situation where shear keys are used. The formula is valid for uncoated tubular piles with normal manufacturing tolerances and where the mill scale has been completely removed. The recommendations are valid when the design parameters fall within the following tolerances:

1. Unconfined compressive strength: 20 MPa $\leq f_{ck} \leq$ 80 MPa
2. Sleeve geometry: $50 \leq \frac{D_s}{t_s} \leq 140$
3. Pile geometry: $20 \leq \frac{D_p}{t_p} \leq 40$
4. Sleeve geometry: $30 \leq \frac{D_s}{t_s} \leq 140$
5. Grout annulus geometry: 10 $\leq \frac{D_g}{t_g} \leq$ 45
6. Mechanism height ratio: $\frac{h}{D_p} \leq$ 0.012
7. Mechanism ratio: 0 $\leq \frac{h}{s} \leq$ 0.10
8. Length interface to pile diameter ratio 1 $\leq \frac{L}{D_p} \leq$ 10

3.2.3. Design stress

According to the Norsok, the design stress that the connection must withstand consists of two different components; $f_{ba,Ed}$, the design interface stress due to normal force and $f_{bt,Ed}$, the design interface stress due to bending moment.

The design interface stress due to normal force, $f_{ba,Ed}$, is defined by:

$$f_{ba,Ed} = \frac{N_{Ed}}{\pi \cdot D_c \cdot L} \quad \text{(Eq. 3.16)}$$

where:

N_{Ed} = design normal force (N)
D_c = outer diameter of the concrete plug (mm)
L = length of connection (mm)

The design interface stress due to bending moment, $f_{bt,Ed}$, is defined by:

$$f_{bt,Ed} = \frac{M_{Ed}}{\pi \cdot D_c^2 \cdot L} \quad \text{(Eq. 3.17)}$$

where:

M_{Ed} = design bending moment on the connection (Nmm)
D_c = outer diameter of the concrete plug (mm)
L = length of connection (mm)

The combined normal and bending design interface shear stress can then be determined with the following formula:

$$f_{Ed} = f_{ba,Ed} + f_{bt,Ed} \quad \text{(Eq. 3.18)}$$

However, this way of determining the design stress is considered a conservative method, specifically for transferring the bending moment, neglecting phenomena such as the small-scale movement of the plug due to the bending moment, better known as wrenching. With this phenomenon of wrenching, a horizontal pressure is exerted between the steel pile and the concrete plug to transfer the bending moment, resulting in a higher contact stress and therefore often a higher bending moment capacity. Another additional effect caused by this phenomenon is that there are both additional vertical and horizontal friction forces that contribute to the transfer of the bending moment. An overview of how these horizontal contact stresses and friction forces occur as a result of the bending moment in the connection is shown in Figure 3.9.

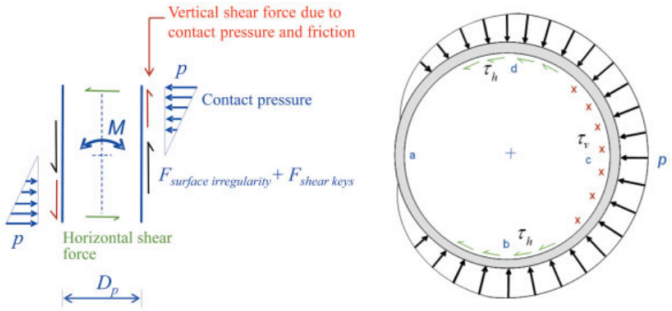

Figure 3.9: Contact pressure and resistance to bending moment (Lotsberg, 2012).

An analytical method for taking into account these occurring contact stresses and friction forces is given in the Det Norske Veritas (DNV) and is based on project results from Lotsberg et al. (2012). To draw up this method, a number of assumptions have been made regarding the pressure distribution. Firstly, it is assumed that a constant pressure is applied around half the circumference of the steel pile from point b to point d in the figure above. It was then also assumed that from point d to a and point b to a the pressure distribution is reduced according to a cosine function. This total stress distribution is based on the ovalization of the cross-section of the pipe pile as a result of the acting bending moment. Sequentially, using the given assumptions, the contribution to the bending moment capacity can be determined for both the contact pressure and the contribution of the horizontal and vertical friction forces.

The moment capacity due to the maximum contact pressure is derived by integrating the contact pressure half the circumference from point b to d and is therefore given by the following function:

$$M_p = p \cdot \frac{D_p \cdot L^2}{3} \qquad \text{(Eq. 3.19)}$$

where:

p = maximum nominal pressure at the top and the bottom of the connection (MPa)
D_p = outer radius of pile (mm)
L = length of the interface of the connection (mm)

The moment capacity due to the horizontal friction force is derived by integrating the contact pressure from point a to c with pressure 0.75 p and is therefore given by the following function:

$$M_{\mu h} = \mu \cdot p \cdot \frac{D_p \cdot L^2}{\pi} \qquad \text{(Eq. 3.20)}$$

where:

μ = Coulomb friction (-)
p = maximum nominal pressure at the top and the bottom of the connection (MPa)
D_p = outer radius of pile (mm)
L = length of the interface of the connection (mm)

The moment capacity due to the vertical friction force is derived by integrating the contact pressure from point a to c with pressure 0.5 p and is therefore given by the following function:

$$M_{\mu v} = \mu \cdot p \cdot {D_p}^2 \cdot L \qquad \text{(Eq. 3.21)}$$

where:

μ = Coulomb friction (-)
p = maximum nominal pressure at the top and the bottom of the connection (MPa)
D_p = outer radius of pile (mm)
L = length of the interface of the connection (mm)

The total moment capacity is the sum of three components and is therefore given by the following function:

$$M_{Rd} = M_p + M_{\mu h} + M_{\mu v} \qquad \text{(Eq. 3.22)}$$

Substituting equations 3.18, 3.19 and 3.10 into equation 3.21 then gives the following function:

$$M_{Rd} = p \cdot \frac{D_p \cdot L^2 \cdot (\pi + 3 \cdot \mu) + 3 \cdot \pi \cdot \mu \cdot {D_p}^2 \cdot L}{3 \cdot \pi} \quad \text{(Eq. 3.23)}$$

In this formulation for the total bending moment capacity, according to the DNV, the maximum allowable nominal contact pressure, p_{nom}, must be used for the contact pressure p, which is limited to 1.2 N/mm^2 where fatique has been taken into account during the service life of the connection. For the coulomb friction, μ, according to the Eurocode and the fib Model Code for Concrete Structures, a number of 0.5 can be used for the friction between unpainted steel and concrete.

3.2.4. Comparison of recommendations bond strength

This section sets up a standard situation for comparing different input parameters of the model. It provides input parameters for the geometry of the elements involved in the connection, such as steel pipe pile dimensions and concrete plug dimensions. It also specifies material properties for concrete and steel.

3.2.4.1. Input parameters

To compare the different input parameters of the model, a standard situation must be set up as a basis from which the different parameters can be varied. All input parameters in the analysis are the same as those given in this section, unless stated otherwise.

First, the geometry of the elements that make up the connection must be determined. The input parameters required for the geometry of the model input are shown in Figure 3.10.

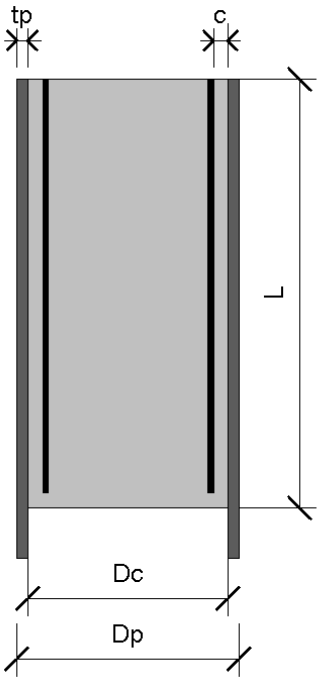

Figure 3.10: Element geometry connection.

The dimensions of this design using a concrete plug can be read from Table 3.1. A number of assumptions have been made in this design example. Firstly, the concrete plug length, L, is assumed to be three times the pipe pile diameter D, because this has not yet been determined in the actual design. Secondly, the concrete cover, c, is assumed to be 40 mm. This assumption is made to meet the Eurocode minimum concrete cover requirement for using their bond strength value, f_{ba}.

Table 3.1: Element geometry connection

Element geometry		
Outer diameter steel pipe pile	D_p	= 600 mm
Wall thickness steel pipe pile	t_p	= 10 mm
Outer diameter concrete plug	$D_c = D_p - 2 \cdot t_p$	= 580 mm
Length of the concrete plug	$L = 3 \cdot D_p$	= 1800 mm
Concrete cover	c	= 40 mm

The material properties of the concrete and steel are given in this section. Strength class C30/37 has been used for the concrete as the base input for the comparison. The characteristic compressive strength, f_{ck}, is known for this strength class. Using this compressive strength, the other material properties of the concrete can then be estimated using the formulas from NEN EN 1992-1-1.

Table 3.2: Material properties comparison recommendations

Material properties		
Characteristic cylinder compressive strength	f_{ck}	= 30 MPa
Mean compressive strength	$f_{cm} = f_{ck} + \Delta f$, $\Delta f = 8$	= 38 MPa
Concrete Young's modulus after 28 days	$E_{cm} = 22000 \cdot (0.1 \cdot f_{cm})^{0.3}$	≈ 30589 MPa
Steel Young's modulus	E_s	= 210 GPa

3.2.4.2. Adjustment of radial stiffness grouted connections for plug connections

In the formulas for the bond strength, both the United Kingdom Department of Energy Code recommendations and the Norsok recommendations use the same radial stiffness factor, K and C_s respectively. However, this stiffness factor is based on a grouted connection and must therefore be adjusted when it is applied in a connection with a concrete plug. Nezamian et al. (2002) made a recommendation for this in their research, which is shown in the formula below. One of the adjustments in this new formula is the elimination of the s term, because there is no sleeve in this type of connection. Another adjustment is that the term t_g has been replaced by the term t_c, which now represents the distance from the outer reinforcement in the plug to the inside of the steel pipe pile instead of the thickness of the grout.

$$K = \frac{1}{m} \cdot (\frac{D_c}{t_c})^{-1} + (\frac{D_p}{t_p})^{-1} \quad \text{(Eq. 3.24)}$$

where:

D_p = outer diameter of pile (mm)
D_c = outer diameter of concrete plug (mm)
t_p = wall thickness of pile (mm)
t_c = distance from outer diameter reinforcement to inner diameter pile (mm) = c
m = steel-grout elastic modular ratio (to be taken as 18 in lieu of actual data) = $\frac{E_s}{E_c}$

3.2.4.3. Influence of D/t ratio on allowable bond strength

The diameter/thickness ratio, D/t, of the steel pipe pile is the first variable analysed for its impact on the bond strength, f_{ba}, across the applicable recommendations. This analysis was conducted by evaluating bond strength for different D/t ratios using the design example. Figure 3.11 illustrates the influence of this variable for each recommendation, considering all applicable constraints.

The figure indicates that the Norsok, United Kingdom Department of Energy Code, and Roeder guidelines suggest a lower bond strength for higher D/t ratios in steel pipe piles. This observation aligns with test results showing a decrease in bond strength as the D/t ratio increases. In contrast, other standards like the Eurocode and BSI, which do not account for this parameter, do not exhibit this decrease, potentially making them less conservative for higher D/t ratios.

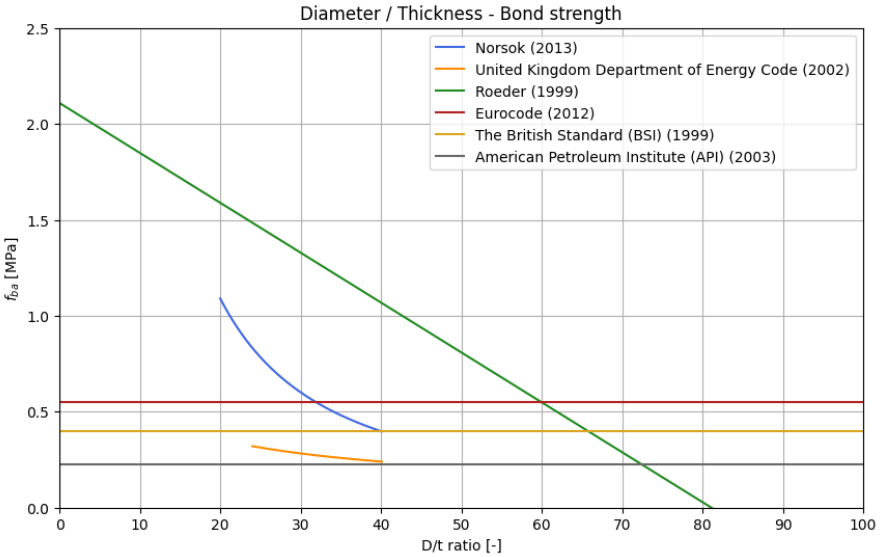

Figure 3.11: Influence of D/t ratio on different recommendations.

3.2.4.4. Influence of L/D ratio on allowable bond strength

The second variable analysed is the length/diameter ratio (L/D) of the concrete plug, to determine its effect on the bond strength, f_{ba}, according to the applicable recommendations. The bond strength was evaluated for different L/D ratios using the design example. Figure 3.12 illustrates the impact of this variable for each recommendation, considering all relevant constraints.

The figure indicates that only the United Kingdom Department of Energy Code establishes a relationship between the L/D ratio and bond strength, showing a decrease in bond strength as the L/D ratio increases. This finding is consistent with Nezamian et al. (2002), who concluded that bond strength diminishes with an increasing L/D ratio, but contradicts Virde and Dowling et al. (1980), who found no significant influence of the L/D ratio on bond strength. Other codes and recommendations do not show a connection between the L/D ratio and bond strength, making it challenging to determine the exact influence of this parameter.

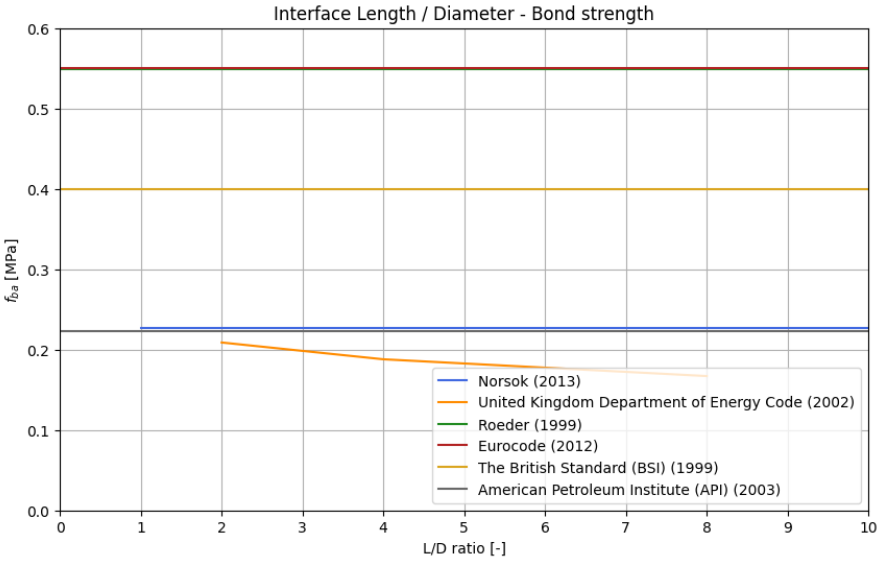

Figure 3.12: Influence of L/D ratio on different recommendations.

3.2.4.5. Influence of concrete compressive strength on allowable bond strength

The final variable investigated is the compressive strength, f_{ck}, of the concrete plug, to understand its influence on bond strength, f_{ba}, across various recommendations. The bond strength was analysed for different f_{ck} values using the design example. Figure 3.13 depicts the impact of this variable for each applicable recommendation, considering all applicable constraints.

The figure shows that both the Norsok and United Kingdom Department of Energy codes assume a relationship between bond strength and the compressive strength (f_{ck}) of the concrete plug, indicating an increase in bond strength with higher f_{ck}. This contradicts the conclusions of Virdi and Dowling et al. (1980), who found no influence of f_{ck} on bond strength, and Aly et al. (2009), who observed a decrease in bond strength with increasing f_{ck}. Other provisions and recommendations do not show a relationship between bond strength and f_{ck}, aligning with the conclusion of Virdi and Dowling et al. (1980) but not with conclusion of Aly et al. (2009).

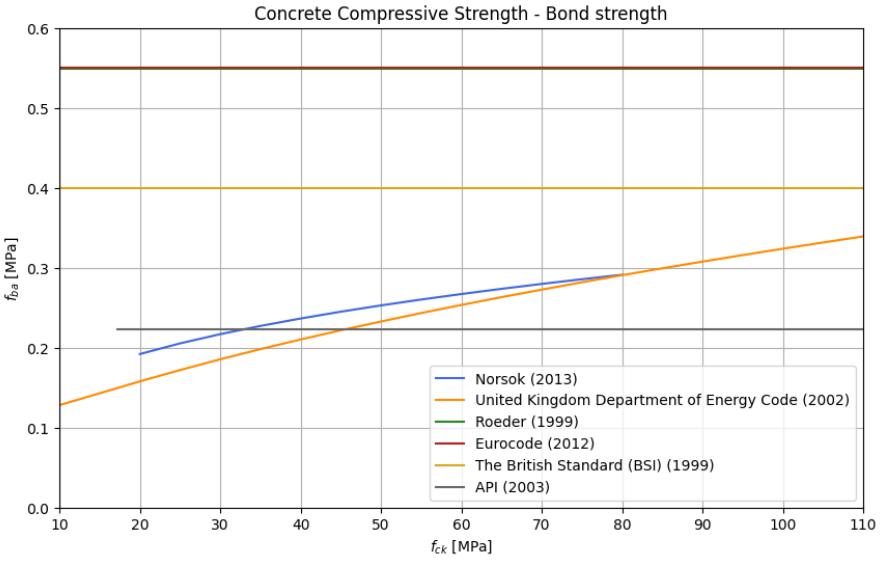

Figure 3.13: Influence of concrete compressive strength on different recommendations.

3.3. Conclusion literature study

This section contains the conclusion of the literature review. This conclusion can again be divided into two parts. Namely part of the parameter study and part for the current code provisions and recommendations. Ultimately leading to a final conclusion of the literature review.

3.3.1. Conclusion parameter study

From the parameter study it can be concluded that various factors influence the bond strength between steel and concrete at concrete plug connections. For example, researchers such as Nezamian et al. (2003) and Virdi and Dowling et al. (1975) mention concrete shrinkage and surface roughness and shape variations as important influencing factors on the transferable load due to friction. As the shrinkage increases and the surface roughness decreases, the bond strength will also decrease.

Various factors surrounding the geometry of the connection are also mentioned as influencing factors surrounding the bond strength. According to Roeder et al. (1999) and Nezamian et al. (2003), the diameter also plays an important role in bond strength. For example, the bond strength would decrease as the diameter of the pipe pile increases. The thickness of the pipe pile also plays a role in the transferable load due to friction, according to Roeder et al. (1999). As the thickness of the pile increases, the level of confinement increases, allowing more load to be transferred through friction. There are several conflicting conclusions about the influence of the interface length of the connection. For example, Virdi and Dowling et al. (2002) describe that the length has no significant influence on the bond strength, while Nezamian concludes that as the length of the plug increases, the bond strength decreases.

The concrete compressive strength is also uncertain as to its exact influence on the bond strength. There are also various conclusions for this. For example, Virdi and Dowling et al. (1980) describe that this has no major influence, while Aly et al. (2009) describe that the bond strength decreases as the concrete compressive strength increases. The level of concrete compaction also influences bond strength, as described by Virdi and Dowling et al. (1980). The better the compaction of the concrete, the higher the bond strength.

Finally, cyclical loading of the plug would also cause a decrease in bond strength. This is described by Nezamian et al. (2003) in his study, in which he recommends that when the concrete plug is cyclically loaded, the bond strength can be reduced by multiplying it by a factor of 0.74.

3.3.2. Conclusion current code provisions and recommendations

The conclusion of the analysis of the current code provisions and recommendations is that there are few comprehensive models available for determining the bond strength regarding the concrete plug connections. For example, there are two code provisions, from Eurocode 4 and The British Standard (BSI), which only prescribe a fixed value for the bond strength between steel and concrete. These values do not depend on any influencing factors. In addition, recommendations are also available from Roeder et al. (1999), which proposes a linear regression model between the bond strength and the diameter / thickness radio of the steel pipe pile. However, once again this recommendation leaves out many influencing factors such as long-term shrinkage.

A second conclusion is that there are many models for the bond strength regarding grouted sleeve connections. These models depend on more parameters than those for plugged connections. However, the question is whether these are applicable to plugged connections, because they have not been validated for this application.

3.3.3. Final conclusion literature study

The final conclusion of the literature review is that a new model is required to determine the bond strength between steel and concrete at concrete plug connections. This model must be set up in such a way that it is dependent on several influencing factors identified in the parameter study, so that the bond strength can be determined for different specific situations.

There is a need for such a model, because the current code provisions and recommendations for concrete plug connections are quite limited and mainly prescribe fixed values. As a result, the bond strength, which depends on several parameters, can probably be underestimated or overestimated in many cases by applying a fixed value. Furthermore, it is also not certain how well applicable the design recommendations for sleeve grouted connections are for concrete plug connections, because they have not been verified for this application.

4

Proposed model transfer of normal force through friction

In this chapter, a new analytical model is proposed for determining the transferable normal force through friction between the steel and concrete with a concrete plug connection. This model is necessary because current design practice lacks recommendations that take into account the various factors that contribute to the force transferable via friction in this specific connection.

To find this model, the following steps were completed in this chapter:

1. First, the concept of friction that is applicable for determining the transferable normal force in the connection via friction was determined.
2. The behavior of the interface between the concrete plug and steel pipe pile was investigated.
3. An expression for the normal force transfer between the concrete plug and steel pipe pile was determined for a small strip of the connection.
4. The expression found for the normal force transfer of a small strip of the connection was extended to a model that can be used to determine the normal force transfer of the entire connection.

4.1. Friction definition

This section describes which friction concept is used in the determination of the resistance due to friction. In the previous chapters it was found that the resistance due to friction can be described on the basis of three different friction components, which are shown in Figure 4.1.

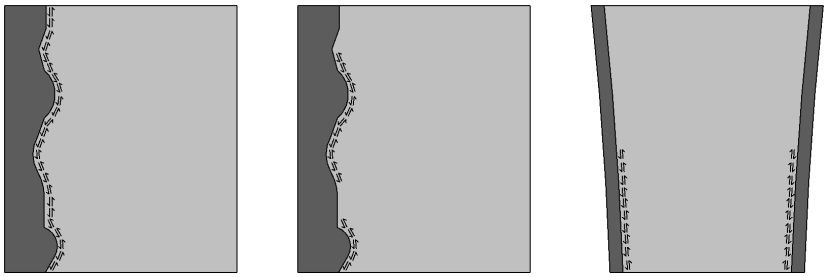

Figure 4.1: Interface friction components.

These three different components consist of chemical adhesion, micro-friction and macro-friction. Each component provides frictional resistance in a different way.

1. Chemical adhesion: Chemical adhesion is related to the bond that is created at molecular level between the concrete of the plug and the steel of the pipe pile. Concrete typically consists of various compounds such as cement, aggregates and water. When concrete cures, a chemical reaction occurs that ensures strong bond formation between the compounds. Additionally, if the surface of the steel pipe pile is properly prepared, for example by cleaning the surface, chemical bonds can also be formed between the concrete of the plug and the steel of the pipe pile.

2. Micro-friction: Micro-friction is related to the resistance created by micro-locking of the concrete of the plug into the steel of the pipe pile. This micro-locking occurs because, when the concrete is loaded vertically, i.e. parallel to the contact surface, the concrete comes into contact with the small irregularities of the steel of the pipe pile. This creates resistance that can be expressed using the friction coefficient and the contact pressure.

3. Macro-friction: Macro-friction refers to the frictional resistance of the concrete and steel to movement at a macroscopic level between the entire surface areas of the concrete plug and the steel pipe pile. This resistance is caused by mechanical resistance, also reffered to as macro-locking, which is caused by manufacturing tolerances associated with the internal pipe pile dimensions. These can, for example, consist of differences in the cross-section of the pipe pile over the height of the connection.

In the past, research has been done into these three different friction components between the concrete and steel by carrying out push-out tests. One of the researchers who has conducted push-out tests is Nezamian et al. (2003). The research by Nezamian et al. (2003) showed that two different load-slip curves can occur when performing push-out tests. These load-slip behaviors are shown in Figure 4.2.

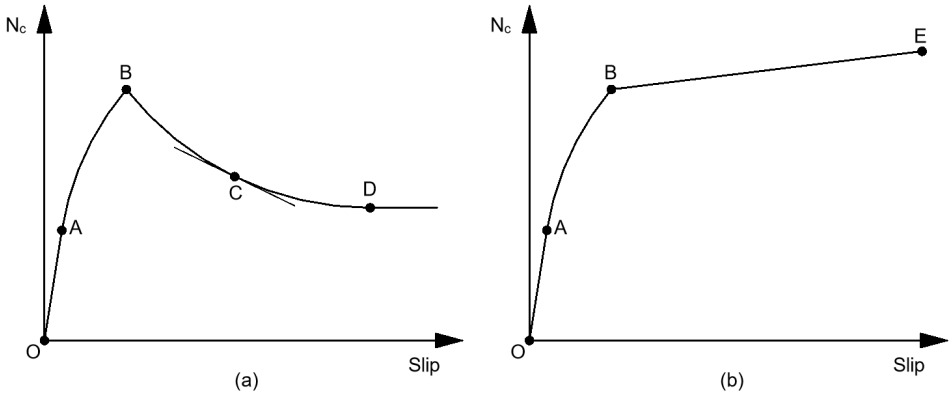

Figure 4.2: Two types of observed load-slip behavior in push-out tests.

Corresponding to the above diagrams of the figure, there are four stages of the whole-load-slip curve: (1) micro slip phase (O-A); (2) slip development phase (A-B); (3) slip increases rapidly phase (B-C, B-E); and (4) residual phase (C-D).

1. Micro slip phase (O-A): In this phase the initial load is relatively small and the relative slip between the concrete and steel is very minimal. In this stage the load is mainly carried by the chemical bond between the concrete and steel, also known as chemical adhesion, until the limit value of this chemical adhesion is reached at point A, where the slip increases. In this initial phase the load-slip behavior is a linear relationship.

2. Slip development phase (A-B): In this phase when the maximum value for the adhesion has been exceeded from point A, the linear relationship of the bond-slip curve will change to a non-linear relationship. In this phase the relative slip will increase more compared to the load on the plug, compared to the previous phase. In this phase, as point B is reached and therefore more slip occurs, the chemical adhesive stress will gradually decrease and more load will be transferred through the micro-friction between the concrete and steel.

3. Slip increases rapidly phase (B-C, B-E): At this stage, when the maximum resistance caused by chemical adhesion and micro-friction have both been exceeded, the relative slip will increase relatively rapidly as load continues to be applied to the concrete plug. In this phase, resistance is still offered by macro-friction between the concrete and steel.

4. Residual phase (C-D): At this stage when the slip has increased drastically, the surface of the concrete plug in contact with the pipe pile will have become smooth due to grinding action between the surfaces of the concrete and steel sliding against each other. As a result, the last resistance, originating from macro friction, will continue to decrease, which will ultimately increase the slip even further.

The difference between the two load-slip behaviors from the figure above is that in the left diagram (a) a decay can be seen after the initial peak (B) has been reached and in the right diagram (b) an increase can be seen after the initial peak has been reached. A possible explanation according to Nezamian et al. (2003) for this difference is that in the case of the right diagram the pipe pile was not as straight or completely round in the cross-section as the pipe pile in the left diagram. However, the proposed model will only consider chemical adhesion and micro-friction, the behavior up to the initial peak (B), so this will make no difference for the model. The reason why only the resistance resulting from chemical adhesion and micro-friction will be included in the model is because at the maximum resistance resulting from these two phenomena, the slip between the concrete and steel is relatively small, in contrast to later phases in the load-slip curve, where with larger slip failure can also occur due to grinding.

This resistance from adhesion and micro-friction, further referred to in this model as the bond strength f_{ba}, can be determined with an adhesion plus micro-friction model between the concrete and steel in contact using the expression below.

$$f_{ba} = a + f_{mf} \tag{Eq. 4.1}$$

where:

a = adhesion (MPa)
f_{mf} = micro-friction (MPa)

The part in the formula which represents the micro-friction, f_{mf}, can be defined using the principle of Coulomb friction. This principle is shown in Figure 4.3. The principle consists of an object with a mass, m, on which a tangential force, F_t, acts. This object is prevented from slipping because the self weight of the object multiplied by the Coulomb force coefficient, μ, and the gravitational constant, g, creates a frictional resistance, F_f, that is equal to the tangential force acting on the object.

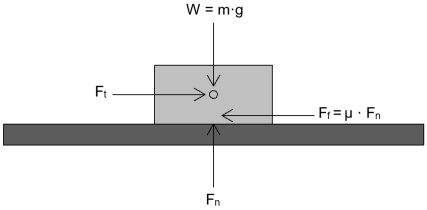

Figure 4.3: Coulomb friction.

To apply this principle to the situation of the connection, the principle must be adopted to the given situation where the resistance is caused differently than in the given example. In the case of a connection with a concrete plug, the resistance to slippage is provided by the contact stress, $\sigma_{i,rr}$, between the steel of the pipe pile and the concrete of the plug multiplied by the Coulomb friction coefficient, μ. This contact stress, $\sigma_{i,rr}$, is caused by the differences in vertical stress, further referred to as longitudinal stress, in the concrete plug and the steel pipe pile along the length of the connection. These stress differences, in combination with the Poisson's effect, cause both the plug and the pipe pile to move horizontally relative to each other, which can therefore cause contact stress. More about this is described in section 4.2. When this principle is applied to the previously found formula for the normal load resistance stress, f_{ba}, the formula for this changes to:

$$f_{ba} = a + \sigma_{i,rr} \cdot \mu \qquad \text{(Eq. 4.2)}$$

where:

a = adhesion (MPa)
μ = Coulomb friction coefficient (-)
$\sigma_{i,rr}$ = contact pressure between the concrete plug and steel pipe pile (MPa)

4.2. Behaviour of the steel-concrete interface

The vertical load that can be transferred by the interface between steel and concrete depends on a number of factors. These factors can be explained by the different states in which the connection can be. These states are shown in Figure 4.4.

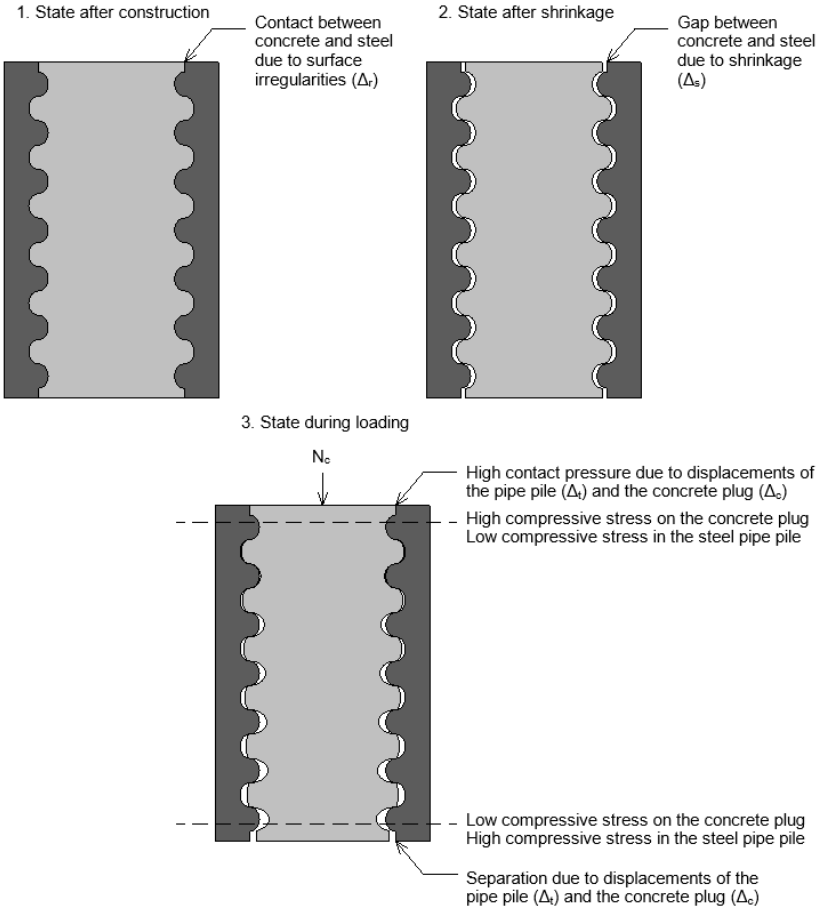

Figure 4.4: States of the connection.

Corresponding to the above figure, there are three states in which the connection can be: (1) state after construction; (2) state after shrinkage; and (3) state during loading.

1. State after construction: The first state of the connection is the state just after construction, where the plug has just been poured and there is full contact between the concrete and the steel because the concrete has been poured into the irregularities in the surface of the steel tubular pile, Δ_r.

2. State during shrinkage: At a later stage, this contact decreases due to concrete shrinkage, Δ_s, causing the concrete to withdraw from these surface irregularities. The extent to which contact decreases therefore depends on the degree of shrinkage of the concrete.

3. State during loading: In the third state, in which the interface is loaded by a compressive force acting on the concrete plug, different contact stresses arise along the length of the interface, which depend on the horizontal displacement of the concrete plug, Δ_c, and the horizontal displacement of the tubular steel pile, Δ_t. These horizontal displacements arise because the longitudinal load transfer stresses in combination with the Poisson ratio effect cause expansions of the elements in the horizontal direction. This creates a high contact stress at the top of the interface, because a high compressive stress is exerted on the concrete compared to the steel, causing the concrete to have a relatively high displacement. The opposite applies at the bottom of the interface, where a relatively low compressive stress still acts on the concrete and a relatively high compressive stress on the steel. This will cause the steel to move relatively much in the horizontal direction relative to the concrete, which can cause separation between the elements and therefore a low contact stress.

The contact regime between the steel and the concrete is therefore mainly dependent on four different components, namely the surface irregularities of the steel pipe pile, the concrete shrinkage, the horizontal displacement of the concrete plug and the horizontal displacement of the steel pipe pile. These are the same four factors that were previously found in research by Nezamian et al. (2003), which is described in subsection 3.1.1. In his research, Nezamian distinguishes between three different states in which the four different components could contribute to the reliability of the connection. These states are as follows:

- State A: $\Delta_{tube} - \Delta_{rugosity} < \Delta_{concrete} - \Delta_{shrinkage}$
- State B: $\Delta_{tube} - \Delta_{rugosity} = \Delta_{concrete} - \Delta_{shrinkage}$
- State C: $\Delta_{tube} - \Delta_{rugosity} > \Delta_{concrete} - \Delta_{shrinkage}$

In state A, the concrete continues to exert pressure on the interface after shrinkage has occurred, and initial bond strength is provided by the chemical adhesion between the steel and the concrete. As the load increases on the connection, this chemical adhesion will break down due to the shear, after which the resistance will depend more on the mechanical characteristics at the interface. Here are two features: the resistance created by the interface contact pressure and the friction coefficient (micro-friction) and the resistance resulting from the mechanical interlock between the steel and the concrete (macro-friction). State B is an intermediate state where chemical adhesion decreases, and also mechanical resistance decreases in an unpredictable manner as state C is reached. In state C there is relatively no bond strength left and the two materials behave separately from each other.

Only state A is used for this analytical model, because this state is the only one that offers a relatively reliable starting point to guarantee the strength of the interface. The given precondition of state A must therefore always be guaranteed.

4.3. Bond strength of a strip of the connection

Over the length of the concrete plug, it is uncertain which stress profile can be assumed for the transfer of the longitudinal stress from the concrete plug to the pipe pile. As a result, initially a very small strip was considered, where the bond strength, f_{ba}, can be considered constant over the length of the strip in both the concrete plug and the steel pipe pile.

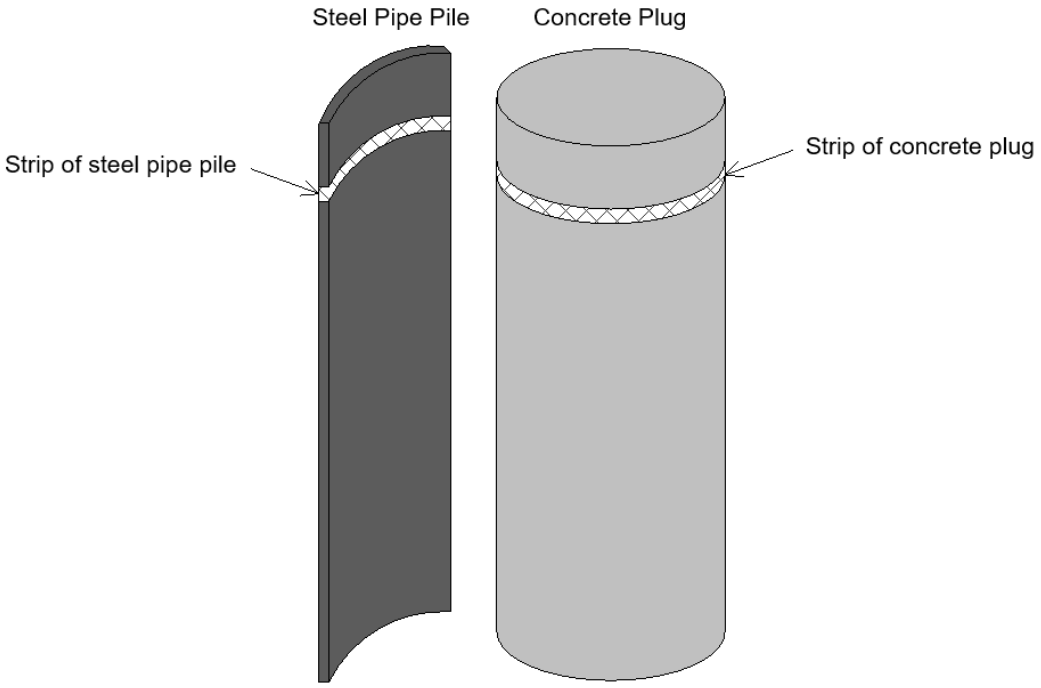

Figure 4.5: Strip of the connection.

To find this constant load transfer stress, f_{ba}, the following steps were completed in this section:

1. First, the contact stresses, which arise between the concrete plug and steel pipe pile and the steel pipe pile and the surrounding soil, were formulated as expressions depending on the horizontal displacements and stiffness factors of the system.

2. To determine these horizontal displacements, the stresses that cause these displacements were determined. In this section the expressions for these stresses have therefore been determined for both the strip of the concrete plug and the strip of the steel pipe pile.

3. After the stresses were determined for the concrete and steel, the horizontal displacements were determined by entering the stresses into the formula for the circumferential strain of both the concrete plug and the steel pipe pile.

4. After the expressions for the horizontal displacements have been determined, the stiffness factors have been determined for both the interface between the concrete and steel and the interface between the steel and the surrounding soil layer. This means that all unknowns have been solved for completing the expressions for the contact stress.

5. Using the expressions for contact stresses, the bond strength can then be determined. This was done by filling in the expressions for the contact stresses in the expression found for the bond strength from section 4.1.

4.3.1. Contact stresses

The contact stresses can be defined using Figure 4.6. The figure shows that the system consists of two interfaces. The first interface is the interface between the concrete plug and the steel pipe pile and the second interface is the interface between the steel pipe pile and the surrounding soil layer. At both interfaces it is assumed that the contact pressure is caused by the sum of the horizontal displacements, $u_{rel,rr}$, and the steel pipe pile, $u_{s,rr}$ respectively multiplied by the spring constants K_i and K_s which represent the stiffness of the steel pipe pile and the stiffness of the surrounding soil, respectively.

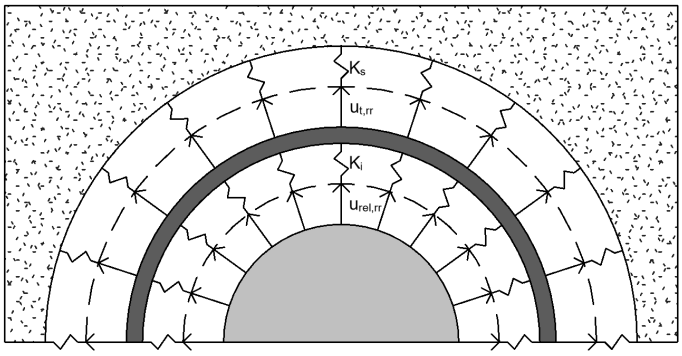

Figure 4.6: Contact stresses in cross-section of the strip.

4.3.1.1. Concrete plug - steel pipe pile interface

The contact pressure between concrete plug and the steel pipe over the height of the interface can be determined with the formulation below. This formulation is constructed from multiplying the identified displacements of the system, as described by Nezamian et al. (2003), by a normal contact stiffness of the interface.

$$\sigma_{i,rr} = u_{rel,rr} \cdot K_i \qquad \text{(Eq. 4.3)}$$

where:

$u_{rel,rr}$ = relative displacement (mm) = $u_{c,rr} + u_{irr,rr} - u_{s,rr} - u_{shr,rr}$
$u_{c,rr}$ = horizontal displacement of the concrete plug (mm)
$u_{irr,rr}$ = surface irregularities (mm)
$u_{s,rr}$ = horizontal displacement of the steel pipe pile (mm)
$u_{shr,rr}$ = shrinkage of the concrete plug (mm)
K_i = normal stiffness interface (N/mm^3)

4.3.1.2. Steel pipe pile - subsoil interface

The contact pressure between the steel pipe pile and the subsoil on the outside of the pile can be determined using the formulation below. This formulation is based on multiplying the displacement of the pile by the horizontal bedding stiffness of the soil of the surrounding layer.

$$\sigma_{o,rr} = u_{s,rr} \cdot K_i \qquad \text{(Eq. 4.4)}$$

where:

$u_{s,rr}$ = horizontal displacement of the steel pipe pile (mm)
K_s = horizontal bedding stiffness of the surrounding soil (N/mm^3)

4.3.2. Concrete stresses

In this section the stresses in the concrete plug are determined. This was done using Figure 4.7, which indicates the stresses on both the concrete and steel. Three different stress components act on the concrete plug, as can be assumed for thick-walled cylinders. A cylinder can be assumed to be thick-walled if the condition ($\frac{D_p}{t_p} \leq 20$) is guaranteed. In practical cases this is always the case for the concrete plug. The three stress components of the concrete plug therefore consist of the longitudinal stress, the radial stress and the circumferential stress. These are given by $\sigma_{c,zz}$, $\sigma_{c,rr}$ and $\sigma_{c,,r\theta}$ respectively. Here, the radial stress in the concrete plug is assumed to be equal to the contact stress between the concrete plug and steel pipe pile, $\sigma_{i,rr}$.

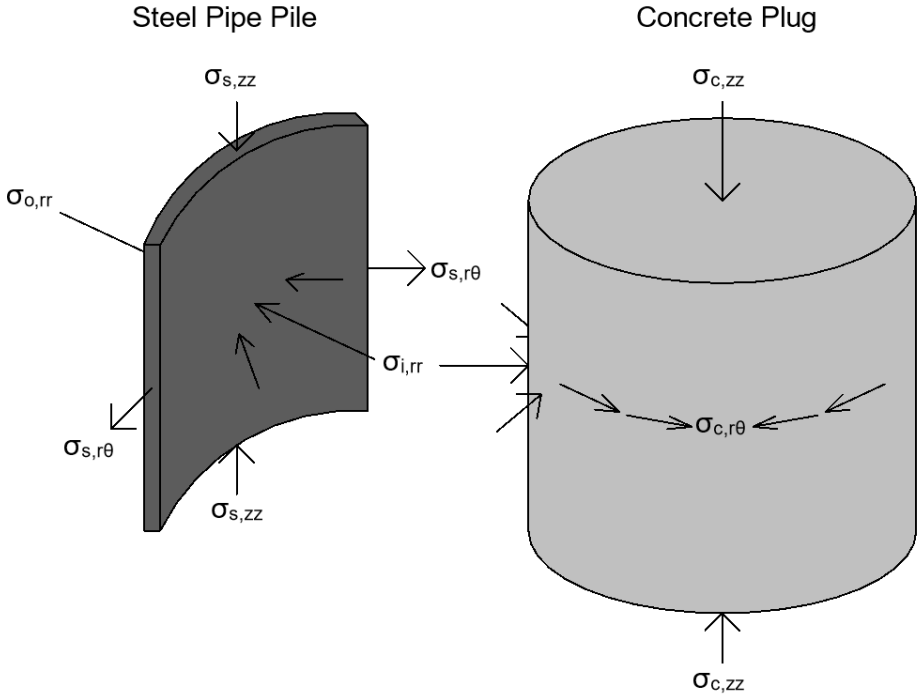

Figure 4.7: Stresses acting on strip of the steel pipe pile and concrete plug.

4.3.2.1. Concrete longitudinal stress

In the model, the contact stresses, $\sigma_{i,rr}$, are caused by the difference in longitudinal stresses between the concrete and steel. To determine the contact stresses for a single strip, the longitudinal stress in the concrete must be entered in the model. The longitudinal stress for a single strip of concrete can be denoted as $\sigma_{c,zz}$.

4.3.2.2. Concrete radial and circumferential stress

Lame's equations (CIEM0000, (2022)) are used to determine the concrete radial and circumferential stress. These equations can be used for thick-walled cylinders, such as the concrete plug in this case. Here the radial and circumferential stress respectively are given by:

$$\sigma_{c,rr}(R_c) = a + \frac{b}{R_c^2} \quad \text{(Eq. 4.5)}$$

$$\sigma_{c,r\theta}(R_c) = a - \frac{b}{R_c^2} \quad \text{(Eq. 4.6)}$$

where:

R_c = radius at point in the concrete plug (mm)

To solve for the constant a and b in the equations, boundary conditions must be established for the equation. These boundary conditions are given in the formula below. Here the radial stress in the inner radius is equal to 0 and the radial stress in the outer radius is equal to the contact pressure of the interface.

$$\begin{cases} \sigma_{c,rr}(R_c = R_i) = 0 \\ \sigma_{c,rr}(R_c = R_o) = -\sigma_{i,rr} \end{cases} \quad \text{(Eq. 4.7)}$$

where:

R_i = inner radius concrete plug (mm)
R_o = outer radius concrete plug (mm)

When equation(4.4) and equation(4.6) are solved using the boundary conditions of equation(4.7) the following values can be found for the constants a and b.

$$\begin{cases} a = \dfrac{R_o^2 \cdot \sigma_{i,rr}}{R_i^2 - R_o^2} \rightarrow R_i = 0 \rightarrow a = -\sigma_{i,rr} \\ b = \dfrac{R_i^2 \cdot R_o^2 \cdot \sigma_{i,rr}}{R_i^2 - R_o^2} \rightarrow R_i = 0 \rightarrow b = 0 \end{cases} \quad \text{(Eq. 4.8)}$$

When constants a and b are substituted back in equation(4.4) and equation(4.6) this results in the following formulas for the radial and circumferential stress in the concrete plug:

$$\sigma_{c,rr} = -\sigma_{i,rr} = -u_{rel,rr} \cdot K_i \quad \text{(Eq. 4.9)}$$

$$\sigma_{c,r\theta} = -\sigma_{i,rr} = -u_{rel,rr} \cdot K_i \quad \text{(Eq. 4.10)}$$

4.3.3. Steel stresses

In this section the stresses in the steel are determined. This was done again using figure 4.7. In contrast to the concrete plug, only two different stress components work on the steel pipe pile, as can be assumed for thin-walled cylinders. This assumption can be made because the steel pipe pile can be assumed as a thin-walled cylinder, because the condition for this ($20 \leq \frac{D_p}{t_p}$) is almost always guaranteed in practice. The two stress components that act on the steel pipe pile consist of the longitudinal stress and the circumferential stress, $\sigma_{s,zz}$ and $\sigma_{s,r\theta}$ respectively. The radial stress in the steel $\sigma_{s,rr}$ is therefore neglected due to the assumption that this pipe pile can be regarded as a thin-walled cylinder.

4.3.3.1. Steel longitudinal stress

In the model, the contact stresses are caused by the difference in longitudinal stresses between the concrete and steel. To determine the contact stresses for a single strip, the longitudinal stress in the steel must be entered in the model. The longitudinal stress for a single strip of steel can be denoted as $\sigma_{s,zz}$.

4.3.3.2. Steel circumferential stress

The steel pipe pile can be assumed as a thin walled cylinder. This assumption can be made because the condition for assuming this ($20 \leq \frac{D_p}{t_p}$) is almost always guaranteed for practical cases. With this assumption, the circumferential stress can then be determined using the pressure vessel method, as shown in the figure below. The pressure from within, originating from the contact pressure between the steel and the concrete, creates a circumferential tensile stress in the steel. The contact pressure caused by the stiffness of the surrounding soil creates a circumferential compressive stress in the steel as can be concluded from Figure 4.8.

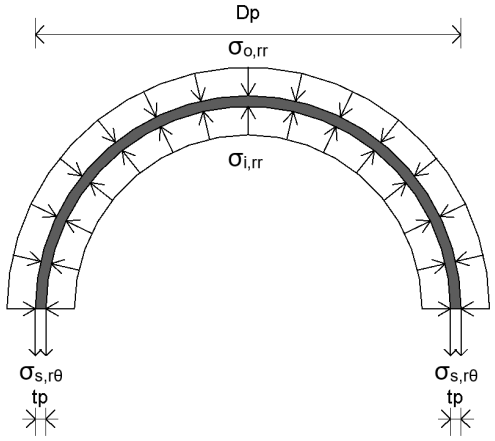

Figure 4.8: Steel circumferential stress.

Using the previous assumptions, the circumferential stress can be determined with the following formula:

$$\sigma_{s,r\theta} = \frac{(\sigma_{i,rr} - \sigma_{o,rr}) \cdot D_p}{2 \cdot t_p} \quad \text{(Eq. 4.11)}$$

where:

D_p = outer diameter of the steel tube (mm)
t_p = thickness of the steel tube (mm)

Substituting the expressions for the contact stresses (equation 4.3 and equation 4.4) into the equation then leads to the following formula:

$$\sigma_{s,r\theta} = \frac{(u_{rel,rr} \cdot K_i - u_{s,rr} \cdot K_s) \cdot D_p}{2 \cdot t_p} \quad \text{(Eq. 4.12)}$$

4.3.4. Displacements

In this section the displacements of the concrete and steel have been determined, so that the total relative displacement in the interface between the concrete and steel can ultimately be determined. The displacements in the concrete and steel are created by the previously found stresses in the concrete and steel from subsections 4.3.2 and 4.3.3 respectively.

4.3.4.1. Concrete horizontal displacement

With all concrete stresses as a function over the height of the plug, the circumferential strain of the concrete can then be determined as a function over the height of the plug. This function can be given by:

$$\epsilon_{c,r\theta} = \frac{1}{E_c} \cdot (\sigma_{c,r\theta} - \nu_c \cdot (\sigma_{c,zz} + \sigma_{c,rr})) \tag{Eq. 4.13}$$

where:

E_c = modulus of elasticity concrete (MPa)
ν_c = Poisson's ratio of concrete (-)

Substituting the expressions for the concrete stresses (equation 4.9 and equation 4.10) into the expression for the concrete strain then gives:

$$\epsilon_{c,r\theta} = \frac{1}{E_c} \cdot (-u_{rel,rr} \cdot K_i - \nu_c \cdot (\sigma_{c,zz} - u_{rel,rr} \cdot K_i)) \tag{Eq. 4.14}$$

The horizontal displacement of the concrete plug can then be determined using the circumferential strain using the formula below:

$$u_{c,rr} = \frac{D_c}{2} \cdot \epsilon_{c,r\theta} = \frac{D_c}{2 \cdot E_c} \cdot (-u_{rel,rr} \cdot K_i - \nu_c \cdot (\sigma_{c,zz} - u_{rel,rr} \cdot K_i)) \tag{Eq. 4.15}$$

4.3.4.2. Steel horizontal displacement

The steel circumferential strain can then be determined using the formula below. The radial stress, unlike the concrete circumferential strain, does not play a part in the equation. This is due to the fact that the steel pipe pile is assumed as a thin-walled cylinder in which the proportion of radial stress is negligible.

$$\epsilon_{s,r\theta} = \frac{1}{E_s} \cdot (\sigma_{s,r\theta} - \nu_s \cdot \sigma_{s,zz}) \tag{Eq. 4.16}$$

where:

E_s = modulus of elasticity steel (MPa)
ν_s = Poisson's ratio of steel (-)

Substituting expressions for the steel stresses (equation 4.12) into the formula for the strain of the steel then leads to the following formula:

$$\epsilon_{s,r\theta} = \frac{1}{E_s} \cdot (\frac{(u_{rel,rr} \cdot K_i - u_{s,rr} \cdot K_s) \cdot D_p}{2 \cdot t_p} - \nu_s \cdot \sigma_{s,zz}) \tag{Eq. 4.17}$$

The displacement of the steel pipe pile can then be determined using the formula below:

$$u_{s,rr} = \frac{D_p}{2} \cdot \epsilon_{s,r\theta} = \frac{D_p}{2 \cdot E_s} \cdot (\frac{(u_{rel,rr} \cdot K_i - u_{s,rr} \cdot K_s) \cdot D_p}{2 \cdot t_p} - \nu_s \cdot \sigma_{s,zz}) \quad \text{(Eq. 4.18)}$$

However, the above formula is a recursive equation. Using Maple, the equation is rewritten to a non-recursive equation, making the formula as follows:

$$u_{s,rr} = \frac{D_p \cdot (u_{rel,rr} \cdot K_i \cdot D_p - 2 \cdot \nu_s \cdot \sigma_{s,zz} \cdot t_p)}{D_p^2 \cdot K_s + 4 \cdot E_s \cdot t_p} \quad \text{(Eq. 4.19)}$$

4.3.4.3. Relative displacement

The relative horizontal displacement in the interface between the concrete plug and the steel pipe pile is a function that can be given as follows:

$$u_{rel,rr} = u_{c,rr} + u_{irr,rr} - u_{s,rr} - u_{shr,rr} \quad \text{(Eq. 4.20)}$$

where:

$u_{irr,rr}$ = surface irregularities (mm)
$u_{shr,rr}$ = shrinkage of the concrete plug (mm)

Substituting the expressions for displacements of both the concrete pug and the steel pipe pile (equation 4.15 and equation 4.19) then leads to the following equation:

$$u_{rel,rr} = \frac{D_c \cdot (-u_{rel,rr} \cdot K_i - \nu_c \cdot (\sigma_{c,zz} - u_{rel,rr} \cdot K_i))}{2 \cdot E_c} - \frac{D_p \cdot (u_{rel,rr} \cdot K_i \cdot D_p - 2 \cdot \nu_s \cdot \sigma_{s,zz} \cdot t_p)}{D_p^2 \cdot K_s + 4 \cdot E_s \cdot t_p} + u_{irr,rr} - u_{shr,rr} \quad \text{(Eq. 4.21)}$$

However, this is again a recursive equation, which has been rewritten with Maple into a non-recursive equation. The result of this is as follows:

$$u_{rel,rr} = \frac{((-2u_{irr,rr}+2u_{shr,rr})E_c+D_c v_c \sigma_{c,zz})K_s D_p^2-4D_p E_c t_p v_s \sigma_{s,zz}+4((-2u_{irr,rr}+2u_{shr,rr})E_c+D_c v_c \sigma_{c,zz})E_s t_p}{((-2K_i-2K_s)E_c+D_c K_i K_s (v_c-1))D_p^2+4E_s(-2E_c+D_c K_i (v_c-1))t_p} \quad \text{(Eq. 4.22)}$$

4.3.5. Stiffness factors

In this subsection the stiffness factors of the model are determined. These stiffness factors consist of the normal stiffness of the interface and the horizontal bedding stiffness of the surrounding soil.

4.3.5.1. Normal stiffness interface

The normal stiffness of the interface between the concrete plug and the steel pipe pile must be determined so that it can be implemented in the formula. The stiffness of the interface depends on the stiffness of the steel pipe pile surrounding the concrete plug. To determine this stiffness, the formula for the circumferential strain of the pile was determined as a function of the radial contact stress using Figure 4.9.

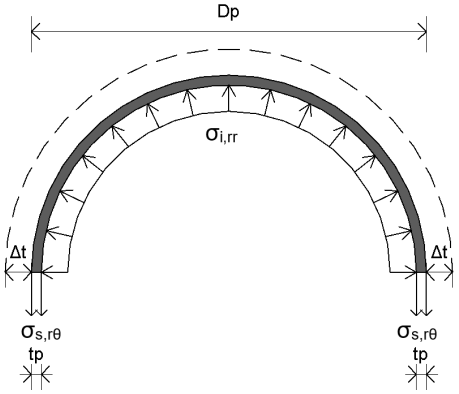

Figure 4.9: Normal stiffness interface.

Using the figure, the following formula for the radial strain can be determined.

$$\epsilon_{s,r\theta} = \frac{\sigma_{s,r\theta}}{E_s} = \frac{\sigma_{s,rr} \cdot D_p}{E_s \cdot 2 \cdot t_p} \tag{Eq. 4.23}$$

where:

E_s = modulus of elasticity steel (MPa)
D_p = outer diameter of the steel tube (mm)
t_p = thickness of the steel tube (mm)

The formula for the displacement of the steel pipe pile can then be determined using the formula for the circumferential strain.

$$u_{s,rr} = \frac{D_p \cdot \epsilon_{s,r\theta}}{2} \tag{Eq. 4.24}$$

Then, by substituting the formula for the displacement (equation 4.24) into the stiffness formula (equation 4.25), and then substituting the radial strain (equation 4.23), a constant can be found that can be taken as the normal stiffness of the interface.

$$K_i = \frac{\sigma_{s,rr}}{u_{s,rr}} = \frac{2 \cdot \sigma_{s,rr}}{D_p \cdot \epsilon_{s,r\theta}} = \frac{4 \cdot \sigma_{s,rr} \cdot E_s \cdot t_p}{D_p^2 \cdot \sigma_{s,rr}} = \frac{4 \cdot E_s \cdot t_p}{D_p^2} \tag{Eq. 4.25}$$

When this factor is analysed it can be concluded that this factor is the same as that established by Roeder et al. (1999) for determining displacements of the steel pipe pile as a result of the internal pressure, which is given in equation 3.2.

4.3.5.2. Horizontal bedding stiffness of the surrounding soil

The horizontal bedding stiffness of the surrounding soil layer, K_s, is determined using the Ménard theory. This theory is based on field tests using a pressureometer. The horizontal bedding constant can be approximated using an empirical formula, depending on the soil type, the pile diameter and the cone resistance. This theory was chosen because it is relatively easy to apply in practice and requires little exact determination.

From an elastic modulus, E_p, determined with the Ménard pressure test or using a parameter β from the cone resistance q_c, the horizontal bedding constant is determined with the following formula:

$$\frac{1}{K_s} = \frac{1}{3 \cdot E_p} \cdot [1,3 \cdot R_0 \cdot (2,65 \cdot \frac{R}{R_0})^{\alpha} + \alpha \cdot R] \quad \text{(Eq. 4.26)}$$

where:

R_0 = reference radius (mm) = 300 mm
R = $\frac{D_p}{2}$
E_p $\approx \beta \cdot q_c$

α, β and q_c are equal to the value in Table 4.1.

Table 4.1: Rheological factors according to Ménard and cone resistance (Menard et al. (1975)).

Soil type	α	β	q_c (MPa)
Peat	1	3,0	0 - 4
Clay	2/3	2,0	0 - 8
Sand	1/3	0,7	5 <

4.3.6. Shrinkage

The displacement of the concrete plug due to shrinkage must also be determined so that it can be included in the model. The shrinkage can be determined using the formula below:

$$u_{shr,rr} = \frac{\epsilon_s \cdot D_c}{2} \quad \text{(Eq. 4.27)}$$

where:

ϵ_s = total shrinkage strain (-)
D_c = outer diameter of the concrete plug (mm)

The shrinkage strain in this formula is a complex value that depends on many factors. The model adopted for this determination is described in chapter 5.

4.3.7. Bond strength

With the determined relative displacement, $u_{rel,rr}$, and the found stiffness's, K_i and K_s, from the previous sections, the bond strength, f_{ba}, of the strip can be determined . This can be done by multiplying the found horizontal contact stress, $\sigma_{i,rr}$, with the coulomb friction coefficient, μ, so that the horizontal stress can be converted into a vertical stress. This process is shown below.

$$f_{ba} = a + \sigma_{i,rr} \cdot \mu = 0 + \sigma_{i,rr} \cdot \mu = u_{rel,rr} \cdot K_i \cdot \mu \quad \text{(Eq. 4.28)}$$

where:

a = adhesion (MPa)
μ = friction coefficient (-)

In this formula, the adhesion, a, is set equal to 0. This is a conservative assumption based on the fact that in order to activate the resistance of micro-friction, a small relative slip is required between the concrete and steel, whereby this adhesion could partially or completely break off. The second reason for neglecting the share of adhesion in the resistance is the occurrence of shrinkage and the relative displacement between the steel and concrete. These horizontal movements could possibly cause separation, making adhesion very uncertain. The third and final reason for neglecting adhesion is that with multiple load cycles, the resistance caused by adhesion in most cases, based on cyclic push-out tests by Nezamian et al. (2003), eventually failed. Therefore, when this model is used in practice, usually for longer periods involving multiple load cycles, the adhesion will most certainly be broken.

When the expressions for the relative displacement (equation 4.22) and stiffness of the interface (equation 4.25) are then substituted into the expression for the bond strength (equation 4.28), the following ultimate formulation for the bond strength capacity of the strip is found.

$$f_{ba} = \frac{2E_s t_p \mu(((4E_c\epsilon_s+4v_c\sigma_{c,zz})D_c-8E_c u_{irr,rr})E_s-4v_s\sigma_{s,zz}D_pE_c)t_p+K_s((E_c\epsilon_s+v_c\sigma_{c,zz})D_c-2E_c u_{irr,rr})D_p^2}{\left(8D_cE_s^2t_p^2(v_c-1)+2t_p(-4E_c+(v_c-1)K_sD_c)E_sD_p^2-D_p^4E_cK_s\right)} \quad \text{(Eq. 4.29)}$$

As can be deduced from the above formula, the bond strength of the strip depends on both the longitudinal stress in the concrete plug and the longitudinal stress in the steel pipe pile, respectively $\sigma_{c,zz}$ and $\sigma_{s,zz}$. However, these two stresses and their distribution are unknown over the length of the interface between the steel and concrete. In order to ultimately arrive at a method to determine the total normal force resistance that can be transferred via friction between the concrete plug and the steel pipe pile, a method must be found to determine this longitudinal distribution over the height. Various methods are possible for this, such as determining a differential equation for this distribution or making an assumption for the distribution based on test results. In the next section it was decided to draw up a numerical differential equation for the progression.

4.4. Numerical method for determining the normal force capacity

In this section, a numerical method has been developed for determining the longitudinal stress in the concrete plug and the steel pipe pile and its distribution over the length of the interface. This was done so that, in combination with the method for finding the bond strength of a strip, the total normal force capacity, $N_{Rd,c}$, can be found that can be transferred via friction between the steel and concrete. This numerical method is necessary because the longitudinal stress distribution over the height of the concrete plug and the steel pipe pile are both unknown and can only be solved by formulating a differential equation. This differential equation will be solved numerically.

4.4.1. Longitudinal stress distributions over the length of the interface

The stress distribution over the height of the pipe pile and the concrete plug were determined using a numerical method. In this method, the concrete plug and the steel pipe pile are divided over the length of the interface into very small equal strips, each with a length Δz , whereby a constant bond strength, $f_{ba,i}$, is assumed in each strip. Using this assumed constant load transfer stress in each of the strips, $f_{ba,i}$, the longitudinal stress in both the concrete and steel, respectively $\sigma_{c,zz,i+1}$ and $\sigma_{s,zz,i+1}$, can then be determined for the next strip, which can then be used to determine the bond strength of the next strip, $f_{ba,i+1}$. By repeating this process until the total length of the interface has been filled in, a relatively accurate estimation of the longitudinal stress distributions in the concrete plug and the steel pipe pile can be made. This process is shown in Figure 4.10.

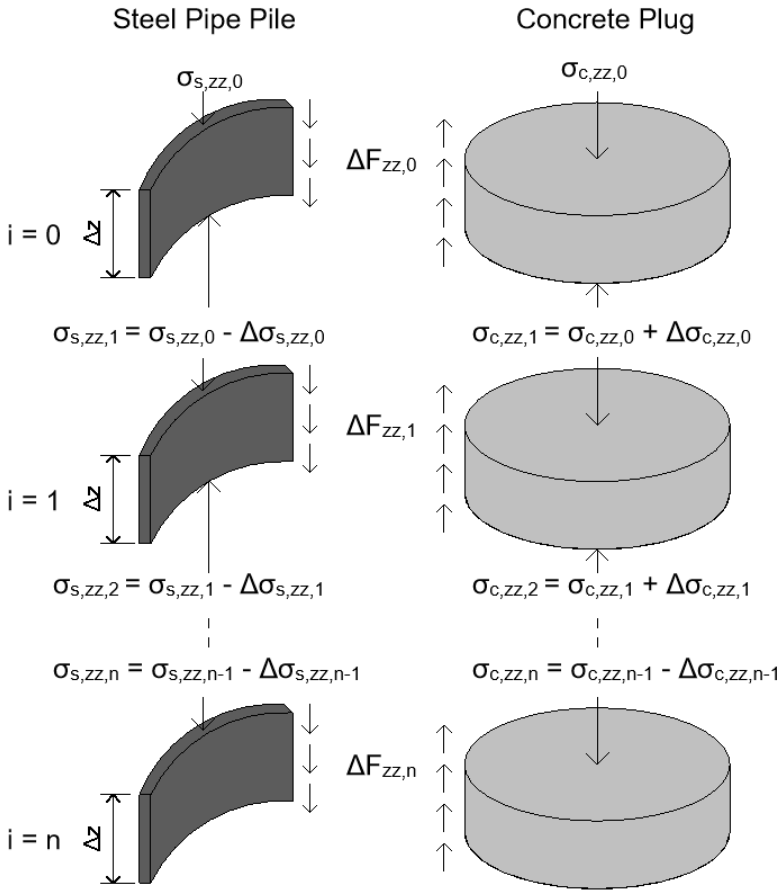

Figure 4.10: Longitudinal stresses over the length of the interface.

The normal force, $\Delta F_{zz,i}$, that will be transferred per strip from the concrete to the steel via friction can be determined using the formula below, where the bond strength of each strip is multiplied by the contact surface between the steel and the concrete of each strip.

$$\Delta F_{zz,i} = \Delta z \cdot f_{ba,i} \cdot D_c \cdot \pi \tag{Eq. 4.30}$$

where:

Δz = size of the mesh (mm)
$f_{ba,i}$ = bond strength (MPa)
D_c = outer diameter of the concrete plug (mm)

The normal force of each strip that is transferred via friction between the concrete plug and the steel pipe pile will also cause a change in the longitudinal stress in both the concrete and the steel between the two adjacent strips, respectively $\Delta\sigma_{c,zz,i}$ and $\Delta\sigma_{s,zz,i}$. These longitudinal stress differences can be determined by dividing the expression for the normal force by the cross-sectional area of the two elements, as is done in the expressions below.

$$\Delta\sigma_{c,zz,i} = \frac{\Delta F_{zz,i}}{A_c} = \Delta z \cdot \frac{f_{ba,i} \cdot D_c \cdot \pi}{\frac{1}{4} \cdot D_c^2 \cdot \pi} = \Delta z \cdot \frac{4 \cdot f_{ba,i}}{D_c} \tag{Eq. 4.31}$$

$$\Delta\sigma_{s,zz,i} = \frac{\Delta F_{zz,i}}{A_s} = \Delta z \cdot \frac{f_{ba,i} \cdot D_c \cdot \pi}{\frac{1}{4} \cdot (D_p^2 - D_c^2) \cdot \pi} = \Delta z \cdot \frac{4 \cdot f_{ba,i} \cdot D_c}{D_p^2 - D_c^2} \tag{Eq. 4.32}$$

where:

D_p = outer diameter of the steel pipe pile (mm)
t_p = thickness of the steel pipe pile (mm)

4.4.2. Concrete longitudinal stress

The longitudinal stress distribution in the concrete is determined numerically using the formula below. In this formula, longitudinal stress in the next strip of concrete, $\sigma_{c,zz,i+1}$, is determined by the change in longitudinal stress of the previous strip, $\Delta\sigma_{c,zz,i}$, added to the longitudinal stress in previous strip, $\sigma_{c,zz,i}$.

$$\sigma_{c,zz,i+1} = \sigma_{c,zz,i} + \Delta\sigma_{c,zz,i} \tag{Eq. 4.33}$$

Entering the expression found for the change in longitudinal stress in the concrete then produces the following expression for the longitudinal stress profile in the concrete.

$$\sigma_{c,zz,i+1} = \sigma_{c,zz,i} + \Delta z \cdot \frac{4 \cdot f_{ba,i}}{D_c} \tag{Eq. 4.34}$$

To determine the stress profile over the length of the interface in the concrete, the initial conditions must also be determined. The initial condition maintained for this stress distribution is equal to the longitudinal stress at the top of the concrete plug. The formula for this stress is known and depends on the normal force introduced via the concrete, N_c.

$$\begin{cases} z_0 = 0 \\ \sigma_{c,zz,0} = -\dfrac{4 \cdot N_c}{D_c^2 \cdot \pi} \end{cases} \tag{Eq. 4.35}$$

where:

N_c = normal force acting on the concrete plug (N)
D_c = outer diameter of the concrete plug (mm)

4.4.3. Steel longitudinal stress

The longitudinal stress distribution in the steel is determined numerically using the formula below. In this formula, longitudinal stress in the next strip of steel, $\sigma_{s,zz,i+1}$, is determined by the change in longitudinal stress of the previous strip, $\Delta\sigma_{s,zz,i}$, subtracted from the longitudinal stress in previous strip, $\sigma_{s,zz,i}$.

$$\sigma_{s,zz,i+1} = \sigma_{s,zz,i} - \Delta\sigma_{s,zz,i} \tag{Eq. 4.36}$$

Entering the expression found for the change in longitudinal stress in the steel then produces the following expression for the longitudinal stress profile in the steel.

$$\sigma_{s,zz,i+1} = \sigma_{s,zz,i} - \Delta z \cdot \frac{4 \cdot f_{ba,i} \cdot D_c}{D_p^2 - D_c^2} \tag{Eq. 4.37}$$

To determine the stress profile over the length of the interface in the steel, the initial conditions must also be determined. The initial condition maintained for this stress distribution is equal to the longitudinal stress at the top of the steel pipe pile. The formula for this stress is known and depends on the normal force introduced via the steel, N_s.

$$\begin{cases} z_0 = 0 \\ \sigma_{s,zz,0} = -\dfrac{4 \cdot N_s}{(D_p^2 - D_c^2) \cdot \pi} \end{cases} \tag{Eq. 4.38}$$

where:

$$N_s = \frac{(D_p^2 - D_c^2) \cdot \pi \cdot f_{cd}}{4} \tag{Eq. 4.39}$$

D_p = outer diameter of the the steel tube (mm)
D_c = outer diameter of the concrete plug (mm) = $D_p - 2 \cdot t_p$
t_p = thickness of the steel tube (mm)
f_{cd} = design compressive strength of concrete (MPa)

4.4.4. Bond strength over the length of the interface

The expression for the bond strength per strip at a constant longitudinal stress has already been found in section 4.3.7. However, to be able to directly enter the expression in the found numerical expressions for the longitudinal stress distributions, f_{ba} has been adjusted to $f_{ba,i}$, with which the stress distribution over the entire length of the interface can be determined using the found contact stresses, $\sigma_{i,rr,i}$, over the length of the interface.

$$f_{ba,i} = a + \sigma_{i,rr,i} \cdot \mu = 0 + \sigma_{i,rr,i} \cdot \mu = u_{rel,rr,i} \cdot K_i \cdot \mu \quad \text{(Eq. 4.40)}$$

where:

a = adhesion (MPa)
μ = friction coefficient (-)

In this formula, the adhesion, a, is again set equal to 0. This is a conservative assumption based on the same assumptions as already mentioned in subsection 4.3.7

When the expressions for the relative displacement (equation 4.22) and stiffness of the interface (equation 4.22) are then substituted into the expression for the bond strength (equation 4.40), the following ultimate formulation for the bond strength capacity of the strip is found.

$$f_{ba,i} = \frac{2E_s t_p \mu(((4E_c\epsilon_s+4v_c\sigma_{c,z,i})D_c-8E_c u_{irr,rr})E_s-4v_s\sigma_{s,z,i}D_pE_c)t_p+K_s((E_c\epsilon_s+v_c\sigma_{c,z,i})D_c-2E_c u_{irr,rr})D_p^2}{\left(8D_cE_s^2t_p^2(v_c-1)+2t_p(-4E_c+(v_c-1)K_sD_c)E_sD_p^2-D_p^4E_cK_s\right)} \quad \text{(Eq. 4.41)}$$

The difference with the expression of section 4.3.7 is that the symbols for the longitudinal stresses in the concrete and steel, $\sigma_{c,zz}$ and $\sigma_{s,zz}$ respectively, have been replaced by $\sigma_{c,z,i}$ and $\sigma_{s,z,i}$. This was done so that the bond strength over the entire length can be determined numerically using the longitudinal stress distributions.

4.4.5. Iterative method for determining the normal force capacity

To determine the total normal force capacity, $N_{Rd,c}$, that can be transferred via friction in the interface between the concrete plug and the steel pipe pile, an iterative method is used. In this method, the normal force, N_c, acting on the concrete is iteratively adjusted until convergence is achieved. Convergence means that the difference between the normal force acting on the concrete plug, N_c, and the normal force capacity due to friction, $N_{Rd,c}$, falls within a very low tolerance. The normal force capacity due to friction, $N_{Rd,c}$, depends on the force acting on the concrete, N_c, because the force acting on the concrete influences the Poisson's effect and therefore ultimately also the contact stresses and therefore the bond strength along the length of the interface.

The normal force capacity is initially calculated by summing the normal forces, $\Delta F_{z,i}$, transferred per strip over the entire length of the interface based on an initial guess for the force acting on the concrete plug, N_c. This provides an initial estimate of $N_{Rd,c}$.

$$N_{Rd,c} = \sum_{i=0}^{i=n} \Delta F_{zz,i} = D_c \cdot \pi \cdot \Delta z \cdot \sum_{i=0}^{i=n} f_{ba,i} \quad \text{(Eq. 4.42)}$$

where:

$$n = \frac{L}{\Delta z} \quad \text{(Eq. 4.43)}$$

L = length of the concrete plug (mm)
Δz = size of the mesh (mm)

The iterative process begins by comparing the calculated normal force capacity, $N_{Rd,c}^{(i)}$, with the initial guess for the normal force acting on the concrete plug, $N_c^{(i)}$. If the absolute difference between these values is within a predefined tolerance, convergence is achieved.

$$|N_{Rd,c}^{(i)} - N_c^{(i)}| < \text{tolerance} \quad \text{(Eq. 4.44)}$$

If convergence is not achieved, the normal force is adjusted using a damping factor, α, to control the step size of the update. The adjusted normal force for the next iteration, $N_c^{(i+1)}$, is calculated as follows:

$$N_c^{(i+1)} = N_c^{(i)} + \alpha \cdot (N_{Rd,c}^{(i)} - N_c^{(i)}) \quad \text{(Eq. 4.45)}$$

where:

α = damping factor to control the step size of the update (-)

This process is repeated iteratively until the calculated normal force capacity closely matches the normal force acting on the concrete plug, indicating convergence. When convergence is achieved, the normal force capacity value determined at that time can be taken as the final capacity.

4.5. Conclusion model transfer of normal force through friction

In this chapter a model has been set up for determining the transfer of normal force due to friction. Friction in this model is expressed as a function of adhesion and micro-friction. However, it was decided to neglect the adhesion part based on the fact that the adhesion in combination with the required slip for utilizing micro-friction, concrete shrinkage and cyclic loading is very uncertain in the long term. The part of micro-friction is expressed using the Coulomb friction model, which depends on the contact pressure between the steel and concrete and the Coulomb friction coefficient.

This contact pressure between the steel and concrete is determined as a function of the longitudinal stresses in both the concrete and steel. Using these stresses, the strains are determined in the concrete plug and in the steel pipe pile, which in turn allows the relative radial displacement between both elements to be determined.

Because the distribution of the longitudinal stresses in both the concrete and steel is unknown, but is required to determine the bond strength over the height of the plug. It was decided to solve this distribution using a differential equation, which can be solved using a numerical scheme about the height of the concrete plug.

The model is dependent on many parameters, including most of those identified in the literature as important influencing factors on bond strength. For example, the bond strength in the model depends on the geometry of the connection, the material properties of both the concrete and steel and other factors such as concrete shrinkage, surface irregularities and the Coulomb friction coefficient. Of all the parameters used in this model, the surface irregularities and the Coulomb friction coefficient are the most uncertain factors, which must be determined with care and some conservatism to be included in the model.

5

Adopted shrinkage model

For the model from Chapter 4, which can be used to determine the normal force transfer through friction, the shrinkage of the concrete plug is required as input. To determine this shrinkage, a shrinkage model must be adopted. In this Chapter, two different shrinkage models have been compared. These shrinkage models come from the Eurocode and the Model Code. Both models describe the total shrinkage as the sum of drying shrinkage and autogenous shrinkage. Drying shrinkage is caused by the loss of capillary water in the concrete cross-section and autogenous shrinkage is caused by uniform reduction of internal moisture due to cement hydration. The formula for the total shrinkage of both models is given as follows:

$$\epsilon_{cs}(t, t_s) = \epsilon_{cd}(t, t_s) + \epsilon_{cs}(t) \quad \text{(Eq. 5.1)}$$

where:

$\epsilon_{cd}(t, t_s)$ = drying shrinkage (-)
$\epsilon_{cs}(t)$ = autogenous shrinkage (-)
t = concrete age (days)
t_s = concrete age at the beginning of drying (days)

5.1. Eurocode 2

The NEN-EN 1992-1-1 describes the drying shrinkage component as a function depending on various factors including the fictional thickness of the cross-section and the relative humidity. The drying shrinkage is less significant when the relative humidity and fictitious thickness have high values. The function is as follows:

$$\epsilon_{cd}(t, t_s) = \beta_{ds}(t, t_s) \cdot k_h \cdot \epsilon_{cd,0} \quad \text{(Eq. 5.2)}$$

where:

$$\beta_{ds}(t, t_s) = \frac{t - t_s}{(t - t_s) + 0,04 \cdot \sqrt{h_0^3}} \quad \text{(Eq. 5.3)}$$

h_0 = fictitious thickness of the cross-section (mm)
k_h = coefficient dependent on the fictitious thickness h_0 (-)
$\epsilon_{cd,0}$ = coefficient dependent on relative humidity and concrete compressive strength (-)

The autogenous shrinkage is described in the Eurocode as a function depending on the concrete strength. The autogenous shrinkage is typically more significant when the concrete strength has a higher value. The function in the Eurocode for the autogenous shrinkage is given as follows:

$$\epsilon_{ca}(t) = \beta_{as}(t) \cdot \epsilon_{ca}(\infty) \quad \text{(Eq. 5.4)}$$

where:

$$\beta_{ca}(t) = 1 - \exp(-0,2 \cdot \sqrt{t}) \quad \text{(Eq. 5.5)}$$

and:

$$\epsilon_{ca}(\infty) = 2,5 \cdot (f_{ck} - 10) \cdot 10^{-6} \quad \text{(Eq. 5.6)}$$

f_{ck} = characteristic cylindrical compressive strength of concrete after 28 days (MPa)

5.2. CEB-FIP Model Code 2010

The Model Code describes the drying shrinkage as a function that, just like in the Eurocode, depends on the fictional thickness of the cross-section, the relative humidity and the compressive strength, whereby these values also have the same influence on the drying shrinkage. The difference with the Eurocode model is that the function also depends on the type of cement used in the concrete mixture. Typically, when cement that develops strength quickly is used, the drying shrinkage is higher and when cement that develops strength slowly is used, the drying shrinkage is lower. The total function is given as follows:

$$\epsilon_{cd}(t, t_s) = \epsilon_{cds0}(f_{cm}) \cdot \beta_{RH}(RH) \cdot \beta_{ds}(t - t_s) \quad \text{(Eq. 5.7)}$$

where:

$$\epsilon_{cds0}(f_{cm}) = [(220 + 110 \cdot \alpha_{ds1}) \cdot \exp(-\alpha_{ds2} \cdot f_{cm})] \cdot 10^{-6} \quad \text{(Eq. 5.8)}$$

$\alpha_{ds1}, \alpha_{ds2}$ = coefficients dependent on the type of cement (-)
f_{cm} = mean cylindrical compressive strength of concrete after 28 days (MPa)

and:

$$\beta_{RH}(RH) = -1,55 \cdot [1 - (\frac{RH}{100})^3] \quad \text{(Eq. 5.9)}$$

RH = relative humidity ($\%$)

and:

$$\beta_{ds}(t - t_s) = (\frac{(t - t_s)}{0,035 \cdot h^2 + (t - t_s)})^{0,5} \quad \text{(Eq. 5.10)}$$

h = fictitious thickness of the cross-section (mm)

The autogenous shrinkage is described in the Model Code as a function of both the concrete compressive strength and the cement class used in the concrete mixture. Just like with drying shrinkage, this is a difference with the Eurocode, where the Eurocode model only depends on the concrete compressive strength. According to the Model Code model, autogenous shrinkage is more significant when concrete with high compressive strength is used and cement is used which develops strength slowly. The function therefore becomes:

$$\epsilon_{cs}(t) = \epsilon_{cas0}(f_{cm}) \cdot \beta_{as}(t) \quad \text{(Eq. 5.11)}$$

where:

$$\epsilon_{cas0}(f_{cm}) = -\alpha_{bs} \cdot (\frac{0,1 \cdot f_{cm}}{6 + 0,1 \cdot f_{cm}})^{2,5} \cdot 10^{-6} \quad \text{(Eq. 5.12)}$$

α_{bs} = coefficient dependent on the type of cement (-)

and:

$$\beta_{as}(t) = 1 - \exp(-0,2 \cdot \sqrt{t}) \quad \text{(Eq. 5.13)}$$

5.3. Comparison shrinkage models

The two shrinkage models described should ultimately be compared with each other. The purpose of this comparison is to see which model is most suitable to apply for the shrinkage input of the model from Chapter 4.

5.3.1. Input parameters

To compare the shrinkage models, an example situation is required that serves as input parameters for the two models, so that they can be compared. This example situation is described in this subsection.

5.3.1.1. Element geometry and material properties

For the element geometry and the material properties, the design example from subsection 3.2.5 is again used. The length of the concrete plug, L, in this example was equal to 1800 mm. Furthermore in this design example, C30/37 was used for concrete quality, which has a characteristic cylindrical compressive strength, f_{ck}, of 30 MPa. To arrive at an average cylindrical compressive strength, f_{cm}, the Eurocode provisions were used, which describe that mean compressive strength can be obtained by adding 8 MPa to the characteristic value. This gives a value of 38 MPa for the mean compressive strength. For the cement in the concrete mixture, it has been assumed that a type of cement with a normal strength development period is used. This refers to the parameters of the cement; α_{bs}, α_{ds1} and α_{ds2} are assumed to be 700, 4 and 0.012 respectively.

5.3.1.2. Relative humidity

The relative humidity, RH, is assumed to be 80%. This value is prescribed in the fib Model Code for an outdoor environment. This is also still a conservative assumption according to Chen et al. (2023), who investigated the creep and shrinkage behavior of concrete filled steel tubes (CFST) columns. The researcher of the paper stated, using test results, that the drying shrinkage of CFST columns was significantly lower than the values that could be determined using the shrinkage model of the Model Code. This was explained by the fact that the confinement of the steel tube with CFST columns limits drying shrinkage, unlike with regular reinforced concrete (RC) columns. The researcher stated that drying shrinkage could not be neglected with CFST columns, because this would lead to an underestimate of the shrinkage that occurs. However, in the study by Chen et al. (2023), a very high relative humidity of 93% could be maintained, so that the shrinkage best matched the shrinkage test results.

5.3.1.3. Fictitious thickness

The value of the fictitious thickness of the cross-section, h_0, is assumed to be twice the length of the concrete plug, L. This assumption stems from research by Nezamian et al. (2003). The assumption is based on Figure 5.1, which assumes that the drying shrinkage only comes from the top of the concrete plug. This is realistic for the actual situation, where the concrete plug is surrounded by a steel pipe pile around the perimeter and by moist soil at the bottom of the plug on which it is poured.

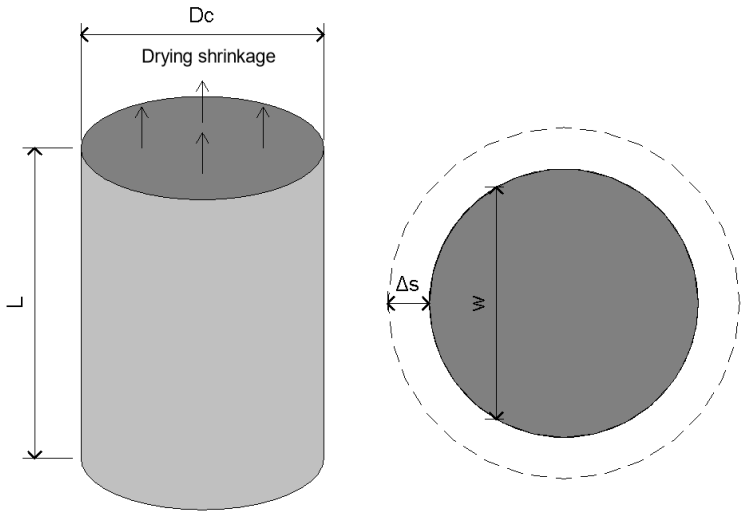

Figure 5.1: Determination fictitious thickness.

The fictitious thickness, h_0, can be determined by using the figure and formula given in the Eurocode and the Model Code:

$$h_0 = \frac{2 \cdot A_c}{u} \qquad \text{(Eq. 5.14)}$$

where:

A_c = cross-sectional area of concrete (mm^2)
u = perimeter of the portion of the cross-section exposed to dehydration (mm)

The cross-section area of the concrete, A_c, can be determined by multiplying the length of the plug, L, by the average width, w, of the round-shaped plug. This is shown in the following formulation:

$$A_c = L \cdot w = L \cdot \frac{\sqrt{\pi} \cdot D_c}{2} \qquad \text{(Eq. 5.15)}$$

where:

L = length of the concrete plug (mm)
w = mean width of the concrete plug (mm) = $\frac{\sqrt{\pi} \cdot D_c}{2}$

The perimeter of the portion of the cross-section exposed to dehydration, u, is, as indicated in the figure, equal to the average width, w, of the top of the concrete plug as shown in the formulation below:

$$u = w = \frac{\sqrt{\pi} \cdot D_c}{2} \qquad \text{(Eq. 5.16)}$$

Substituting equation(5.15) and equation(5.16) into equation(5.14) the final formulation for the fictitious thickness, h_0, can be found, as shown below:

$$h_0 = \frac{2 \cdot A_c}{u} = 2 \cdot L \cdot \frac{\frac{\sqrt{\pi} \cdot D_c}{2}}{\frac{\sqrt{\pi} \cdot D_c}{2}} = 2 \cdot L \qquad \text{(Eq. 5.17)}$$

5.3.2. Comparison with shrinkage diagram

To compare the two different models, the shrinkage was determined with both models for over a period of 100 years. This period of 100 years is equal to the design life time for which many civil structures must be designed. Figure 5.2 shows the result for determining this shrinkage, with the given input parameters. It can be analysed form the figure that over a period of 100 years there is a substantial difference in the final shrinkage of both models.

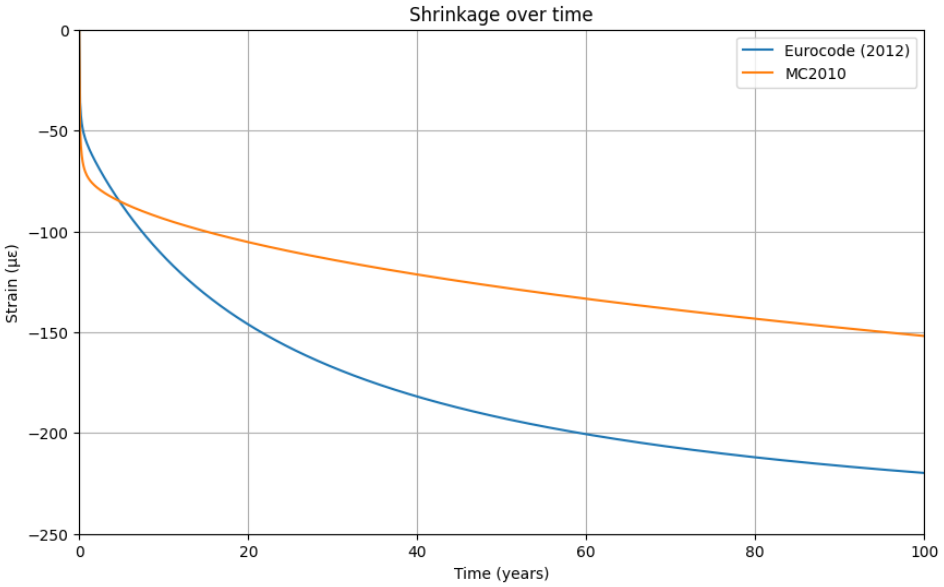

Figure 5.2: Comparison shrinkage models.

The first thing that can be deduced from the figure is that the final shrinkage in the Eurocode shrinkage model is determined much more conservatively than with the model from the Model Code. This is mainly because, as can be deduced from the figure, the drying shrinkage in the Eurocode model is estimated to be larger than with the Model Code model. This drying shrinkage is the shrinkage that continues to develop in the later phase of the figure, in contrast to the autogenous shrinkage which mainly develops at the beginning of the period. This autogenous is equal to the offset that arises over the first period of shrinkage in both cases. It can then be analysed that this autogenous shrinkage, in contrast to the drying shrinkage, is estimated to be larger by the Model Code model than in the Eurocode model.

According to Eurocode 4 (NEN-EN 1994-1-1+C1:2011), experience shows that the values for shrinkage deformations according to NEN-EN 1992-1-1 can overestimate the effects of shrinkage in steel-concrete structures. As a result, the maximum shrinkage strain in the final state for steel-concrete structures may be assumed as in Appendix C of Eurocode 4. This appendix prescribes that in other environments a final shrinkage strain of 200 $\mu\epsilon$ can be maintained for normal concrete. This fact in combination with the fact that with the Eurocode model the drying shrinkage is estimated to be relatively significant, while according to test results by Chen et al. (2023) it is relatively small with CFST columns. Ensures that the Eurocode model is considered less realistic compared to the Model Code model for the application of shrinkage in steel-concrete structures.

5.4. Conclusion shrinkage model

The conclusion is that for the shrinkage model that will be applied in the model of Chapter 4, the Model Code model is considered more realistic. This is firstly because this model estimates the drying shrinkage to be less significant compared to the Eurocode model, which is realistic for concrete filled steel tubes (CFST) columns according to Chen et al. (2023). The second point is that Eurocode 4 (NEN-EN 1994-1-1+C1:2011) states that the shrinkage model of Eurocode 2 (NEN-EN 1992-1-1) can overestimate the shrinkage for steel-concrete structures.

As a result, it was decided to ultimately apply the Model Code model to determine shrinkage. This is also still a conservative model for determining the shrinkage for CFST columns, according to Chen et al. (2023) when a relative humidity of 80% is used. Research by Chen et al. (2023) showed that the test results were best simulated at a relative humidity of 93%, which leads to lower shrink values for the drying shrinkage.

6

Validation proposed model normal force transfer through friction

In this chapter the proposed model for determining the transferable normal force due to friction is validated. This was initially done by analysing the output of the model. This included an analysis of the effect of varying the various parameters on the output of the model. It was specifically analysed whether the various parameters have the same influence on the bond strength as the influence identified in the literature study. An attempt was then made to validate the model using test results. The results of push-out tests were again used for this.

6.1. Input model parameters

To compare the different input parameters of the model, a standard situation must be set up as a basis from which the different parameters can be varied. All input parameters in this chapter are the same as those given in this section, unless stated otherwise.

6.1.1. Element geometry

First, the geometry of the elements that make up the connection must be determined. The input parameters required for the geometry of the model input are shown in Figure 6.1.

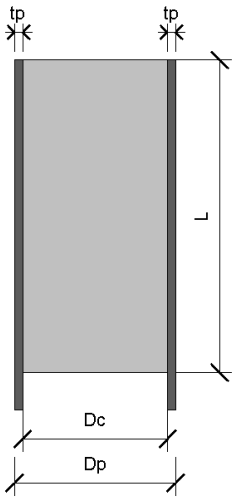

Figure 6.1: Element geometry.

The input values for the parameters shown in Figure 6.1 above are shown in Table 6.1.

Table 6.1: Element geometry

Element geometry		
Outer diameter steel pipe pile	D_p	= 600 mm
Wall thickness steel pipe pile	t_p	= 10 mm
Outer diameter concrete plug	$D_c = D_p - 2 \cdot t_p$	= 580 mm
Length of the concrete plug	L	= 6000 mm

6.1.2. Material properties

The material properties of both the concrete and the steel also influence the input of the model. These properties are given in this subsection.

6.1.2.1. Concrete properties

The properties of the concrete are given in this section. Strength class C30/37 has been used for the base input of the model. The characteristic compressive strength, f_{ck}, is known for this strength class. Using this compressive strength, the other material properties of the concrete can then be estimated using the formulas from NEN EN 1992-1-1.

Table 6.2: Concrete material properties (NEN EN 1992-1-1)

Concrete property		
Characteristic cylinder compressive strength	f_{ck}	= 30 MPa
Mean compressive strength	$f_{cm} = f_{ck} + \Delta f$, $\Delta f = 8$	= 38 MPa
Design compressive strength	$f_{cd} = f_{ck}/\gamma_c$, $\gamma_c = 1.5$	= 20 MPa
Young's modulus after 28 days	$E_{cm} = 22000 \cdot (0.1 \cdot f_{cm})^{0.3}$	≈ 30589 MPa
(Initial) Poisson ratio	ν_c	= 0.20

6.1.2.2. Steel properties

The steel parameters used in the model are shown in Table 6.3.

Table 6.3: Steel material properties

Steel property		
Young's modulus	E_s	= 210 GPa
Poisson ratio	ν_s	= 0.30

6.1.3. Shrinkage

The shrinkage of the concrete is determined according to the model of the Model Code 2010, which is described in Chapter 5 Here the properties of the concrete are entered as determined in paragraph 6.2.1.1. Furthermore, a value of 80$\%$ has been used for the relative humidity, RH, based on the substantiation given in Chapter 5 For the cement in the concrete mixture, it has been assumed that a type of cement with a normal strength development period is used. This refers to the parameters of the cement; α_{bs}, α_{ds1} and α_{ds2} to be 700, 4 and 0.012 respectively. The shrinkage is calculated for after a period of 100 years, which is equal to a typical design life time of a bridge.

6.1.4. Surface irregularities

The height of the surface irregularities, Δ_r, is an important parameter for the model. Det Norske Veritas (DNV) prescribes a standard of 0.07 mm for rolled steel surfaces for this height for grouted connections. However, in this design standard the height of the irregularities is not used directly to determine the normal force resistance due to friction, but for the frictional resistance to bending moments. The Eurocode 1 (NEN-EN 1991-1-4) prescribes a value of 0.05 mm for the height of the surface irregularities of bare steel. This value is more conservative to use compared to the DNV, because it will result in lower friction resistance. However, the value is still uncertain to use, because in the Eurocode article it is used to determine the wind load. In this article, a higher value for the surface irregularities is actually more conservative, while in the case of the model for the normal force resistance, a lower value is more conservative.

Many steel producers, who produce steel pipe piles, vary their values for irregularities between 0.0045 mm and 0.09 mm. When the model is used in practice, it will therefore be necessary to determine exactly for the pipe pile that is used and what the manufacturer recommends for the level of these irregularities, because this can vary widely between certain producers. For the comparison of the influence factors of the model, a value of 0.05 mm will be used as prescribed by the Eurocode. This can be seen as a conservative value across the broad spectrum of different sources.

6.1.5. Coulomb friction coefficient

The coulomb friction coefficient, μ, is an important parameter in the model, which determines what share of the contact stress between the concrete and steel can be converted into bond strength. The parameter depends on many different factors, including surface roughness, material properties and environmental conditions. In practice, Coulomb friction coefficient values of between 0.3 and 0.6 are often used for concrete-steel interfaces.

The Eurocode 4 prescribes a Coulomb friction coefficient of 0.5 for concrete-steel interfaces, which involve unpainted steel. This value must be further validated for this type of connection in practical applications of the model, but will be used in this model for the comparison of the different parameters.

6.2. Influence of model parameters on the normal force capacity

In this section it will be analysed how the different input parameters influence the output of the model. This will be done by varying the various input parameters, keeping the other parameters constant when possible. It will be examined whether the influences of the parameters are comparable to those found in the literature.

6.2.1. Stiffness factors

First, the influence of the various stiffness factors on the transferable normal force from the model will be analysed. The mutual influence between the two stiffness factors will be examined, respectively the radial stiffness of the pipe pile and the radial stiffness of the surrounding soil. The hypothesis is that the stiffness of the soil, in relation to the stiffness of the pipe pile, has almost no influence on the contact stress between the concrete plug and the steel pipe pile. This hypothesis arises from the expectation that the steel pipe pile offers a much greater stiffness factor than the surrounding soil. As a result, the influence of the ground could be neglected, which ensures that the model can be simplified to a shorter expression.

To check this hypothesis, a ratio will be calculated for the given parameters between the stiffness of the pipe pile and the stiffness of the surrounding soil. This can be used to determine whether the difference in stiffness is so great that the influence of the ground could be neglected. First, the stiffness factor of the pipe pile, K_i, will be determined using the formula below.

$$K_i = \frac{4 \cdot E_s \cdot t_p}{D_p^2} \qquad \text{(Eq. 6.1)}$$

Entering the parameters in this formula then leads to the following stiffness of the pipe pile:

$$K_i = \frac{4 \cdot 210 \cdot 10^3 \cdot 10}{600^2} = \frac{70}{3} \approx 23.33 N/mm^3 \quad \text{(Eq. 6.2)}$$

The radial stiffness of the surrounding soil, K_s, also known as the horizontal bedding stiffness, using Ménard's method, which was previously described in Chapter 4 The formula of this method is shown below.

$$\frac{1}{K_s} = \frac{1}{3 \cdot E_p} \cdot [1.3 \cdot R_0 \cdot (2.65 \cdot \frac{R}{R_0})^{\alpha} + \alpha \cdot R] \quad \text{(Eq. 6.3)}$$

To check whether the influence of each type of soil layer can be neglected in the model, it was decided to determine the bedding stiffness using the parameters for a fictitious surrounding sand layer. Compared to other common types of soil layers where a pile foundation is used, such as clay and peat, sand is a stiffer soil layer where a higher bedding stiffness is expected. If the stiffness can be neglected for sand, this can also be done for clay and peat. This bedding stiffness is determined below for a fictitious sand layer.

$$\frac{1}{K_s} = \frac{1}{3 \cdot 0.7 \cdot 5} \cdot [1.3 \cdot 300 \cdot (2.65 \cdot \frac{300}{300})^{\frac{1}{3}} + \frac{1}{3} \cdot 300] \approx 60.92 \rightarrow K_s \approx 1.64 \cdot 10^{-2} N/mm^3 \quad \text{(Eq. 6.4)}$$

Now that both stiffness factors are known, the radio can be determined between these two stiffness factors. This is done below.

$$\frac{K_i}{K_s} = \frac{23.33}{1.64 \cdot 10^{-2}} \approx 1421.49 \quad \text{(Eq. 6.5)}$$

From the above ratio it can be concluded that the hypothesis was correct, with the surrounding soil layer having virtually no confinement effect on the interface between the steel and concrete. For the sake of simplicity, it was therefore decided to neglect the influence of the surrounding soil layer in the following comparisons.

6.2.2. Diameter of the pile

The literature study showed that the diameter of the pipe pile is an important influencing factor on force transfer through friction. For example, several recommendations described that as the diameter increases, the transferable force due to friction decreases. The proposed model also shows this relationship in Figure 6.2. In the figure, the influence of the diameter on the average bond strength is analysed for a non-embedded and an embedded pile. The difference between a non-embedded pile and an embedded pile is described in section 2.3. The influence of shrinkage has also been analysed for both types of piles in the figure by examining both the relationship with and without shrinkage.

For a realistic comparison in practice of the influence of the diameter on the bond strength, the other parameters have been taken into account, which also change as the diameter increases. In practice, the thickness of the pile, t_p, increases as the diameter of the pipe pile, D_p, increases. For this purpose, a constant ratio of $D_p/t_p = 50$ has been maintained between these two parameters. Also, in practice, the length of the interface, L, increases as the diameter of the pile increases. Therefore, a constant ratio of $L/D_p = 10$ was also maintained for these parameters in the analysis.

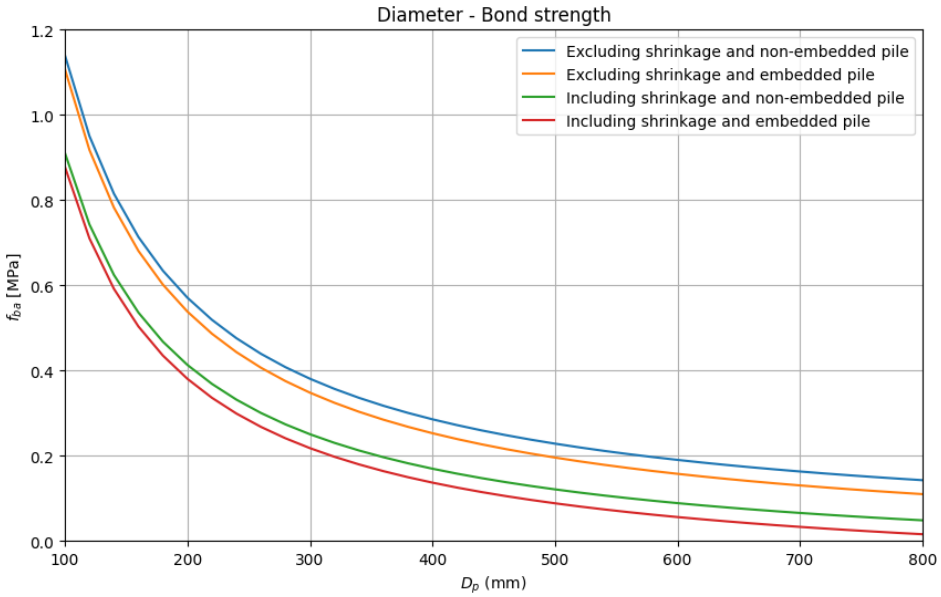

Figure 6.2: Bond strength versus different diameters of the steel pile.

The figure shows that as the diameter of the pipe pile increases, the average bond strength decreases. This relationship can be explained by several factors that influence the proposed model. For example, one of the most important factors is the stiffness of the interface, K_i, which determines the level of confinement by means of the radial stiffness of the pipe pile, decreasing quadratically as the diameter of the pipe pile increases. This will cause the contact stress to decrease, causing the average bond strength to also decrease. Secondly, the difference between the model in which shrinkage is taken into account and the model in which shrinkage is not taken into account can be explained by the fact that with larger diameters the concrete shrinkage will increase linearly, and therefore the contact stress will again decrease and therefore also the transferable bond strength. Another factor that influences the decrease in the average bond strength is that as the diameter increases, the difference in longitudinal stress between the steel pipe pile and the concrete plug will increase more. This will cause the steel pipe pile to move more horizontally relative to the concrete plug, which will reduce contact and therefore the bond strength. This relationship can be demonstrated analytically by equating the expressions for the increase in longitudinal stresses as follows.

$$\Delta\sigma_{c,z,i} \leq \Delta\sigma_{s,z,i} \rightarrow \Delta z \cdot \frac{4 \cdot f_{ba,i}}{D_c} \leq \Delta z \cdot \frac{f_{ba,i} \cdot D_c}{D_p \cdot t_p} \rightarrow \frac{4}{D_c} \leq \frac{D_c}{D_p \cdot t_p} \qquad \text{(Eq. 6.6)}$$

If the above ratio between the diameter of the concrete plug, D_c, and the diameter and thickness of the pipe pile is guaranteed, the stress in the steel will increase relatively more, causing the difference in longitudinal stress to increase. This ratio can also be converted into a minimum ratio, D_p/t_p, where this can also be guaranteed. This is shown below.

$$\frac{4}{D_p - 2 \cdot t_p} \leq \frac{D_p - 2 \cdot t_p}{D_p \cdot t_p} \rightarrow \frac{D_p}{t_p} \geq 2 \cdot (2 + \sqrt{3}) \approx 7.46 \qquad \text{(Eq. 6.7)}$$

In practice, this minimum ratio found between the diameter and thickness of the pipe pile is almost always exceeded. This factor can therefore also be taken into account in the reasoning for the decrease in the bond strength with larger diameters. However, if this ratio is not exceeded, the effect will be opposite.

A factor that should also be considered is that even though the average bond strength decreases with increasing diameter, the total normal force capacity can still increase as the diameter increases. This is shown in Figure 6.3. This figure shows the total normal force resistance, N_{Rd}, of the connection of the concrete cap and steel pipe pile. This total resistance is made up of the normal force that can be transferred by friction, $N_{Rd,c}$, and the normal force that can be introduced directly into the pile from the top, $N_{Rd,s}$. This last component only influences the total resistance when the pile is embedded in the concrete cap. If the total normal force capacity continues to increase with larger diameters, this can be explained by the fact that the contact surface between the steel and concrete in these cases continues to increase faster than the bond strength decreases. The figure also shows that from a certain point this is no longer the case and that the bond strength therefore decreases faster than the contact surface increases.

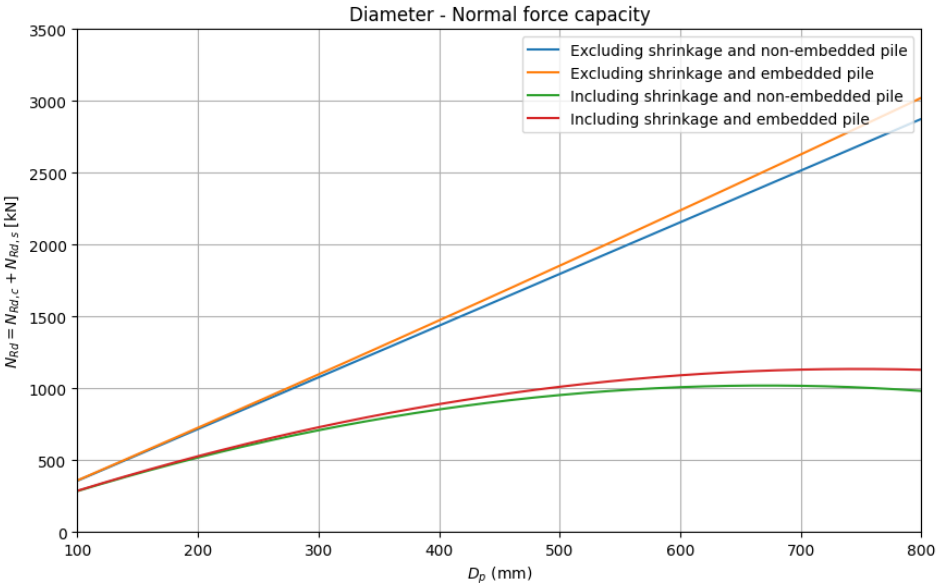

Figure 6.3: Normal force capacity versus different diameters of the steel pile.

6.2.3. Thickness of the pile

According to the literature, the thickness of the pipe pile is also an important influencing factor on the bond strength, which can be transferred through friction. This was explained by the fact that a greater thickness of the pipe pile leads to a higher level of confinement of the pipe pile. A higher level of confinement results in a higher stress capacity. This relationship also results from the proposed model, as can be analysed from Figure 6.4.

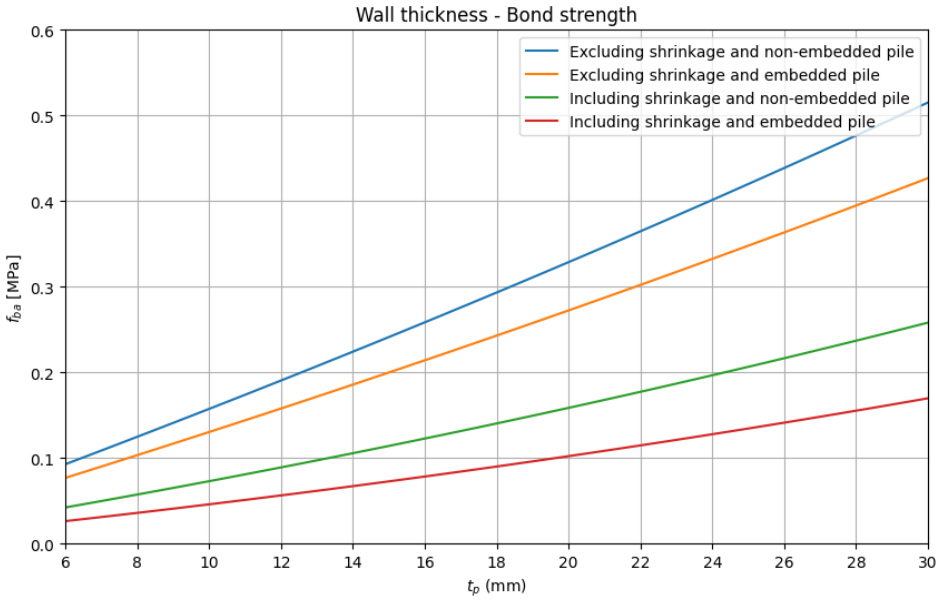

Figure 6.4: Bond strength versus different wall thicknesses of the steel pile.

The figure therefore shows that when a greater wall thickness of the pipe pile is applied, the bond strength also increases. This can be explained by several factors to which the thickness of the pipe pile contributes. The first factor is the level of confinement, as described earlier. This level of confinement, which is expressed in the model with the stiffness of the interface, K_i, increases linearly as the thickness of the pipe pile increases. As a result, the contact pressure increases, which also increases the total bond strength. The second factor is that as a greater thickness is applied, the longitudinal stress in the steel pipe pile increases relatively less compared to the longitudinal stress in the concrete, so that the steel pipe pile will expand less horizontally. This will create more contact pressure between the pipe pile and the plug and therefore more bond strength.

A greater wall thickness of the pipe pile will also ensure that the total surface area of the steel pipe will increase. As a result more load can be directly introduced into the steel piep pile in case of an embedded pile. This will increase the total normal force capacity compared to a non-embedded pile as shown in Figure 6.5.

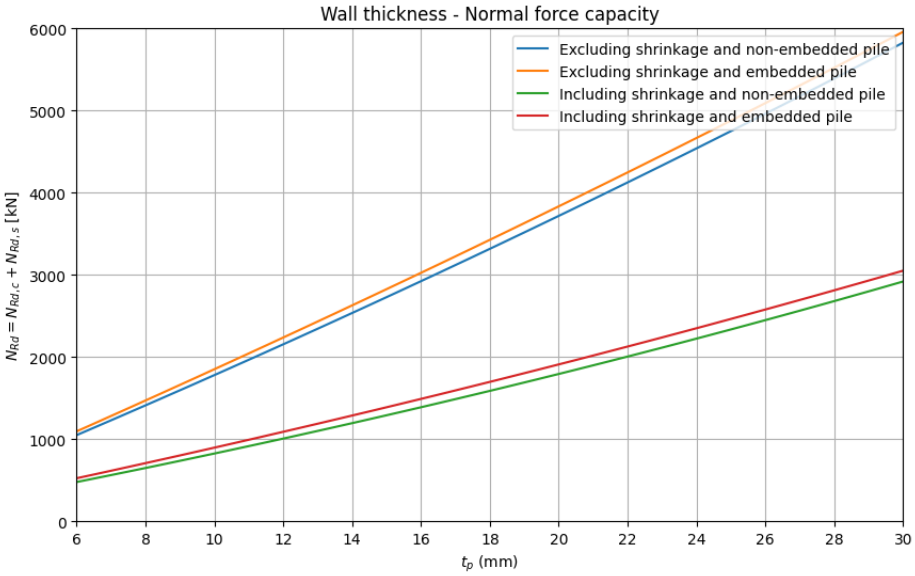

Figure 6.5: Normal force capacity versus different wall thicknesses of the steel pile.

6.2.4. Length of the concrete plug

No clear answer can be found in the literature regarding the influence of the length of the concrete plug on the bond strength. For example, Nezamian et al. (2002) describe that the bond strength decreases with increasing plug length, while Virdi and Dowling et al. (1980) conclude that the length of the plug has no significant influence on this capacity. In Figure 6.6, the influence on the bond strength has been examined for different plug lengths using the proposed model. These results of the proposed model show that as the plug length increases, the average bond strength decreases. This is in accordance with the conclusion of Nezamian et al.'s (2002) study.

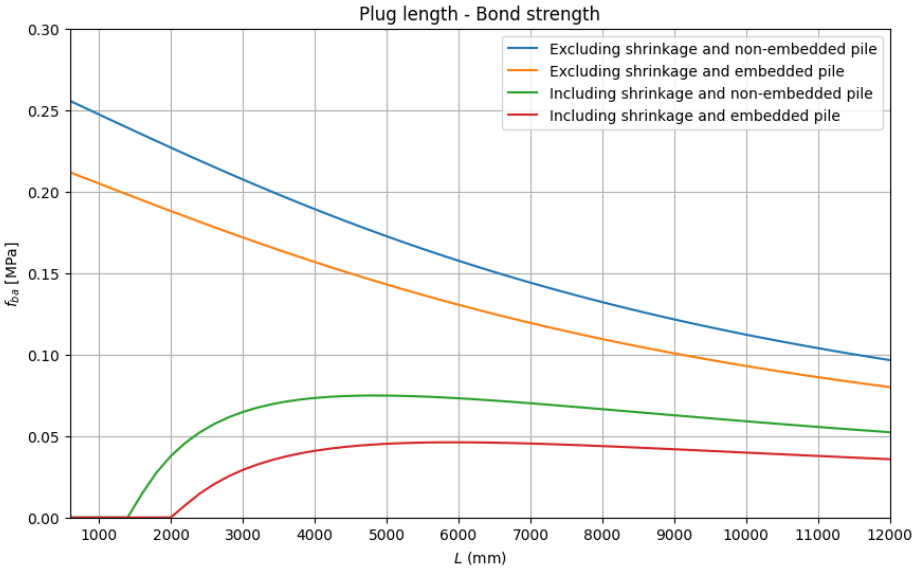

Figure 6.6: Bond strength versus different plug lengths.

That the average bond strength decreases in the model as the length of the plug is increased can be explained by the bond stress distribution over the length of the interface. At the top of the plug (connection plug to pile cap) there is still a relatively large amount of longitudinal stress present in the concrete, and relatively little in the steel, causing a locally high contact pressure in combination with the Poissons effect. As a result, a relatively large amount of normal force is transferred directly from the concrete to the steel. Below this point, the longitudinal stress will immediately be present increased in the steel compared to the concrete where this longitudinal stress will be decreased. This effect results in less contact pressure at this point and therefore less contact stress and therefore less normal force transfer. As the plug is made longer, this effect will become increasingly stronger, to the point that virtually no load is transferred anymore, resulting in an average low normal force transfer capacity. Figure 6.7 shows for the example situation how the normal force transfer stress develops over the length of the interface.

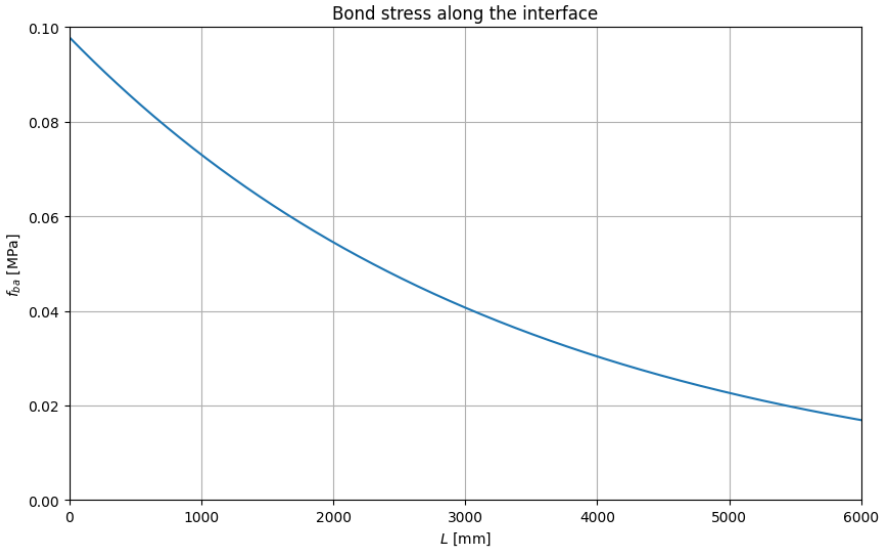

Figure 6.7: Bond stress along the interface.

The distribution of the longitudinal stresses of the concrete and steel over the length of the interface is shown in Figure 6.8.

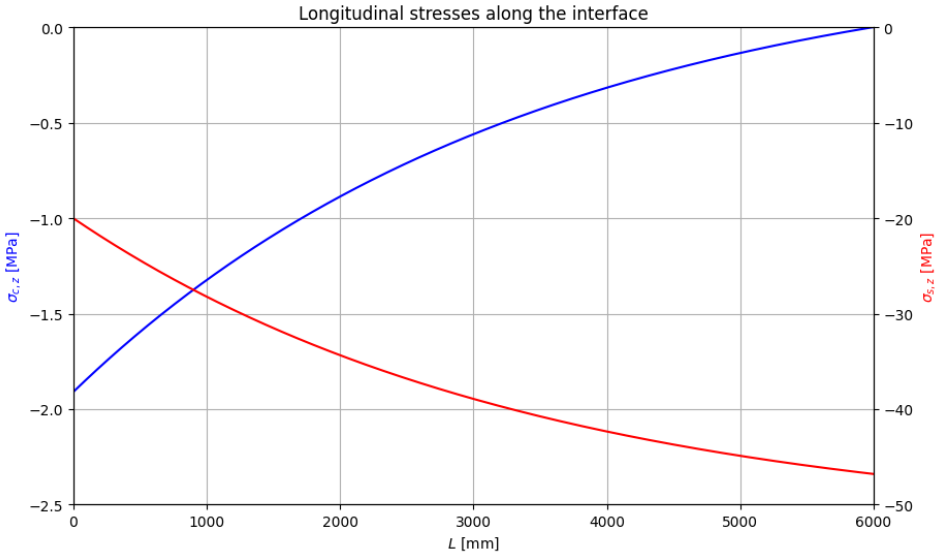

Figure 6.8: Longitudinal stresses along the interface.

Although the mean bond strength decreases as the plug length increases, the total normal force capacity does increase as the plug length increases as shown in the Figure 6.9. This can be simply explained by the fact that the contact surface continues to increase as the prop length increases, allowing more force to be transferred. However, it can be analysed that this capacity barely increases from a certain length, so that in practice from a certain point it is hardly advantageous to use a plug with a greater length.

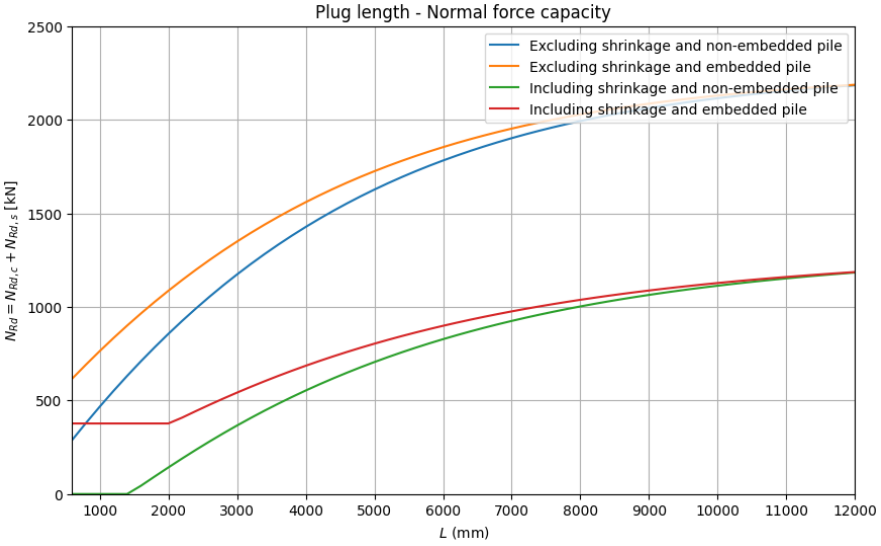

Figure 6.9: Normal force capacity versus different plug lengths.

6.2.5. Concrete compressive strength

The literature showed that, according to Virdi and Dowling et al. (1980), this factor has no significant influence on the bond strength. On the other hand, research by Aly et al. (2009) showed that the bond strength decreased as a higher compressive strength was applied. The influence of the concrete compressive strength on the bond strength has also been analysed using the proposed model. The results of this are shown in Figure 6.10.

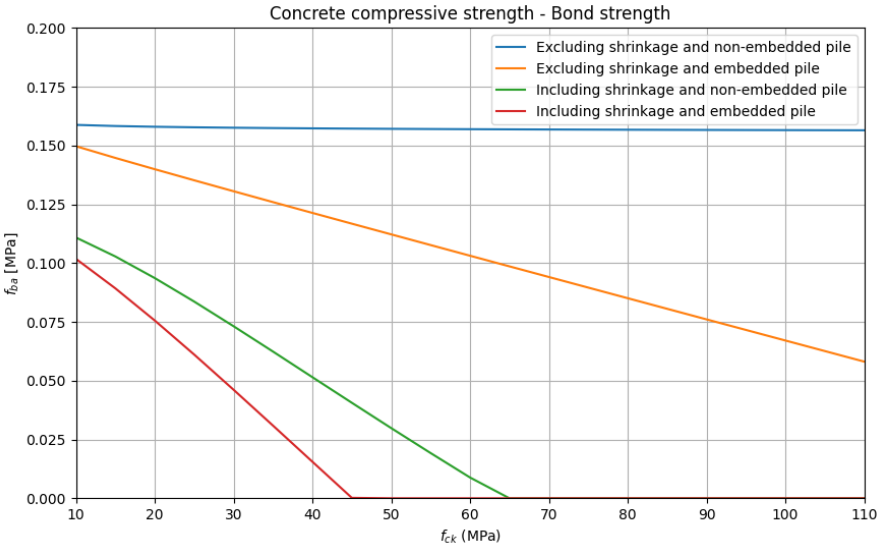

Figure 6.10: Bond strength versus different concrete compressive strengths.

The results of the proposed model show that as the concrete strength increases, in all cases except the non-embedded pile without shrinkage, the concrete stress capacity decreases. The first reason why this capacity decreases, according to the model, is because as the concrete strength increases, more concrete shrinkage occurs and therefore there is less contact between the steel and concrete, resulting in less friction. The second reason, in the case of an embedded pile, is that when a higher concrete strength is applied, more force can be directly introduced into the steel pipe pile. This ensures that the difference in longitudinal stress between the steel and concrete at the top of the plug is greater, resulting in less contact and therefore less friction.

The results of the model are in accordance with the results of Aly et al. (2009), but not in accordance with the conclusion of Virdi and Dowling et al. (1980). A possible explanation for this could be that in the study by Aly et al. (2009) the tests were carried out at a later stage after pouring the concrete than in the study by Virdi and Dowling et al. (1980). Virdi and Dowling tested all their samples after 28 days, compared to an average of 58 days in Aly's study. This could mean that the effect of shrinkage was better reflected in Aly's study, because more concrete shrinkage can occur over a longer period of time.

Figure 6.11 shows what influence the concrete compressive strength has on the total normal force capacity of the connection. It can be analyzed that when the pile is not embedded in the pile cap, the influence of the compression strength depends on including the concrete shrinkage in the model. When shrinkage is included in this case, the total capacity decreases, because shrinkage according to the Model Code increases with higher concrete strength. If shrinkage is neglected, the concrete strength will have no influence on the normal force capacity of a non-embedded pile. When considering an embedded pile, it can be concluded that if shrinkage is not taken into account, the total capacity of the connection increases, because more load can be transferred directly into the top of the pipe pile. If shrinkage is taken into account for an embedded pile, it can be analyzed that this ensures that from the point at which the plug no longer experiences capacity due to friction, the total capacity also starts to increase again.

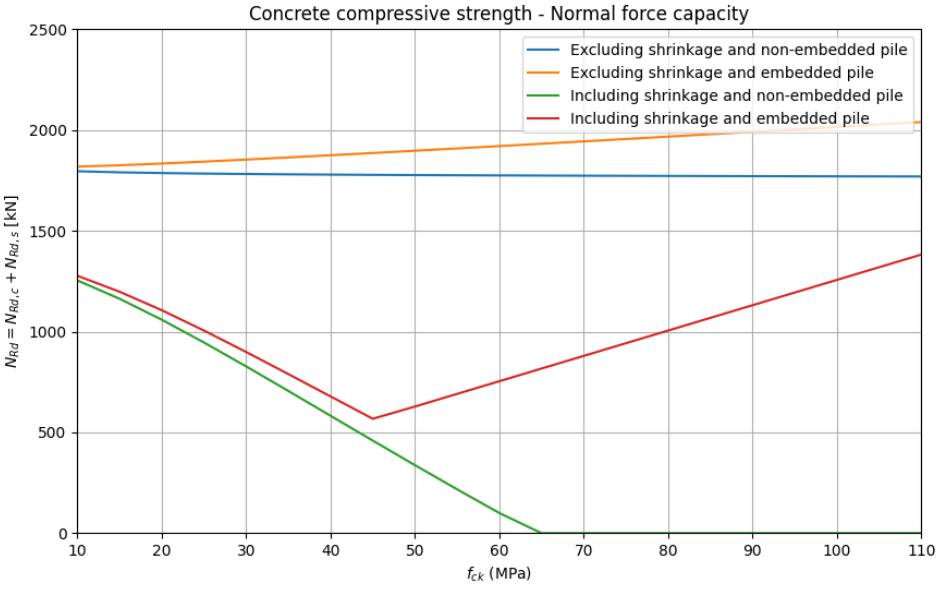

Figure 6.11: Normal force capacity versus different concrete compressive strengths.

6.2.6. Surface irregularities

Another important influencing factor is the surface roughness according to a study by Virdi and Dowling et al. (1975). This factor is expressed in the model as the surface irregularities. Figure 6.12 shows the influence of the for the surface irregularities value on the bond strength.

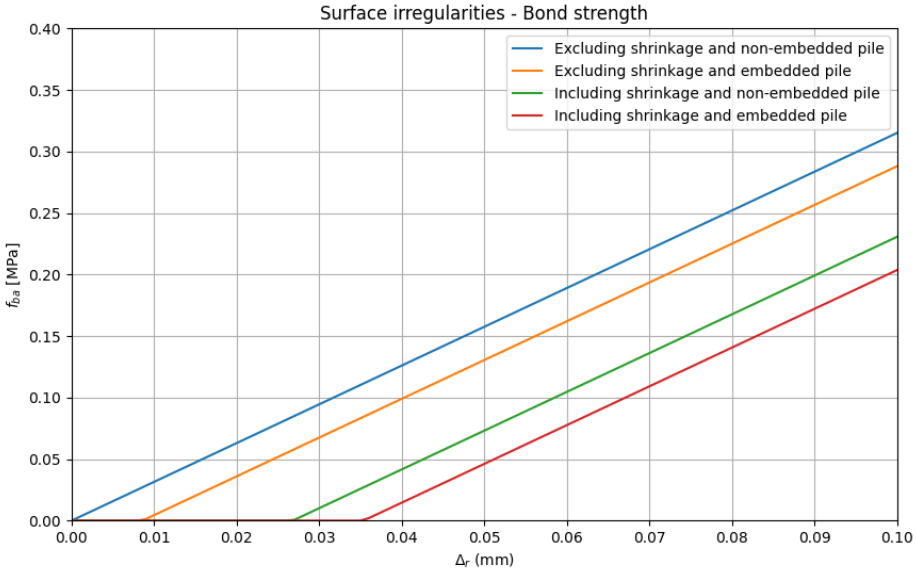

Figure 6.12: Bond strength versus different surface irregularities of the steel pipe pile.

As would logically be expected, the bond strength increases as the value for the surface irregularities increases as input to the model. It can clearly be concluded that the relationship between this factor and the bond strength is linear. As mentioned earlier, the value of these irregularities can be very uncertain and should therefore be assumed conservatively if no reliable value has been determined for this. Especially because this parameter has so much influence on the output of the model. How this bond strength increases linearly with the value for the surface irregularities can also be seen in Figure 6.13, which shows that the bond stress across the interface increases equally between the different values for the surface irregularities.

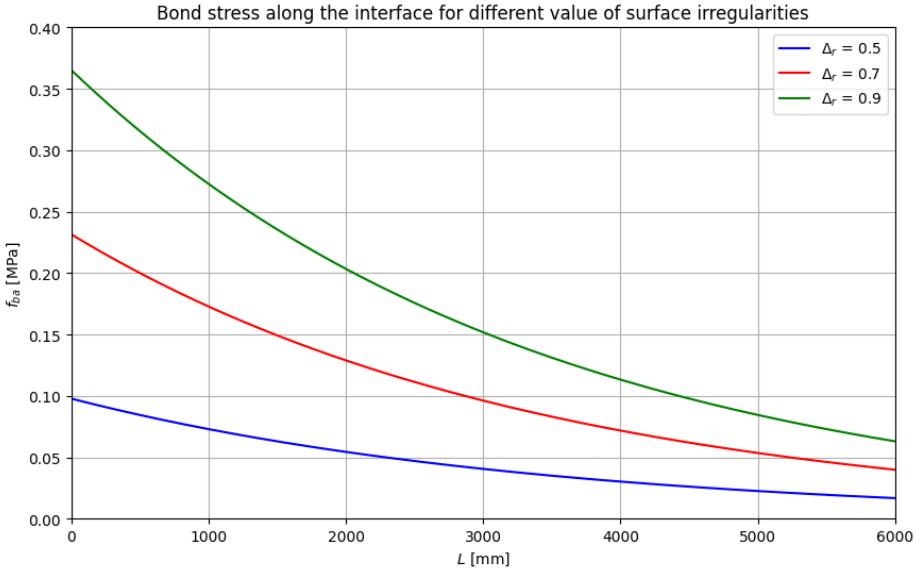

Figure 6.13: Bond stress along the interface for different value of surface irregularities.

6.2.7. Coulomb friction coefficient

The Coulomb friction coefficient is also an important input parameter in the model, which determines how much contact stress is converted into bond strength. The influence of this parameter on the average bond strength is shown in Figure 6.14.

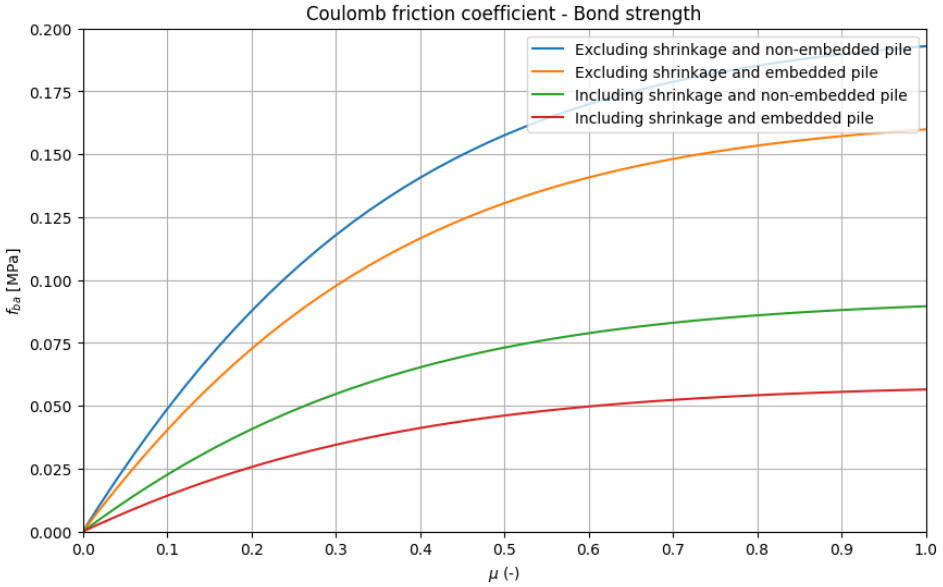

Figure 6.14: Bond strength versus different Coulomb friction coefficients.

It can be clearly concluded, as expected, that as the Coulomb friction coefficient increases, the average bond strength also increases. It can also be concluded that this capacity almost no longer increases from a certain value for the coefficient. This can be explained by the fact that in the model, with a higher value for the coefficient, the transfer of the normal force localizes even more at the top of the plug, so that the average value no longer increases so much. This phenomenon is shown in Figure 6.15.

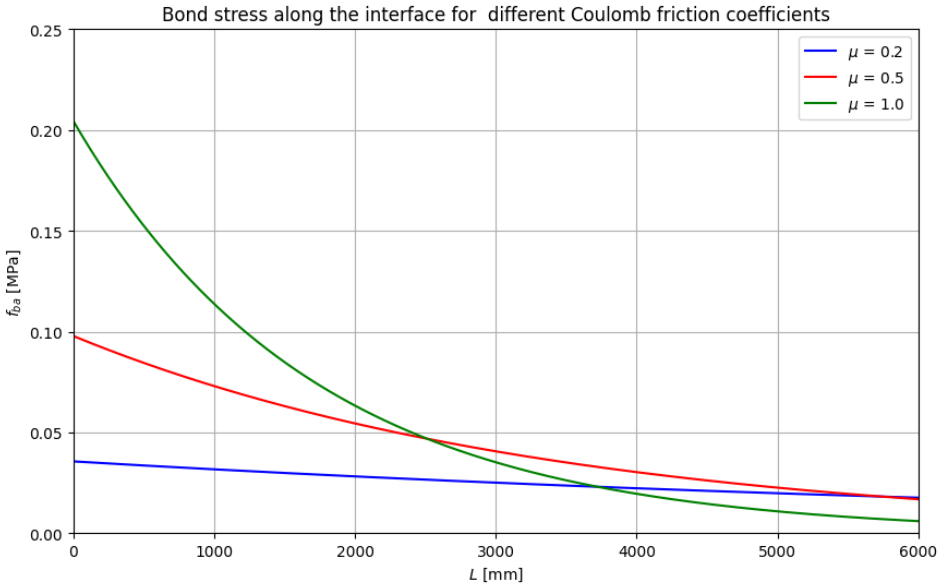

Figure 6.15: Bond strength along the interface for different Coulomb friction coefficients.

6.3. Comparison model with test results

The model can also be verified using test results from Appendix A. These test results are the same test results as those shown in the literature review. The test results were obtained using push-out tests with a non-embedded pile, i.e. without loading the steel pipe pile. Initially, the results of the model were compared with the test results using only the initial parameters for the surface irregularities and the Coulomb friction coefficient. After these were compared, an attempt was made to update the parameters so that they better fit the test results, so that the model could give a better estimate of the bond strength. After the parameters have been updated, a safety factor has also been drawn up with which the results of the model can be translated into a safe design value for the bond strength that can be applied in design.

6.3.1. Comparison with initial model parameters

In figure 6.16 the initial comparison between the results of the model for the bond strength, f_{ba}, is plotted against the experimental results for the bond strength, $\overline{f}_{ba}$. The figure shows that the model, which uses the initial parameters for the surface irregularities and the Coulomb friction coefficient, both overestimates and underestimates the experimental values. This can be seen by the dots above the dotted line and by the dots below the dotted line respectively.

The large scatter of the points, mainly in the results of Virdi and Dowling et al. (1980) and Nezamian et al. (2002), is due to the fact that there was already a large scatter present in these test sets themselves. In these test sets there was large scatter in identical or nearly identical test specimens.

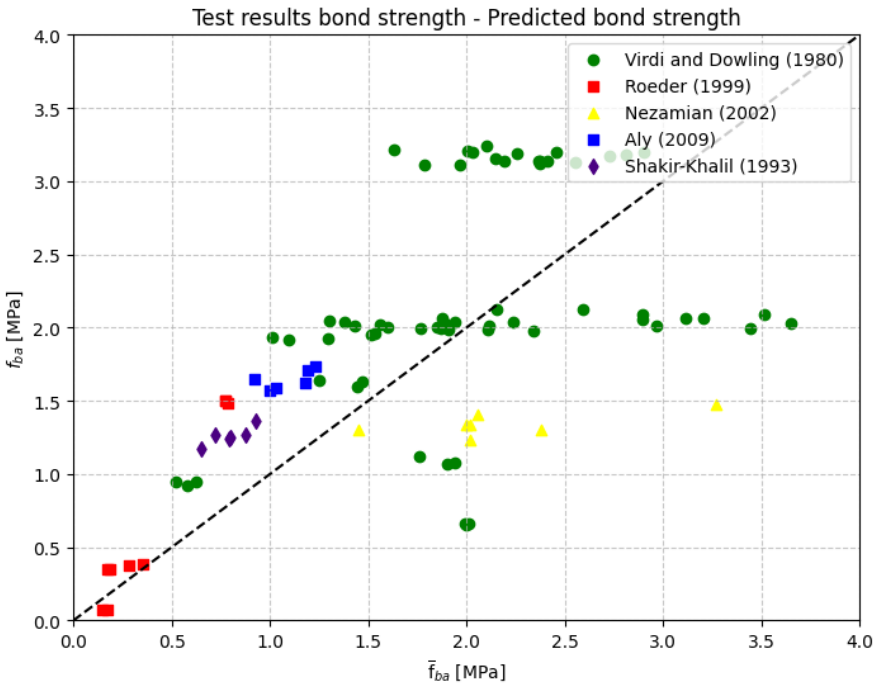

Figure 6.16: Test results bond strength versus predicted bond strength

6.3.2. Updating model parameters

A method to ensure that the results of the model correspond better with the experimental results is by updating the initially assumed parameters from the model. The parameters that were the most uncertain and therefore assumed, and also have a major influence on the results of the model, consist of the surface irregularities and the Coulomb friction coefficient. For this purpose it was decided to update these parameters.

6.3.2.1. Updating methodology

This section describes the procedure for updating the model parameters. The first step in updating the model is to deal with the scatter that was more significant in certain test sets than in other test sets. It is desirable to update the model based on more accurate test results so that the updated model is more reliable. At the same time, this will also lead to a more conservative model as the test sets with little scatter are currently overestimated by the model. By updating the model, these values will be less overestimated by the model, resulting in the model being more conservative.

To deal with the uneven scatter of the different test sets, it was decided to apply the inverse variance weighting method. In this method, the variance, σ_i^2, is determined for each set of test results. The magnitude of the variance value indicates the extent to which the test results are spread. Because test sets with a high variation should be less included in the update of the parameters, the weighting of these test sets should be lower than for test sets with little variation. As a result, the inverse of the variance must be determined for the weighting as shown in the formula below.

$$w_i = \frac{1}{\sigma_i^2} \tag{Eq. 6.8}$$

where:

$$\sigma_i^2 = \frac{1}{m_i - 1} \cdot \sum_{j=1}^{m_i} (f_{ba}^{(i,j)} - \overline{f}_{ba}^{(i)})^2 \tag{Eq. 6.9}$$

m_i = number of test results inside of test set i (-)
$f_{ba}^{(i,j)}$ = observed bond strength corresponding to test result i, j (MPa)
$\overline{f}_{ba}^{(i)}$ = mean observed bond strength corresponding to test set i (MPa)

To better represent the weightings in relation to each other, it was decided to normalize the weightings as well. This can be done by dividing each weighting separately by the total sum of the weightings, as shown below. The total sum of the normalized weightings always equals 1.

$$w_i^* = \frac{w_i}{\sum_{i=1}^{N} w_i} \tag{Eq. 6.10}$$

To update the parameters, a cost function, J, had to be defined. A function that uses absolute difference was chosen. This method is an alternative to the least squared method and in this case it is particularly useful to deal with the outliers, because this method is less sensitive to these outliers. As shown in the formula for J, for each individual test set the absolute differences for the test results and the model results are summed and multiplied by the weighting of the test set. These are then added together again and lead to a total value for the cost function for a certain composition of the input parameters. The goal of optimization is to minimize this cost function and thus arrive at the updated parameters for the model.

$$J(\Delta_r, \mu) = \sum_{i=1}^{n} w_i^* \sum_{j=1}^{m_i} \left| f_{ba}(\Delta_r, \mu, x^{(i,j)}) - \overline{f}_{ba}^{(i,j)} \right| \tag{Eq. 6.11}$$

where:

n = number of test sets (-)
m_i = number of test results inside of test set i (-)
w_i^* = normalised weight of test set i (-)
$f_{ba}(\Delta_r, \mu, x^{(i,j)})$ = predicted bond strength using input $x^{(i,j)}$ and parameters Δ_r and μ (MPa)
$\overline{f}_{ba}^{(i,j)}$ = observed bond strength corresponding to test result i, j (MPa)

To minimize the cost function, `minimize` from `scipy.optimize` is used in Python. This function employs an optimization algorithm to find the values of the input parameters while satisfying the specified bounds.

$$\Delta_r{}^*, \mu^* = \arg\min_{\Delta_r, \mu} J(\Delta_r, \mu) \quad \text{subject to} \quad \Delta_r \in [\Delta_{r,min}, \Delta_{r,max}], \quad \mu \in [\mu_{min}, \mu_{max}] \qquad \text{(Eq. 6.12)}$$

6.3.2.2. Updating results

This section shows the results of the update. Table 6.4 shows the variance and corresponding weighting of each test set in the update. As can be concluded from the table, the test results of Virdi and Dowling et al. (1980) and Nezamian et al. (2002) contain the largest scatter. This could already be concluded from the plot of the test results in Figure 6.15. The test results of Aly et al. (2009) and Shakir-Khalil et al. (1993) contain the least scatter and therefore carry the most weight in the update of the model parameters.

Table 6.4: Weight for every test

Test set	Variance σ_i^2 (MPa^2)	Weight w_i (-)	Normalised weight w_i^* (-)
Virdi and Dowling (1980)	0.466	2.145	0.012
Roeder (1999)	0.082	12.203	0.070
Nezamian (2002)	1.238	0.808	0.005
Aly (2009)	0.016	63.871	0.365
Shakir-Khalil (1993)	0.010	95.877	0.548

The updated parameters are shown in table 6.5. It can be seen that the Coulomb friction coefficient has remained virtually the same, while the value of the surface irregularities has decreased significantly. This will lead to the model giving less high values for the bond strength, making the model more conservative.

Table 6.5: Initial and updated model parameters

Model	Surface irregularities Δ_r (mm)	Coulomb friction coefficient μ (-)	Objective function $J(\Delta_r, \mu)$ (MPa)
Initial model	0.050	0.500	3.499
Updated model	0.036	0.512	0.953

A point of attention is that two parameters in the model are updated based on only the difference in bond strength between the test results and the model results. Because the surface irregularities and the Coulomb friction coefficient have almost the same influence on this value, in theory several updated combinations of these parameters could occur, which makes the actual combination uncertain. An improvement option could be, for example, if the longitudinal stress distribution over the height of the plug would be available for different push-out tests. To include this distribution in the cost function of the parameter update. This can ensure that the actual combination of parameters can be estimated better, because the Coulomb friction coefficient has a different influence on this distribution than the surface irregularities. The Coulomb friction coefficient ensures that, in contrast to surface irregularities, the longitudinal stress is transferred more to the top of the connection as the value increases.

However, the updated combination of parameters in table 6.5 can be used as they are considered conservative. This is because the value for the surface irregularities mainly decreases in contrast to the value for the Coulomb friction coefficient. The surface irregularities not only influence the ultimate bond strength, such as the Coulomb friction coefficient, but also when the plug detaches from the pile due to shrinkage and there is no resistance at all. This makes lowering this parameter more conservative, especially for larger diameters where more concrete shrinkage is expected.

6.3.3. Comparison with updated model parameters

Figure 6.17 shows the comparison between the results of the model, in which the updated parameters have been applied, and the test results. As expected, updating the model parameters leads to a more conservative model, because these parameters are updated more closely to the test results with little scatter, which were initially overestimated by the model.

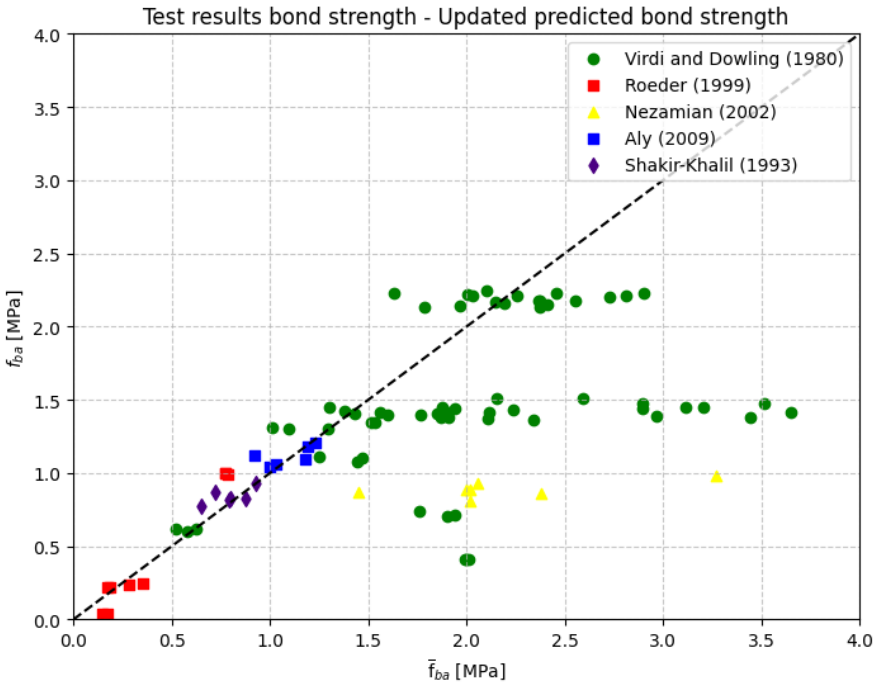

Figure 6.17: Test results bond strength versus updated predicted bond strength

The quality of the update can also be measured by the Mean Absolute Error (MAE). The lower this value, the better the quality of the update. The MAE can be determined using the formula below.

$$\text{MAE}(\Delta_r, \mu) = \frac{1}{n} \sum_{i=1}^{n} \left| f_{ba}(\Delta_r, \mu, x^{(i)}) - \overline{f}_{ba}^{(i)} \right| \qquad \text{(Eq. 6.13)}$$

where:

n = number of test results (-)
$f_{ba}(\Delta_r, \mu, x^{(i)})$ = predicted bond strength using input $x^{(i)}$ and parameters Δ_r and μ (MPa)
$\overline{f}_{ba}^{(i)}$ = observed bond strength corresponding to test result i (MPa)

The values for the MAE are shown in table 6.6 for both the initial model and the updated model. The MAE was determined for each individual test set as well as for all test sets combined. It can be analysed that the test sets with a higher weighting in the update logically reduce the value for the MAE the most. The test sets with a low weighting reduce their value for the MAE a lot less, with the exception of the test results of Nezmian et al. (2002) which even results in a higher value for the MAE with the updated parameters.

Table 6.6: Initial and updated MAE for test results

	Initial model	Updated model
Test set	MAE (MPa)	MAE (MPa)
Virdi and Dowling (1980)	0.683	0.625
Roeder (1999)	0.310	0.127
Nezamian (2002)	1.173	1.629
Aly (2009)	0.555	0.064
Shakir-Khalil (1993)	0.466	0.063
Combined test results	0.666	0.589

6.3.4. Determination of design bond strength model

To apply the new model in design, a safety factor is required with which the outcome of the model for the bond strength, f_{ba}, can be translated into a design value for the bond strength, $f_{ba,d}$. This design value can be determined using the method in Annex D of Eurocode 0, whereby a reduction factor can be determined using test results. How this method was applied to determine the safety factor of this model is included in Appendix C of this report.

The reduction factor determined for this model, to obtain a design value for the bond strength, is equal to a value of 0,246. This equals a safety factor, γ, of approximately 3,9. This determination is shown in the formula below. Initially, it suggests that this safety factor is on the high side, since the initial comparison without a safety factor was already quite conservative.

$$f_{ba,d} = 0.256 \cdot f_{ba} \approx \frac{f_{ba}}{3.9} \rightarrow \gamma \approx 3.9 \qquad \text{(Eq. 6.14)}$$

In Figure 6.18 the comparison between the test results, $\overline{f}_{ba}$, and the results of the model in which the reduction factor was applied to arrive at a design value, $f_{ba,d}$.

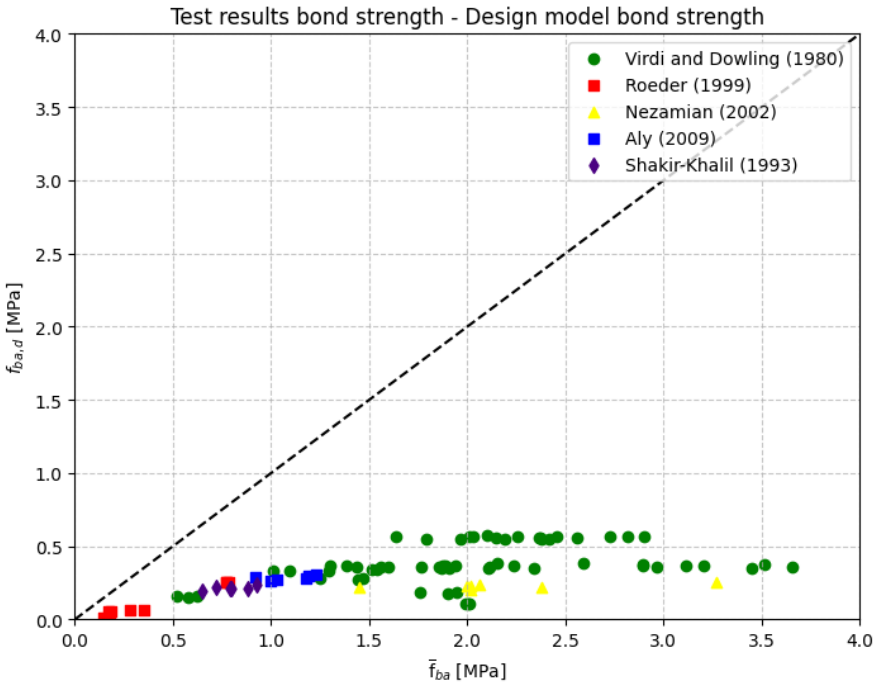

Figure 6.18: Test results bond strength versus design bond strength

It can be analysed from the figure that when the reduction factor is applied to the model, the model is very conservative compared to the test results. This gives rise to the suspicion that the safety factor could be too conservative to actually apply in the model. The reason why this could be is because in certain test sets used to determine the reduction factor there is a large amount of scatter. This ensures that the reduction factor is determined more conservatively based on Eurocode 0, because extra safety must be applied to take this scatter into account. Another reason could be that updating the model parameters has introduced some conservatism in the model. However, it is important that this update is carried out, because the factor for the surface irregularities also determines when the plug detaches from the pile due to shrinkage, and therefore has a major influence on the capacity at larger diameters. It has also been determined that when the reduction factor is determined with the initially adopted parameters, the safety factor becomes even greater, so that the capacity remains approximately the same.

6.4. Results model with updated parameters

In section 6.3 it was concluded that the model with the initial parameters did not correspond well enough with the test results. As a result, it was decided to update the most uncertain parameters of the model, the surface irregularities, Δ_r, and the Coulomb friction coefficient, μ, so that the model corresponds better. This update mainly resulted in a significant reduction for the surface irregularity value. This means that the model with the updated parameters determines the bond strength more conservatively than the model in which the initial parameters have been filled in.

To properly display the effect of the reduction on the bond strength, a plot has been made in Figure 6.19 in which the bond strength is shown for different diameters of the pipe pile. This figure shows the relationship for both the model with the initial parameters and the model with the updated parameters. For a realistic comparison the change of the other parameters have been taken into account, which also change as the diameter increases. In practice, the thickness of the pile, t_p, increases as the diameter of the pipe pile, D_p, increases. For this purpose, a constant ratio of $D_p/t_p = 50$ has been maintained between these two parameters. Also, in practice, the length of the plug, L, increases as the diameter of the pile increases. Therefore, a constant ratio of $L/D_p = 10$ was also maintained for these parameters in the analysis.

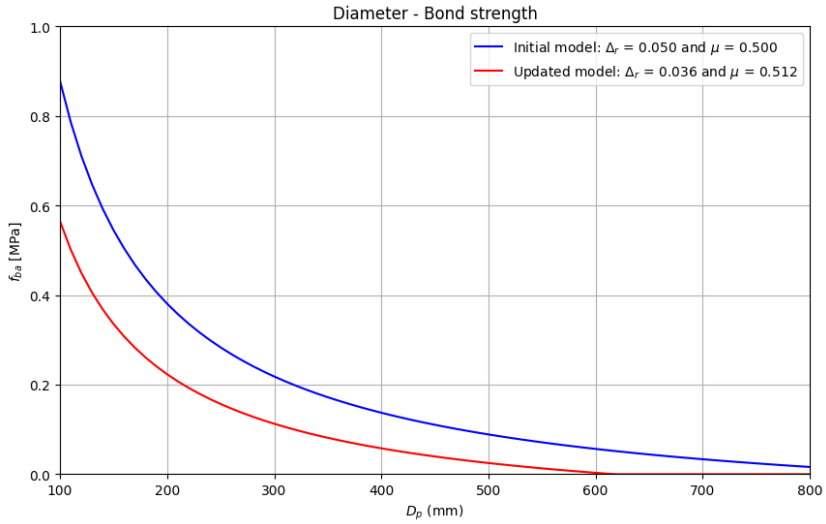

Figure 6.19: Bond strength versus different diameters of the steel pile for different model parameters.

It can be seen from the figure that the bond strength in the updated model is estimated to be significantly lower for all diameters, but also that due to the decrease in surface irregularities, the concrete plug will detach from the pile at smaller diameters. This can be analysed from the fact that from a diameter of approximately 600 mm there is no bond strength at all.

6.5. Conclusion validation model

This section contains the conclusion of the model validation. This conclusion can again be divided into two parts. Namely part of the influence of the model parameters and part where the model was compared to test results. Ultimately leading to a final conclusion of the model validation.

6.5.1. Conclusion influence of model parameters on the normal force capacity

In this chapter, an analysis was first carried out into the influence of the various parameters on the bond strength of the model. From this analysis it can be concluded that the input parameters of the model have the same effect on the bond strength as identified in the literature review. For example, a larger diameter and smaller thickness of the pipe pile ensures that the bond strength is lower than when a small diameter is used with a larger thickness of the pipe pile. Also, increasing the plug length causes a small decrease in the average bond strength.

Furthermore, it can be analysed that increasing the concrete compressive strength has virtually no influence on the bond strength, unless shrinkage is taken into account. This is because the Model Code model determines more shrinkage for higher concrete strength. This equates to the effect of shrinkage, as shrinkage also causes, as expected, a decrease in bond strength. This is because the plug will become more detached from the steel pipe pile due to shrinking, resulting in less contact. In final design situations it may therefore be recommended to use concrete with less shrinkage, so that the bond strength is less reduced.

It can also be concluded that the bond strength increases linearly as the value for the surface irregularities increases. This input variable therefore has a major influence on the outcome of the model, although it is difficult to estimate. This effect is comparable to that of the Coulomb friction coefficient, while more literature is available on this, it also remains one of the most uncertain factors in the model with a great influence on the output.

6.5.2. Conclusion comparison model with test results

When the model is verified with the parameters initially adopted from the literature for the surface irregularities and the Coulomb friction coefficient, it can be concluded that the model overestimates a fair share of the test results, making the model not conservative enough. As a result, it was decided to update the most uncertain factors in the model, namely the surface irregularities and the Coulomb friction coefficient, based on the test results, so that the model better fits these results. This update showed that the model with respective values of 0.036 and 0.512 for the surface irregularity and the Coulomb friction coefficient firstly contained a smaller Mean Average Error (MAE) and secondly became more conservative compared to the initial model.

After updating the model parameters, an attempt was made to determine a safety factor for the model using Appendix D from Eurocode 0. This resulted in a very conservative safety factor of 3.9. This factor is considered to be very conservative compared to the test results, making its application uncertain. This factor is due to a large degree of scatter of certain test sets used, which means that the Eurocode 0 method gives a more conservative value than when these test results are not used. It is therefore recommended to collect more accurate test results, with less scatter, with which a new safety factor can be drawn up or to determine a safety factor using a more specialized method.

6.5.3. Final conclusion validation model

The final conclusion of the validation is that the model can estimate the bond strength values reasonably accurately for test results with little scatter. Almost all input parameters also have the same influence on the bond strength as found in the literature, which means that this model is considered realistic. The only point for improvement is that the safety factor is currently on the very conservative side, which means that values for the bond strength could possibly be underestimated too much. It is therefore recommended to determine a safety factor using accurate test results or a more specialist method.

7

Transfer of normal force with mechanical connections

In the previous chapters, the normal force capacity due to friction has been worked out for concrete plug connections. If this capacity is not sufficient to transfer the design normal force from the concrete to the steel, mechanical connections must be used to realize this force transfer. This chapter discusses the possible mechanical connections that can be applied in that case. For one of these options for mechanical connections, it is also shown how the capacity of this mechanical connection can be determined and verified.

7.1. Alternatives for mechanical connections

Various alternatives are available in the literature to realize mechanical connections for transmitting the normal force. Figure 7.1 (Gebman et al. 2006) shows some of the most commonly used alternatives for these mechanical connections. These mechanical connections are all installed by welding them to the inside of the steel pipe pile, creating a mechanical connection between the concrete of the plug and the pipe pile.

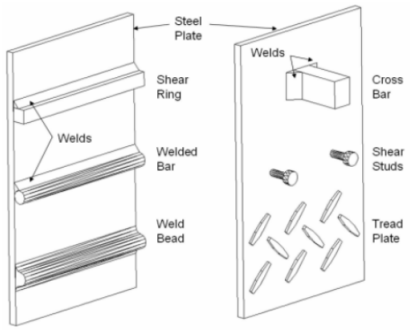

Figure 7.1: Alternatives for the mechanical connections (Gebman et al. 2006).

Research by Gebman et al. (2006) concluded that mainly the mechanical connections that were installed around the entire inner circumference of the steel pipe pile were effective in transferring the normal force. This was explained by the fact that test results showed that these mechanical connections offered much better ductile performance compared to, for example, the shear studs, which are distributed over the internal surface of the pile. This was confirmed in an article by Wiersma et al. (2023), who partly preferred shear rings over shear studs for the same reason.

7.2. Verification of shear rings

From the previous section, it can be assumed from literature that shear rings, compared to shear studs, are more effective in transferring the normal force from the concrete plug to the steel pipe pile. It has therefore been decided to further discuss this alternative in detail and to provide a calculation method for how the capacity of this alternative can be determined and how it should be verified. Figure 7.2 shows the geometry of a concrete plug connection in which shear rings have been applied.

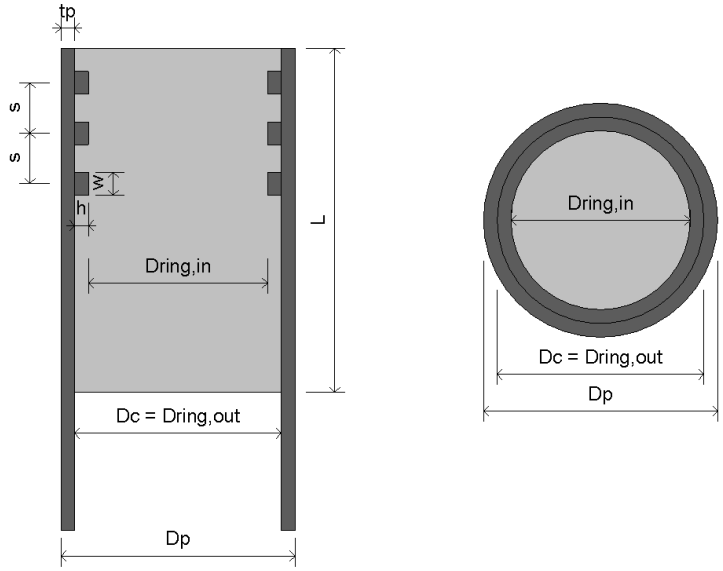

Figure 7.2: Shear rings in steel pipe pile.

The total normal force capacity, $N_{Rd,c}$, of the concrete plug provided with mechanical connections can be given as the function of the number of rings, n, multiplied by the normal force capacity per shear ring, $N_{Rd,ring}$. It is therefore assumed that at the moment of failure each ring will be loaded to its maximum capacity.

$$N_{Rd,c} = n \cdot N_{Rd,ring} \quad \text{(Eq. 7.1)}$$

where:

n = number of shear rings (-)
$N_{Rd,ring}$ = normal force resistance per shear ring (kN)

7.2.1. Concrete verifications

The normal force resistance per shear ring, $N_{Rd,ring}$, can be determined as a function where the surface area of the shear ring, A_{f1}, is multiplied by the maximum allowable concrete compressive stress, $\sigma_{c,max}$. It is therefore assumed that the failure mechanism of the connection is the crushing of the concrete on the steel rings. So logically if the normal force resistance per ring is not exceeded, it can be assumed that the concrete will not fail. The function for this normal force resistance per shear ring is as follows:

$$N_{Rd,ring} = A_{f1} \cdot \sigma_{c,max} \quad \text{(Eq. 7.2)}$$

where:

$$A_{f1} = \frac{\pi \cdot (D^2_{ring,out} - D^2_{ring,in})}{4} \quad \text{(Eq. 7.3)}$$

and:

$D_{ring,out}$ = outer diameter shear ring (mm)
$D_{ring,in}$ = inner diameter shear ring (mm) = $D_{ring,out} - h$
h = height of shear ring (mm)
$\sigma_{c,max}$ = maximum concrete compressive stress (MPa)

The maximum allowable concrete stress, $\sigma_{c,max}$, can be determined using the method for block dowels in solid concrete flanges from Annex F of Eurocode 4. This standard states that shear connections may be considered and calculated as block dowels when the front of these are not wedge-shaped and furthermore so stiff that it can be assumed that the stress on the concrete in front of the shear connection is evenly distributed at the moment of failure. The geometry definitions required for this determination of the allowable concrete stress is shown in Figure 7.3.

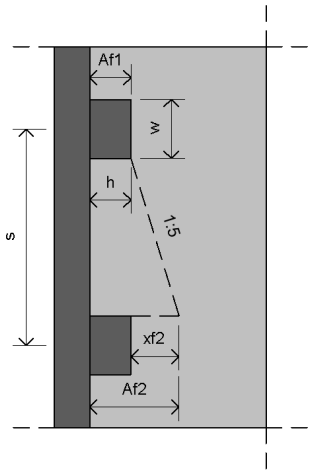

Figure 7.3: Determination of maximum allowable concrete stress on shear ring.

The maximum stress on the concrete, $\sigma_{c,max}$, is a function of the characteristic strength of the concrete, f_{ck}, divided by the partial material factor of concrete, γ_c, and multiplies by a factor, C_A, This factor depends on the geometry of the shear rings.

$$\sigma_{c,max} = \frac{C_A \cdot f_{ck}}{\gamma_c} \quad \text{(Eq. 7.4)}$$

where:

C_A = factor (-)
f_{ck} = characteristic cylinder compressive strength (MPa)
γ_c = partial factor concrete (-)

The factor, C_A, can be determined using the formula below. In this formula it is assumed that the stress on the concrete between the rings will spread at a slope of 1:5 over a larger projection surface, so that a greater stress on the dowels can be assumed. C_A may not exceed 2.5 for normal concrete. When lightweight concrete is used, a factor of 2.0 may not be exceeded.

$$C_A = \min\left(\sqrt{\frac{A_{f2}}{A_{f1}}}; 2.5\right) \quad \text{(Eq. 7.5)}$$

where:

$$A_{f1} = \frac{\pi \cdot (D^2_{ring,out} - D^2_{ring,in})}{4} \quad \text{(Eq. 7.6)}$$

and:

$$A_{f2} = \frac{\pi \cdot (D_{ring,out}^2 - (D_{ring,in} - 2 \cdot x_{f2})^2)}{4} \quad \text{(Eq. 7.7)}$$

$D_{ring,out}$ = outer diameter shear ring (mm)
$D_{ring,in}$ = inner diameter shear ring(mm) = $D_{ring,out} - h$
h = height of shear ring (mm)
x_{f2} = extra distance projection surface (mm) = $(s - w)/5$
s = spacing of the shear rings (mm)
w = width of shear ring (mm)

CUR Recommendation 77 also specifies preconditions that must be met for the use of steel strips on piles. These can be applied to the situation where shear rings have been applied. The conditions concern the geometry of the rings themselves and their mutual distance. The shear rings must meet the following conditions:

1. Height of shear ring: $25\,\text{mm} \leq h \leq 35\,\text{mm}$
2. Spacing of the shear rings: $85\,\text{mm} \leq s \leq 120\,\text{mm}$

7.2.2. Steel verifications

In addition to the concrete verifications, the steel of the pipe pile must also be verified for the stresses occurring as a result of the transmission of normal force through shear rings. At a local level, steel stresses occur at the location of the introduction of the forces on the shear rings in the wall of the pipe pile. The local moment generates stresses perpendicular to the plane of the steel pipe pile wall. How exactly these stresses arise is shown in Figure 7.3

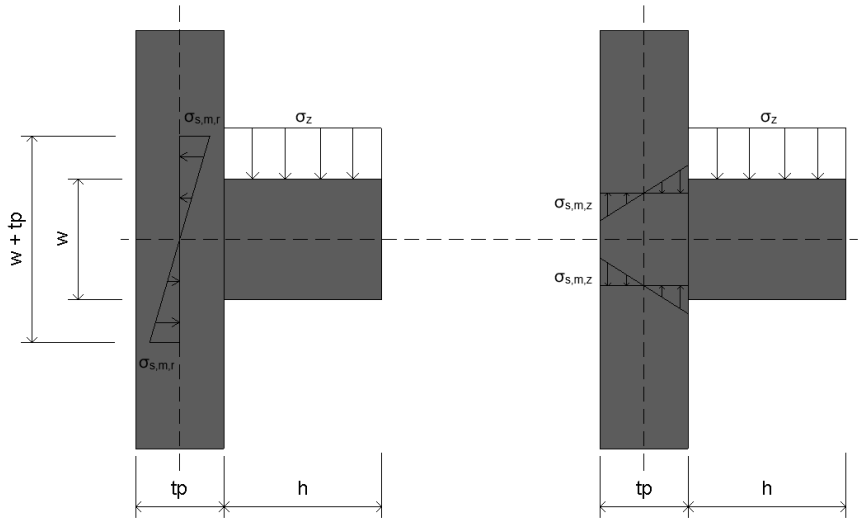

Figure 7.4: Determination of maximum allowable concrete stress on shear ring.

The stresses as shown in the figure above can be determined using the following formulas:

$$\sigma_{s,m,r} = \frac{6 \cdot M_{Ed,r}}{(w + t_p)^2} \quad \text{(Eq. 7.8)}$$

$$\sigma_{s,m,z} = \frac{3 \cdot M_{Ed,r}}{t_p^2} \quad \text{(Eq. 7.9)}$$

where:

$$M_{Ed,r} = \sigma_z \cdot h \cdot (\frac{t_p}{2} + \frac{h}{2}) \quad \text{(Eq. 7.10)}$$

w = width of shear ring (mm)
h = height of shear ring (mm)
t_p = wall thickness of the steel pipe pile (mm)
σ_z = stress acting on shear ring (MPa)

The given equations show how the local stresses in the steel can be determined from the stress acting on the shear rings, σ_z. When it is assumed that the failure mechanism of the connection is concrete compression failure, it can be assumed that this stress, σ_z, is equal to the maximum allowable concrete stress, $\sigma_{c,max}$. Once the steel stresses have been determined using this stress, they must be verified using the Von Mises criterion in which the stresses can be combined in the three-dimensional direction and tested against the yield stress of the material, f_{yd}.

7.3. Conclusion force transfer with mechanical connections

This chapter discusses how the normal force can be transferred with mechanical connections, when the resistance due to friction is insufficient. It has been assumed from the literature of Gebman et al. (2006) and Wiersma et al. (2023) that the use of shear rings as an mechanical connection is the most effective for this.

The capacity of these shear rings can be determined according to Appendix F of Eurocode 4. For this it must be assumed that the failure mechanism that occurs at the moment of failure is concrete in compression. With this method the capacity of the shear ring can be assumed and calculated like the capacity of a block dowel.

When the full strength of the shear rings is utilized, as can be determined according to Eurocode 4, the failure mechanism of concrete in compression must be assumed. To this end, it must be verified that the other structural components do not fail premature before this desired failure mechanism occurs. For example, the pipe pile must be verified for the stresses that this maximum concrete compressive stress introduces into the steel pipe pile. These stresses must be able to be absorbed by the pipe pile, so that it does not fail before the concrete does.

8

Transfer of bending moment and interaction with normal force

In many practical scenarios, a concrete cap must transfer not only a normal force but also a bending moment to the steel pipe pile. This bending moment is often caused by the horizontal variable loads acting on the structure, but can also be permanent when, for example, the permanent loads are transferred eccentrically to the pipe pile. Therefore, it is important to examine how the concrete plug transfers these bending moments in addition to the normal forces.

This chapter explores how the bending moment can effectively be transferred through the concrete plug. The focus is on the horizontal wrenching effect generated by the bending moment, which facilitates the transfer of loads without requiring additional mechanical connections. In addition, the bending moment resistance of the cross-section of the concrete plug was also examined. It was investigated whether this resistance is possibly the governing bending moment resistance of the concrete plug, which limits the moment that can be transferred using the concrete plug connection.

The chapter also investigates the interaction between stresses induced by the bending moment and those caused by the normal force. A model is proposed to estimate this interaction, hypothesizing that the bending moment-induced contact stresses could enhance normal force resistance through increased friction between the concrete plug and the steel pipe pile. This potential increase in friction could positively influence the overall capacity of the concrete plug connection.

8.1. Wrenching bending moment resistance

The bending moment is introduced from the concrete plug into the steel pipe pile by means of the wrenching mechanism. This mechanism is shown in Figure 8.1. Because wrenching occurs in the concrete plug in the pipe pile as a result of the bending moment that occurs, contact stresses arise along the interface between the concrete and the steel of the pile. If no stresses occur that are higher than the maximum concrete compressive stress, a linear distribution can be assumed for this stress distribution in the vertical direction as shown in the figure.

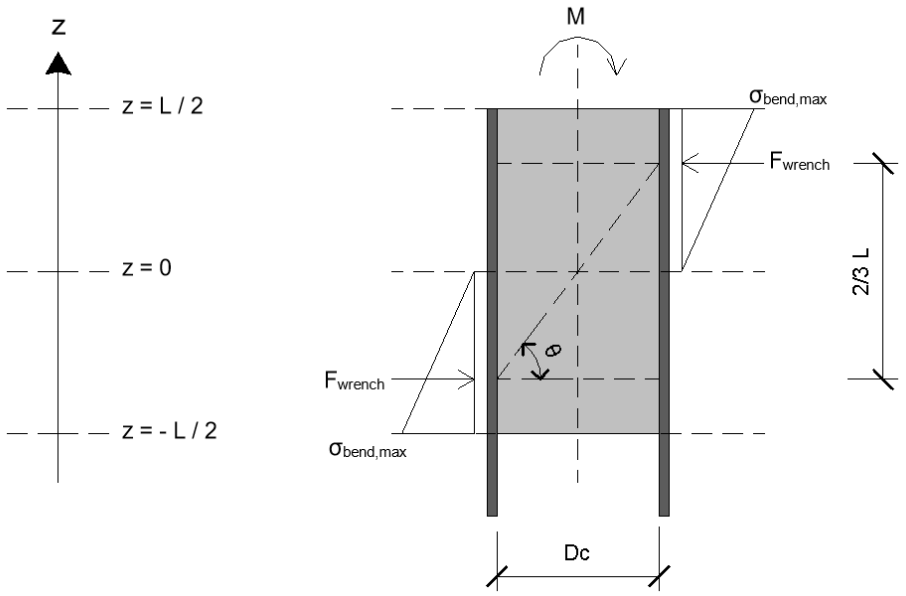

Figure 8.1: Transfer bending moment in pipe pile.

According to Eurocode 2 (NEN-EN 1992-1-1), the compression diagonals that arise as a result of wrenching must be within a certain margin for the compression diagonal angle with respect to each other. This margin is summarized in the formulation below.

$$1.0 \leq \tan(\theta) \leq 2.5 \rightarrow 45^\circ \leq \theta \leq 68^\circ \qquad \text{(Eq. 8.1)}$$

If a small compression diagonal angle is assumed, this means that the concrete plug uses a smaller length to transfer the bending moment and therefore also a smaller internal lever arm, which results in both higher contact stresses between the concrete and steel. Resulting from this there will also be higher ring tensile stresses in the pipe pile. If a larger compression diagonal angle is assumed, this will lead to a longer concrete plug, but to both lower contact and ring tensile stresses. In an optimal design for the concrete plug, such a diagonal angle should be assumed whereby the concrete plug is as short as possible but remains within the allowable contact and ring tensile stresses. The allowable contact stress is equal to the design compressive strength of concrete, f_{cd}. Therefore the following condition needs to hold true.

$$\sigma_{bend,max} \leq f_{cd} \qquad \text{(Eq. 8.2)}$$

This condition must also be maintained in order to assume the linear stress progression over the height of the plug, because no stresses may occur that are higher than the maximum concrete compressive stress.

In addition to a vertical distribution for the contact stress, a horizontal distribution for the contact stress around the concrete plug must also be assumed. Two different options are described in the following subsections, including a sinusoidal distribution and a quadratic sinusoidal distribution. These different options arise from a study by Wiersma et al. (2023). According to this study, these distributions are realistic to occur for concrete plug connections, when the maximum contact stress does not exceed the maximum compressive stress of the concrete.

8.1.1. Sinusoidal distribution

The first stress distribution that can be assumed for the contact stress around the concrete plug is a sinusoidal distribution. This distribution is shown in Figure 8.2.

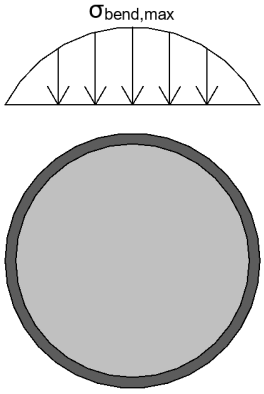

Figure 8.2: Sinusoidal stress distribution.

This sinusoidal distribution for the stress over both the height and along the circumference of the concrete plug can be described using the following formula:

$$\sigma_{bend}(z,x) = \sigma_{bend,max} \cdot \sin(\frac{x \cdot \pi}{D_c}) \cdot \frac{2 \cdot z}{L} \quad \text{(Eq. 8.3)}$$

where:

$\sigma_{bend,max}$= maximum wrenching stress on top and bottom of the concrete plug (MPa)
D_c = outer diameter of the concrete plug (mm)
L = length of the concrete plug (mm)

To determine the wrenching force, F_{wrench}, using the linear stress distribution, the integral equation below must be solved. The contact stress is integrated over half the height of the plug, L and integrated over the outer diameter of the concrete plug, D_c.

$$F_{wrench} = \int_0^{D_c} \int_0^{\frac{L}{2}} \sigma_{bend}(z,x)\, dz\, dx = \frac{\sigma_{bend,max} \cdot D_c \cdot L}{2 \cdot \pi} \quad \text{(Eq. 8.4)}$$

To arrive at the wrenching moment from the wrenching force, M_{wrench}, the wrenching force must be multiplied by the internal lever arm between the compression diagonals over the height of the concrete plug. This is shown in the formula below:

$$M_{wrench} = F_{wrench} \cdot \frac{2 \cdot L}{3} = \frac{\sigma_{bend,max} \cdot D_c \cdot L^2}{3 \cdot \pi} \quad \text{(Eq. 8.5)}$$

8.1.2. Quadratic sinusoidal distribution

The second stress distribution that can be assumed for the contact stress around the concrete plug is a quadratic sinusoidal distribution. This distribution is shown in Figure 8.3.

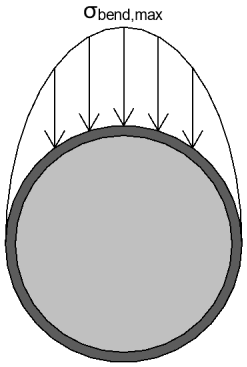

Figure 8.3: Quadratic sinusoidal stress distribution.

This quadratic sinusoidal distribution for the stress over both the height and along the circumference of the concrete plug can be described using formula below:

$$\sigma_{bend}(z,\theta) = \sigma_{bend,max} \cdot \sin(\theta)^2 \cdot \frac{2 \cdot z}{L} \tag{Eq. 8.6}$$

where:

$\sigma_{bend,max}$= maximum wrenching stress on top and bottom of the concrete plug (MPa)
D_c = outer diameter of the concrete plug (mm)
L = length of the concrete plug (mm)

To determine the wrenching force, F_{wrench}, using the linear stress distribution, the integral equation below must be solved. The contact stress is integrated over half the height of the plug, L and integrated over half the outer radius of the concrete plug, θ.

$$F_{wrench} = \int_0^{\pi} \int_0^{\frac{L}{2}} \sigma_{bend}(z,\theta) \cdot \frac{D_c}{2}\, dz\, d\theta = \frac{\pi \cdot \sigma_{bend,max} \cdot D_c \cdot L}{16} \tag{Eq. 8.7}$$

To arrive at the wrenching moment from the wrenching force, M_{wrench}, the wrenching force must be multiplied by the internal lever arm between the compression diagonals over the height of the concrete plug. This is shown in the formula below:

$$M_{wrench} = F_{wrench} \cdot \frac{2 \cdot L}{3} = \frac{\pi \cdot \sigma_{bend,max} \cdot D_c \cdot L^2}{24} \tag{Eq. 8.8}$$

8.1.3. Comparison stress distributions

To compare the stress distributions along the circumference of the concrete plug, Table 7.1 shows the relationship between the concrete stress and the wrenching force and wrenching moment for the different distributions. This table also includes a linear and uniform stress distribution for comparison, although these will not be used because they are not considered realistic to occur given the shape of the pipe pile. How these were determined is shown in Appendix D.

Table 8.1: Comparison of stress distributions

Stress distribution		Linear	Sinusoidal	Quadratic sinusoidal	Uniform
$F_{wrench} = \alpha \cdot \sigma_{bend,max} \cdot D_c \cdot L$	$\alpha =$	$\frac{1}{8} = 0.125$	$\frac{1}{2 \cdot \pi} \approx 0.159$	$\frac{\pi}{16} \approx 0.196$	$\frac{1}{4} = 0.250$
$M_{wrench} = \beta \cdot \sigma_{bend,max} \cdot D_c \cdot L^2$	$\beta =$	$\frac{1}{12} \approx 0.083$	$\frac{1}{3 \cdot \pi} \approx 0.106$	$\frac{\pi}{24} \approx 0.131$	$\frac{1}{6} \approx 0.167$

From the comparison between the sinusoidal and quadratic sinusoidal distributions from the table it can be concluded that the sinusoidal stress distribution provides a more conservative capacity for the bending moment capacity, M_{wrench}, of the connection, making this distribution governing in determining this capacity. However, if a check regarding the wrenching forces, F_{wrench}, must be carried out at a given bending moment, the quadratic sinusoidal distribution is governing. This conservative approach was chosen because it is not certain which of the two stress distributions is closer to the actual distribution in practice. To provide a definitive answer to this, more research is needed into the actual distribution, for example with test results. But for now, the sinusoidal distribution will be used to determine the wrenching bending moment resistance, $M_{Rd,wrench}$. If the crushing of the concrete is assumed as the failure mechanism, the maximum contact stresses between the steel and concrete, $\sigma_{bend,max}$, can be taken to be equal to the design concrete compressive strength, f_{cd}, for determining this resistance.

8.2. Cross-sectional bending moment resistance

The bending moment is transferred from the capping beam to the concrete plug by means of reinforcement in the concrete cross-section of the plug. The reinforcement that is applied also influences the length of the concrete plug because it affects the anchorage length in the concrete plug and therefore the total length of the plug. This section explains how the capacity of the applied reinforcement can be verified and how the required anchorage length can be determined.

8.2.1. Stress distribution in the cross section

The stress distribution used to determine the cross-sectional moment resistance is based on the rectangular model from Eurocode 2 (NEN-EN 1992-1-1). The distribution applied to the circular cross-section of the concrete plug with an example for the reinforcement configuration is shown in Figure 8.4.

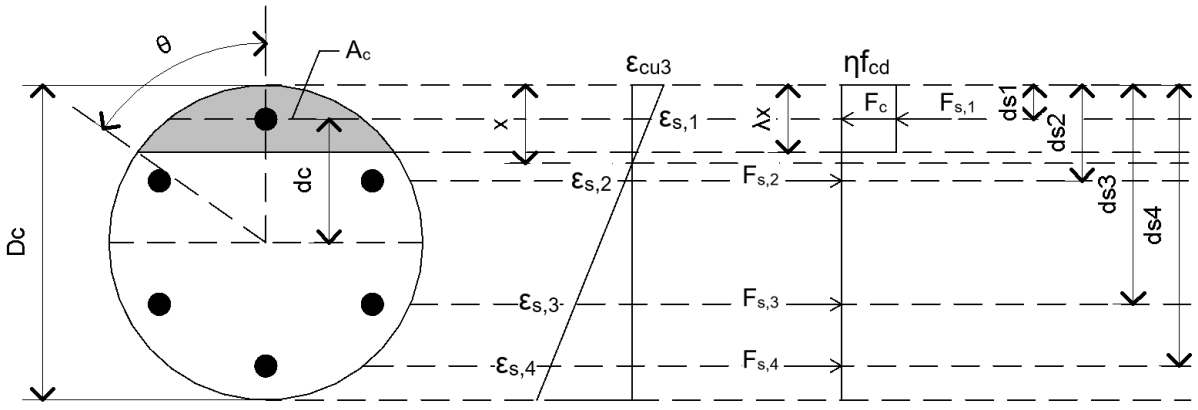

Figure 8.4: Strains, Forces and Moment arms.

The compressive force, F_c, in the part of the concrete cross-section that is subject to compression can be determined using the following formula:

$$F_c = A_c \cdot \eta \cdot f_{cd} \quad \text{(Eq. 8.9)}$$

where:

$$A_c = D_c^2 \cdot \frac{\theta - \sin(\theta) \cdot \cos(\theta)}{4} \quad \text{(Eq. 8.10)}$$

η = 1.0 for $f_{ck} \leq 50$ MPa
f_{cd} = design compressive strength concrete (MPa)
D_c = outer diameter concrete plug (mm)

In the formula for the concrete compressive force, the angle, θ, must be determined so that the surface area of the concrete that will be under compression can be determined. This angle can be determined with the formula below from ACI 318-14.

$$\theta = \cos^{-1}\left(\frac{\frac{D_c}{2} - \lambda \cdot x}{\frac{D_c}{2}}\right) \quad \text{(Eq. 8.11)}$$

where:

λ = 0.8 for $f_{ck} \leq 50$ MPa
x = distance from the fiber of maximum compressive strain to the neutral axis (mm)

The force per reinforcement layer, $F_{s,i}$, can be determined using the formula below. This formula takes into account the possibility that the reinforcement will yield.

$$F_{s,i} = A_{s,i} \cdot \min(\epsilon_{s,i} \cdot E_s; f_{yd}) \quad \text{(Eq. 8.12)}$$

where:

$$\epsilon_{s,i} = \epsilon_{cu3} \cdot \frac{x - d_{s,i}}{x} \quad \text{(Eq. 8.13)}$$

$A_{s,i}$ = area of reinforcement layer (mm^2)
E_s = modulus of elasticity reinforcement steel (MPa)
f_{yd} = design yield strength reinforcement steel (MPa)
ϵ_{cu3} = ultimate compressive strain concrete (-)
$d_{s,i}$ = distance reinforcement from the fiber of maximum compressive strain (mm)

The total internal force, F_{int}, in the cross-section of the concrete plug can then be determined using the expression below:

$$F_{int} = F_c + \sum F_{s,i} \quad \text{(Eq. 8.14)}$$

Using the internal forces in the cross-section, the moment capacity, M_{Rd}, of the cross-section can then be determined. However, because the distance from the fiber or maximum compressive strain to the neutral axis, x, is initially assumed to be a certain value, it must be verified whether this is the correct value. This can be done using an iterative process where the value of x is varied until the condition below is guaranteed. In this condition, the internal forces, F_{int}, must be equal to the external forces, F_{ext}, on the cross-section, creating vertical equilibrium.

$$\sum F = F_{int} + F_{ext} = 0 \quad \text{(Eq. 8.15)}$$

When the value of x has been determined in such a way that the vertical force balance is guaranteed, the moment capacity, $M_{Rd,cross-section}$, can be determined using the formula below. The capacity is the sum of the internal forces multiplied by their moment arms.

$$M_{Rd,cross-section} = F_c \cdot d_c + \sum (F_{s,i} \cdot (\frac{D_c}{2} - d_{s,i}) \quad \text{(Eq. 8.16)}$$

where:

$$d_c = \frac{D_c^3 \cdot \sin^3(\theta)}{12 \cdot A_c} \quad \text{(Eq. 8.17)}$$

8.2.2. Anchorage length of reinforcement

When the cross-sectional reinforcement has been verified for sufficient moment capacity, the required anchorage length, l_{bd}, can be determined. This length can be determined using the method from NEN-EN 1992-1-1, which is shown below.

$$l_{bd} = \alpha_1 \cdot \alpha_2 \cdot \alpha_3 \cdot \alpha_4 \cdot \alpha_5 \cdot l_{b,rqd} \geq l_{b,min} \quad \text{(Eq. 8.18)}$$

where:

α_1 = effect for the shape of the bars = 1.0 ($c_d \leq 3 \cdot \phi$)
α_2 = effect of the minimum concrete cover = $0.70 < 1 - 0.15 \cdot \frac{c_d - \phi}{\phi} < 1.00$
α_3 = effect of confinement by transverse reinforcement = 1.0 (conservative)
α_4 = influence of one or more welded cross bars = 1.0 (conservative)
α_5 = effect of a compressive stress perpendicular to the cleavage plane = 1.0 (conservative)
$l_{b,rqd}$ = base anchorage length = $36 \cdot \phi$ for concrete C30/37
$l_{b,min}$ = minimum anchorage length = $\max(0.3 \cdot l_{br,rqd}; 10 \cdot \phi; 100)$

The required anchoring length must be realized from the bottom of the part of the concrete plug in which the bending moment is transferred to the pipe pile. This means that the anchorage length must be added to this length for the total length of the concrete plug. However, the ROK V2.0 imposes an additional requirement on the anchorage length for concrete plugs, which means that the reinforcement must extend to the level of twice the anchorage length below the place where the reinforcement is no longer necessary from a mathematical point of view. This changes the formula for the required anchorage length, l_{bd}, to the following:

$$l_{bd} = 2 \cdot \alpha_1 \cdot \alpha_2 \cdot \alpha_3 \cdot \alpha_4 \cdot \alpha_5 \cdot l_{b,rqd} \geq 2 \cdot l_{b,min} \quad \text{(Eq. 8.19)}$$

8.3. Governing bending moment resistance

To determine which of the two bending moment resistances governs the final bending moment resistance of the connection, these two are compared with each other for different design situations of the concrete plug. The two bending moment resistances that are compared in this section are the previously determined wrenching resistance, $M_{Rd,wrench}$, and the cross-section resistance, $M_{Rd,cross-section}$. To provide a good comparison between the bending moment resistances of both the wrenching and the cross-section, the resistance of both has been determined for different diameters of the concrete plug.

8.3.1. Input parameters

In this subsection the input parameters for determining the bending moment resistances are given. These input parameters are necessary for determining the resistance, as described in sections 8.1 and 8.2.

8.3.2. Input parameters for wrenching bending moment resistance

To determine the wrenching bending moment resistance, in addition to the diameter, the concrete strength class and the length of the plug over which the moment is transferred are also required. The strength class of the concrete is required to determine the maximum allowable contact stress between the steel and concrete. This contact stress may not exceed the design compressive strength of the concrete. For the concrete strength class, class C30/37 has been used, which has a design compressive strength, f_{cd}, of 20 MPa.

The length over which the bending moment is transferred can be determined using Figure 8.1. It can be deduced from this Figure that this length can be determined as a function of the diameter of the plug and the assumed compression diagonal between the wrenching forces. The formula for determining this length is as follows:

$$L = \frac{3 \cdot D_c \cdot \tan(\theta)}{2} \qquad \text{(Eq. 8.20)}$$

where:

D_c = outer diameter concrete plug (mm)
θ = angle of compression diagonal (°) = $45° \leq \theta \leq 68° \rightarrow 1.0 \leq \tan(\theta) \leq 2.5$

According to Eurocode 2 (NEN-EN 1992-1-1), the assumed angle for the compression diagonal must remain within certain limit values. This means that $\tan(\theta)$ may be assumed to be at least equal to 1.0 or at most equal to 2.5.

8.3.3. Input parameters for cross section bending moment resistance

To determine the bending moment resistance of the cross-section, in addition to the diameter of the concrete plug, the strength class of the concrete and the amount of reinforcement in the cross-section are required. Strength class C30/37 will also be used for this. For the amount of reinforcement in the cross-section of the plug, a fixed ratio is maintained for the total area of the steel compared to the area of concrete. The total area of reinforcement can therefore be calculated as a function of the area of concrete, using the following formula:

$$A_s = \rho \cdot A_c \qquad \text{(Eq. 8.21)}$$

where:

ρ = reinforcement ratio (-) = $\rho \leq 0.04$
A_c = total area of concrete plug (mm^2) = $\frac{D_c^2 \cdot \pi}{4}$

According to Eurocode 2 (NEN-EN 1992-1-1) the total area of the reinforcement may not exceed 4$\%$ of the total area of the cross section of the concrete plug. This means that a maximum value of 0.04 may be used for the reinforcement ratio.

The bending moment resistance of the cross section cannot be determined directly as a function of the total reinforcement area, using subsection 8.2.1. As a result, the total surface area of reinforcement must be converted to a reinforcement configuration for each cross section, where the sum and area of rebars must be equal to the total reinforcement area. It must be ensured that the reinforcement ratio remains the same for each cross section so that a good comparison is made. To determine the reinforcement configuration for this number of cross sections, a Python script was used, which determines the rebar diameter based on the number of rebars, while guaranteeing the reinforcement ratio. It was always checked whether the number of rebars was sufficient so that they remained well distributed around the cross-section. Appendix E contains an example in which the bending moment resistance is calculated for a cross-section with a specific diameter.

A consequence of this method is that non-existing rebar diameters can be used by the Python script, because the input reinforcement ratio must be precisely met. When trying to achieve the same reinforcement ratio in practice, existing rebar diameters must be used, which sometimes makes it not possible to achieve exactly the same desired reinforcement ratio. This consequence could be disadvantageous when the resistance for the maximum reinforcement ratio is determined, because in practice this ratio cannot be exactly achieved and may not be exceeded, as a result of which the bending moment resistance in practice could be lower than the one determined with the Python script.

8.3.4. Comparison bending moment resistances

In Figure 8.5 the results for the bending moment resistance are plotted for different diameters of the concrete plug. These results were obtained using the input parameters from subsection 8.2. As can be seen from the figure, the bending moment resistance of the cross-section has been determined for two different reinforcement ratios. One of these is the maximum reinforcement ratio according to Eurocode 2. This ratio is used to determine the maximum bending moment resistance of the cross-section. Because in practice cross-sections are often not reinforced to this maximum ratio, a lower reinforcement ratio has also been used to determine the bending moment resistance of the cross-section for a good comparison. Furthermore, the figure also shows the wrenching bending moment resistances for both the minimum and maximum plug length over which the bending moment may be transferred by wrenching according to Eurocode 2. This is respectively for a situation where $tan(\theta)$ equals 1.0 and a situation where $tan(\theta)$ equals 2.5.

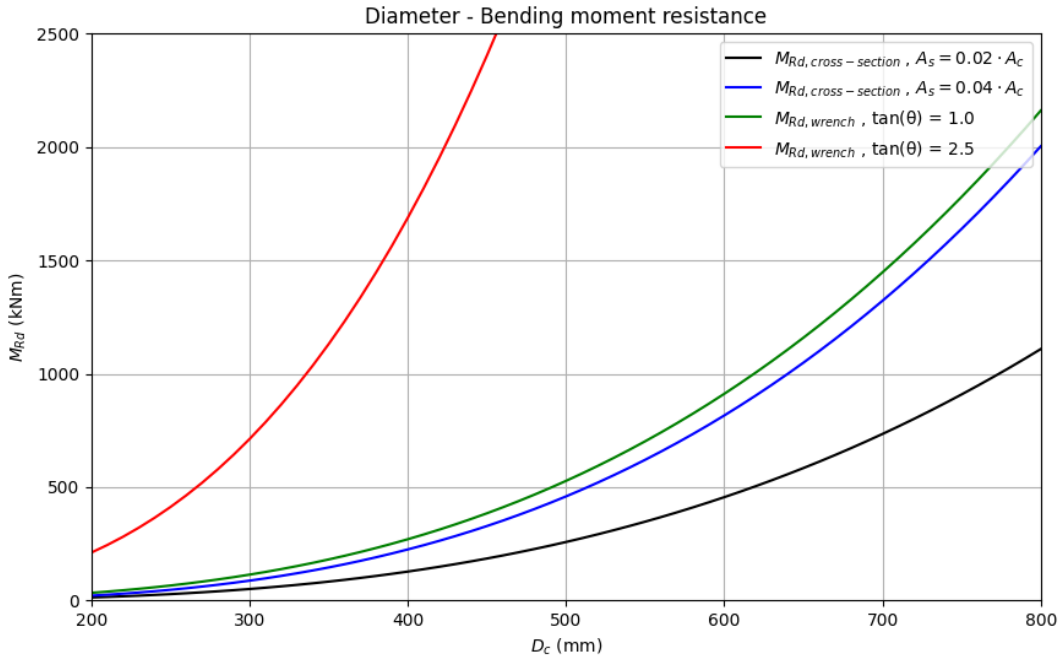

Figure 8.5: Diameter - Bending moment resistance.

As can be analyzed from the figure, the cross-section of the concrete plug has a lower bending moment resistance than the wrenching bending moment resistance. It can be deduced that even when the angle for the compression diagonal is maintained at the minimum limit value, i.e. when the bending moment is transferred over the minimum length by wrenching, the bending moment resistance is higher than that of the cross-section with maximum reinforcement . When the comparison is made with a situation in which the cross-section of the concrete plug is not provided with maximum reinforcement, this difference in resistance is even greater, as expected. From this it can be concluded that the bending moment resistance of the entire connection is limited by the bending moment resistance of the cross-section. As a result, the cross-sectional bending moment resistance governs the final bending moment resistance of the concrete plug connection.

8.4. Conclusion transfer of bending moment

In the previous sections, the bending moment resistance of the concrete plug connection, without mechanical connections, was determined. Initially, the mechanism for transferring the bending moment from the concrete plug to the steel pipe pile was analyzed. It was found that the moment transfer occurs through a wrenching mechanism in the concrete plug induced by the bending moment, creating contact stresses between the concrete plug and the steel pipe pile. These contact stresses facilitate the transfer of bending to the pipe pile via horizontal wrenching forces.

A specific stress distribution must be assumed for these contact stresses, which arise both over the height and around the circumference of the plug. A linear distribution can be assumed over the height of the plug if the contact stresses due to the bending moment do not exceed the compressive strength of the concrete. For the contact stresses around the circumference, a sinusoidal distribution or a quadratic sinusoidal distribution can be assumed. However, when comparing these two distributions, it appeared that the sinusoidal distribution provided a lower moment resistance than the quadratic sinusoidal distribution. Given the uncertainty of the exact distribution in practice, it is more conservative to assume a sinusoidal distribution. Further research into the exact distribution could clarify which one will occur.

Using the identified stress distributions for the contact stresses, the bending moment can be verified in two ways: by evaluating the allowable contact stresses for a given moment or by determining the bending moment resistance from the maximum allowed contact stresses. However, it has been found that the wrenching mechanism does not govern the maximum allowable bending moment resistance of the plug; instead, the bending moment resistance of the plug's cross-section governs. Therefore, this cross-sectional resistance determines the final allowable bending moment of the connection.

8.5. Interaction between normal force and bending moment

As previously determined, the bending moment can be transferred from the concrete plug to the steel pipe pile through a wrenching mechanism induced by the bending moment. This wrenching mechanism creates contact stresses between the concrete plug and the steel pipe pile. This section investigates whether these contact stresses can contribute to additional normal force resistance beyond what is provided by the contact stresses from the normal force in combination with the Poisson's effect, as described in Chapter 4.

As assumed in the model proposed in Chapter 4, these contact stresses between the plug and the pile can be converted into normal force resistance using the Coulomb friction principle. Thus, it is also plausible that the contact stresses caused by the wrenching mechanism could lead to additional normal force resistance. To determine the total normal force resistance, including this additional resistance, an interaction between the contact stresses caused by the normal force, σ_{norm}, and those caused by the bending moment, σ_{bend} must be assumed. In this section, an interaction is proposed to determine the resulting contact stress, σ_{cont}, due to these separate stress components, which can be converted into total normal force resistance using the Coulomb friction principle.

To model the interaction between the contact stress created by the normal force, σ_{norm}, and the contact stress created by the bending moment, σ_{bend}, it is proposed to combine these stress components. This combination will result in a higher contact stress on one side of the plug, as the bending moment will press the plug more firmly against this side. Conversely, on the opposite side of the plug, it is assumed that the contact stresses will be reduced by the bending moment. This reduction occurs because the plug may develop a small deformation due to the bending moment, causing less contact with this side and possibly creating a gap between the plug and the pipe pile.

To model this reduction, it is assumed that the compressive stress arising on one side of the plug due to the bending moment can be mirrored as a tensile stress on the other side of the plug. This assumption creates the stress distribution illustrated in Figure 8.6, showing both the contact stress component originating from the normal force, σ_{norm}, and the assumed contact stress component originating from the bending moment, σ_{bend}. The normal force component will be calculated according to the model from Chapter 4, and the bending moment component will be determined as described in Section 8.1.

Figure 8.6 also shows that it has been decided to distribute the contact stresses σ_{bend}, which are caused by the bending moment over the entire length of the concrete plug. This suggests that the bending moment is introduced over the entire length of the concrete plug and may therefore conflict with the requirements of Eurocode 2 regarding the compression diagonal requirements that restrict the length for moment transfer. However, in this application, where the normal force resistance needs to be determined, it is more conservative to assume a longer length for introducing the bending moment, as this will lead to lower contact stresses and therefore less normal force resistance. In contrast, for verifying the bending moment resistance, a shorter length assumption leads to higher contact stresses, resulting in a more conservative bending moment resistance. Because in practice it is uncertain over which part of the plug length the bending moment is actually transferred, it is therefore conservative to use a different stress distribution for both situations, which will lead to a more conservative resistance.

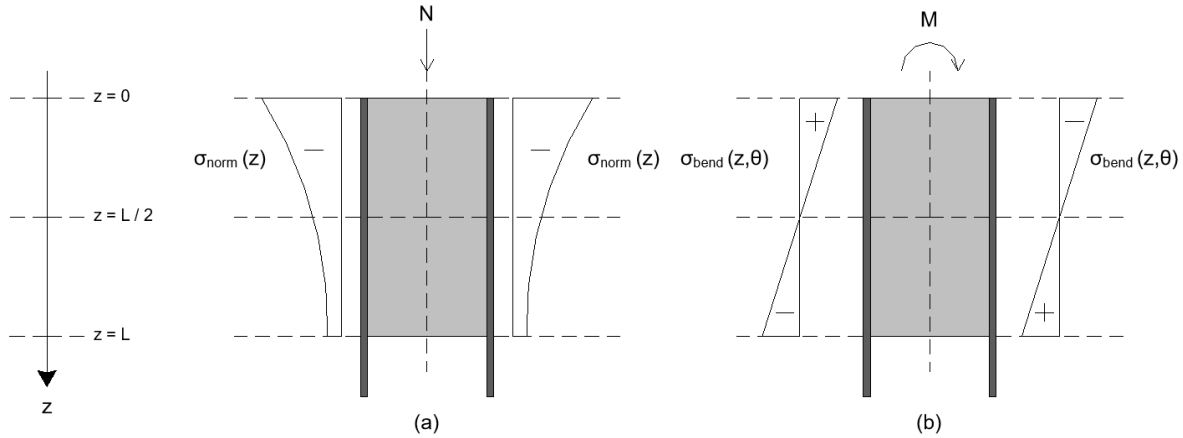

Figure 8.6: Stress distributions over the length of the plug created by normal force and bending moment.

In contrast to the model in which only normal force was included, as in Chapter 4, it can no longer be assumed that the contact stress around the circumference of the plug is uniform. This is because the bending moment creates a non-uniform distribution around the circumference of the plug, as shown in Figure 8.7. As a result, in the model for normal force and bending moment, the plug will have to be divided over both the height and around the circumference of the plug. For the stress profile around the plug, resulting from the bending moment, the quadratic sinusoidal profile will be assumed. This profile was used because it gives lower values for the stresses caused by the bending moment, σ_{bend}, than the sinusoidal profile. This will result in less additional contact stress and therefore less extra normal force capacity. Therefore, assuming the quadratic sinusoidal profile in this case is a conservative assumption in this application.

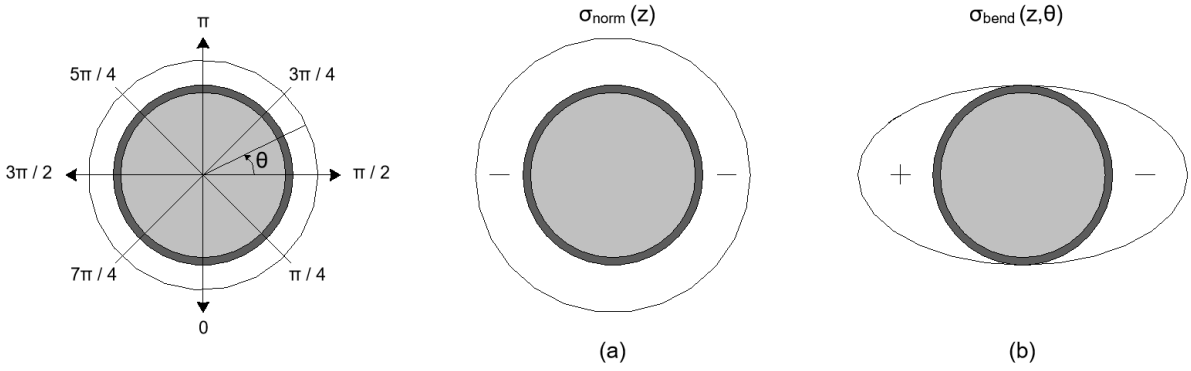

Figure 8.7: Stress distributions around the circumference of the plug created by normal force and bending moment.

8.5.1. Interaction with semi-dominant bending moment

The first situation that can arise because of the assumed interaction between the bending moment and normal force is a situation in which the bending moment is semi-dominant. Semi-dominant means that at the bottom of the plug the maximum contact stress that arises as a result of the bending moment is greater than the maximum contact stress that arises as a result of the normal force. The condition for which this holds true is as follows:

$$\sigma_{norm}(z = L) < \sigma_{bend}(z = L, \theta = \frac{3\pi}{2}) \rightarrow \sigma_{norm}(z = L) < \sigma_{bend,max} \quad \text{(Eq. 8.22)}$$

where:

$$\sigma_{bend,max} = \frac{24 \cdot M}{\pi \cdot D_c \cdot L^2} \quad \text{(Eq. 8.23)}$$

8.5.1.1. Resulting contact stresses over height of the interface

In this condition, at the bottom of the plug (at $\theta = \pi/2$) , the assumed tensile stress as a result of the bending moment will be greater in magnitude than the compressive stress that arises as a result of the normal force. This will theoretically create a resulting tensile stress at the bottom of the plug. However, the connection between the steel and concrete cannot transfer any tensile stresses, so the model will assume that the resulting stress at this point is equal to 0. This sum of contact stresses is shown in the Figure 8.8.

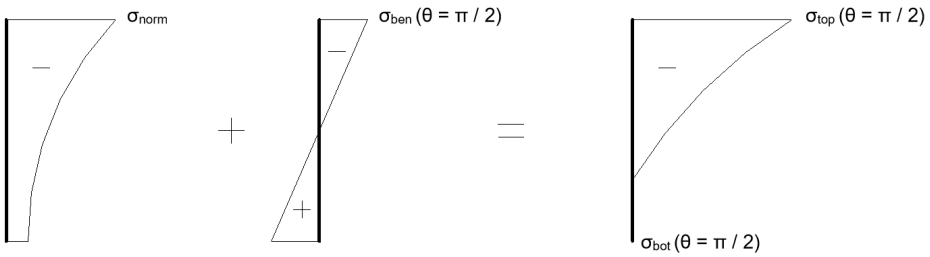

Figure 8.8: Resulting contact stress at $\theta = \pi/2$.

On the opposite side (at $\theta = 3\pi/2$) there is an additional compressive stress due to the bending moment at the bottom of the plug instead of a additional tensile stress. This leads to an increase in the compressive contact stress at the bottom of the plug, while the contact stress at the top of the plug is reduced. However, the magnitude of this tensile stress from the bending moment at the top in this situation is not greater than the magnitude of the compressive stress originating from the normal force. This will still result in a contact compressive stress as shown in Figure 8.9.

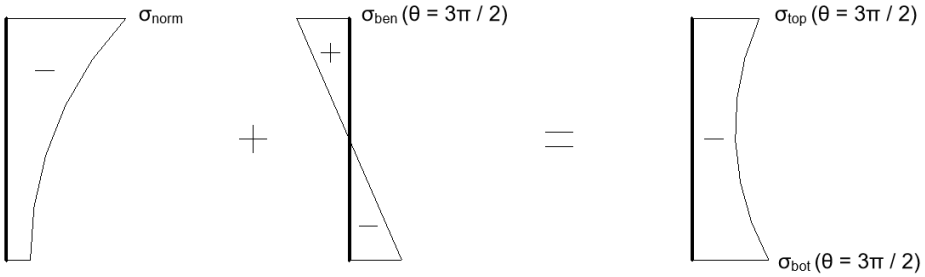

Figure 8.9: Resulting contact stress at $\theta = 3\pi/2$.

When these two resulting stress distributions are combined into an average stress distribution, it can be concluded that the mean contact stress at the bottom of the plug has increased because of the influence of the bending moment, as shown in Figure 8.10.

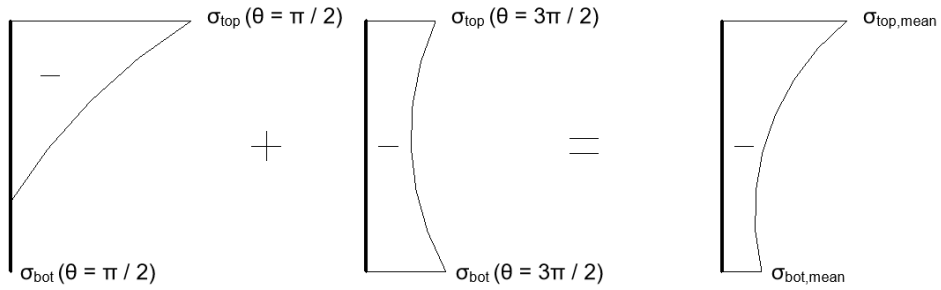

Figure 8.10: Mean resulting contact stress.

This exact increase in contact stress can be determined when the contact stress due to the normal force is subtracted from the average contact stress distribution. When this is done, the exact increase in contact stress due to the bending moment can be visualised as in Figure 8.11. In this situation this turns out to be a local stress triangle at the bottom of the plug.

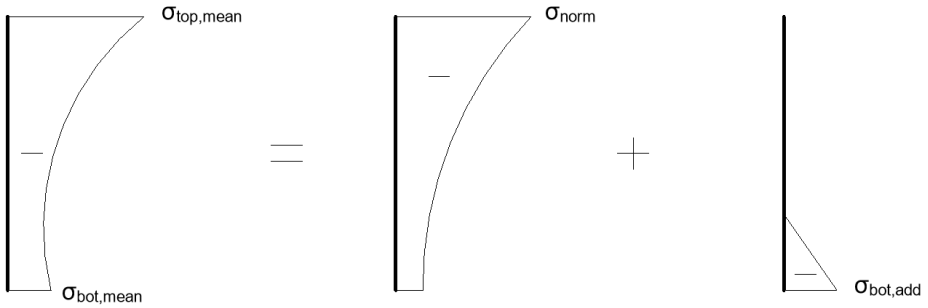

Figure 8.11: Additional contact stress.

8.5.1.2. Resulting contact stresses around circumference of the interface

The resulting contact stresses can also be determined around the circumference of the plug. This resulting contact stress at the top of the plug is shown in Figure 8.12. As can be analysed from the figure, the resulting contact stress because of the bending moment, will be more concentrated towards one side of the concrete plug. However, the total contact stress at the top of the plug will remain the same as the situation without a bending moment, because the increase in stress on one side cancels out the decrease in stress on the other side.

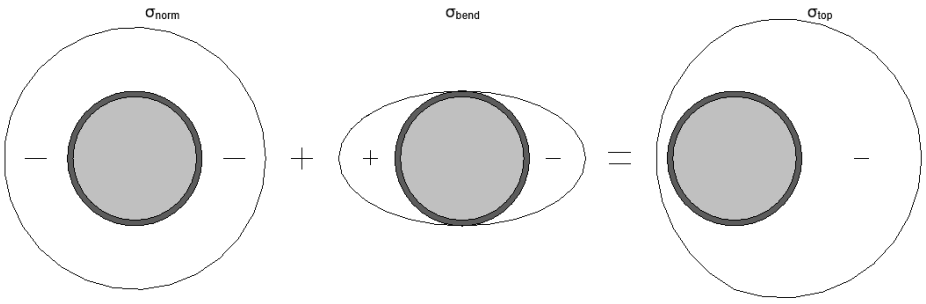

Figure 8.12: Resulting contact stress at $z = 0$.

The resulting contact stress at the bottom of the plug is shown in Figure 8.13. As can be analysed from the figure, the contact stress will also increase towards one side of the concrete plug at the bottom. However on this side, the total contact stress increase compared to the situation without a bending moment. This is because the resulting contact stress on one side cannot be reduced further than 0, so this reduction no longer compensates for the increase in the contact stress on the other side. This results in a total increase in contact stress.

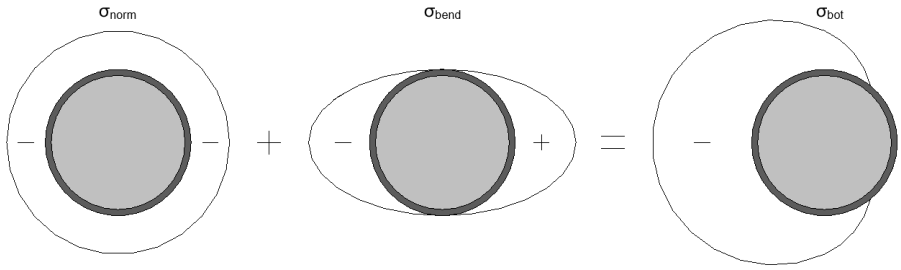

Figure 8.13: Resulting contact stress at $z = L$.

8.5.2. Interaction with dominant bending moment

The second situation that can arise because of the assumed interaction between the bending moment and normal force is a situation in which the bending moment is dominant. Dominant means that the maximum contact stress that arises as a result of the bending moment is greater than the maximum contact stress that arises as a result of the normal force at both the top and bottom of the plug. The condition for which this holds true is as follows:

$$\sigma_{norm}(z=0) < \sigma_{bend}(z=0, \theta=\frac{\pi}{2}) \rightarrow \sigma_{norm}(z=0) < \sigma_{bend,max} \quad \text{(Eq. 8.24)}$$

where:

$$\sigma_{bend,max} = \frac{24 \cdot M}{\pi \cdot D_c \cdot L^2} \quad \text{(Eq. 8.25)}$$

8.5.2.1. Resulting contact stresses over height of the interface

In this condition also, at the bottom of the plug (at $\theta = \pi/2$) , the assumed tensile stress as a result of the bending moment will be greater in magnitude than the compressive stress that arises as a result of the normal force. This will theoretically create a resulting tensile stress at the bottom of the plug. However, the connection between the steel and concrete cannot transfer any tensile stresses, so the model will assume that the resulting stress at this point is equal to 0. This sum of contact stresses is shown in the Figure 8.14.

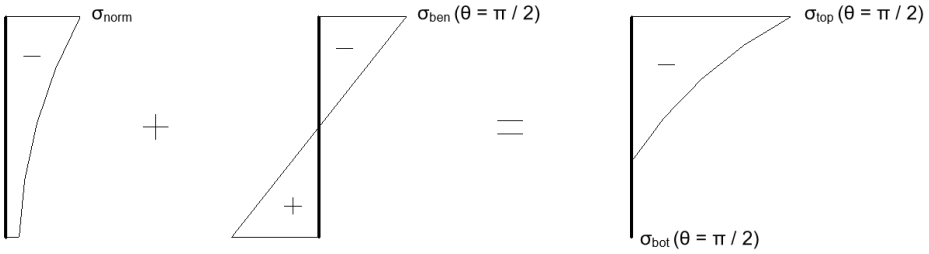

Figure 8.14: Resulting contact stress at $\theta = \pi/2$.

On the opposite side (at $\theta = 3\pi/2$) there is an additional compressive stress due to the bending moment at the bottom of the plug instead of a tensile stress. This leads to an increase in the contact stress at the bottom of the plug, while the contact stress at the top of the plug is reduced. In this case, the tensile stress at the top of the plug, due to the bending moment, is greater in magnitude than the compressive stress due to the normal force. This means that the resulting contact stress is set equal to 0. This sum of contact stresses is shown in the Figure 8.15.

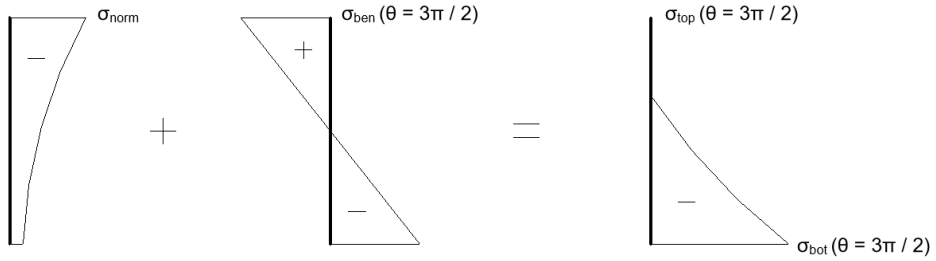

Figure 8.15: Resulting contact stress at $\theta = 3\pi/2$.

When these two resulting stress distributions are combined into an average stress distribution, it can be concluded that the contact stress at both the top as the bottom of the plug has increased because of the influence of the bending moment, as shown in Figure 8.16.

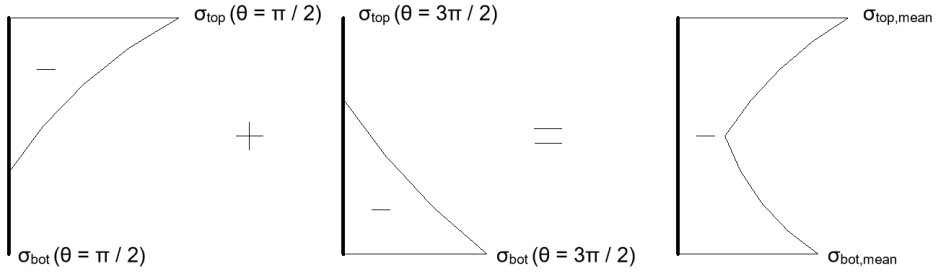

Figure 8.16: Mean resulting contact stress.

This exact increase in contact stress can be determined when the contact stress due to the normal force is subtracted from the average contact stress distribution. When this is done, the exact increase in contact stress due to the bending moment can be visualised as in Figure 8.17. In this situation the increase in contact stress turns out to be a local stress triangle at both the top as the bottom of the plug.

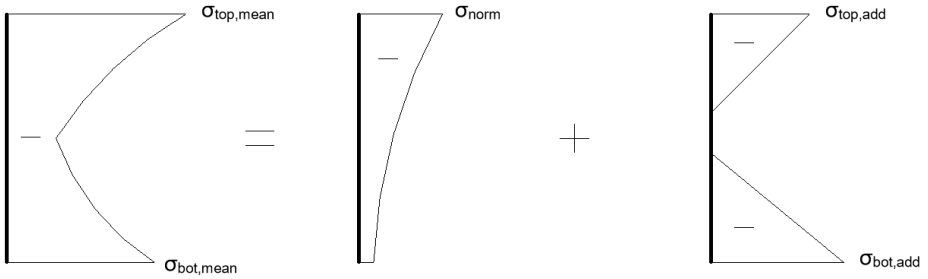

Figure 8.17: Additional contact stress.

8.5.2.2. Resulting contact stresses around circumference of the interface

The resulting contact stresses can also be determined around the circumference of the plug. This resulting contact stress at the top of the plug is shown in Figure 8.18. As can be analysed from the figure, the resulting contact stress because of the bending moment, will be more concentrated towards one side of the concrete plug. In this case, the total contact stress increases compared to the situation without a bending moment. This is because the resulting contact stress on one side cannot be reduced further than 0, so this reduction no longer compensates for the increase in the contact stress on the other side. This results in a total increase in contact stress.

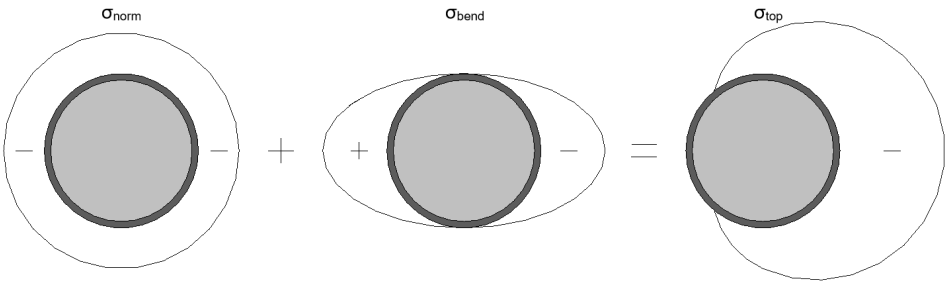

Figure 8.18: Resulting contact stress at $z = 0$.

The resulting contact stress at the bottom of the plug is shown in Figure 8.19. As can be analysed from the figure, the contact stress will also increase towards one side of the concrete plug at the bottom. Also in this case, the total contact stress increase compared to the situation without a bending moment.

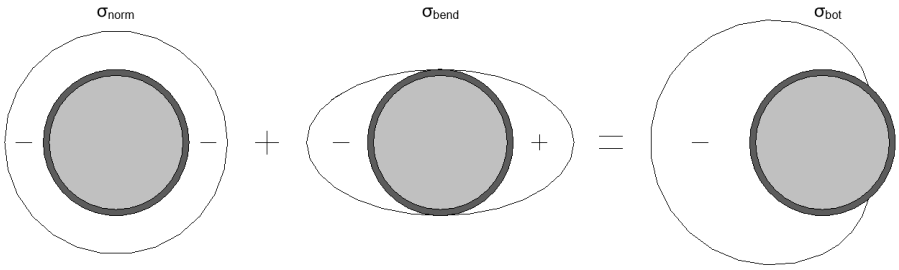

Figure 8.19: Resulting contact stress at $z = L$.

8.5.3. Calculation of total normal force capacity

The assumed resulting contact stresses can be converted into a total normal force capacity of the plug, $N_{Rd,c}$, using the Coulomb friction principle. In this principle, the contact stress, σ_{cont}, is multiplied by the Coulomb friction coefficient, μ, so that total resistance due to friction can be determined.

To determine the total capacity of the plug, a numerical integration method was used in which the plug is divided into smaller surfaces around the height and circumference of the concrete plug. These surfaces have a uniform length of Δz over the height and a uniform width of $\Delta\theta \cdot \frac{D_c}{2}$ around the circumference. For each of these areas, the resulting contact stress was determined by combining the contact stress, σ_{norm}, originating from the normal force with the contact stress, σ_{bend}, originating from the bending moment. The contact stress originating from the normal force is determined using the model from Chapter 4. The contact stress originating from the bending moment is determined as described in section 8.1. The mesh of the concrete plug is shown in Figure 8.20.

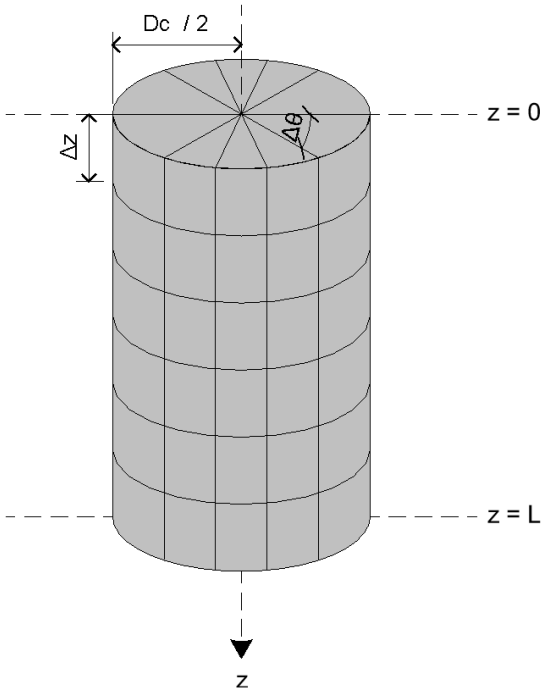

Figure 8.20: Mesh concrete plug.

The formula for determining the normal force capacity, $N_{Rd,c}$, is shown below. This formula makes use of a numerical integration method. In this method the contact stress, $\sigma_{cont}(z_i, \theta_j)$, is determined for each small surface of the plug. This contact stress is then multiplied by the Coulomb friction coefficient, μ, and the area of the surface so that the normal force capacity of that individual surface is determined. This is then determined repeatedly for each individual surface and summed so that the total capacity of the plug can be found. The formula also includes a Heaviside step function, $H(\sigma_{cont}(z_i, \theta_j))$. This function ensures that when a contact stress on a surface becomes negative, it is set equal to 0, because the connection between the steel and concrete cannot transfer tension.

$$N_{Rd,c} = \sum_{j=0}^{n} \sum_{i=0}^{m} \sigma_{cont}(z_i, \theta_j) \cdot \mu \cdot H(\sigma_{cont}(z_i, \theta_j)) \cdot \frac{D_c}{2} \cdot \Delta\theta \cdot \Delta z \qquad \text{(Eq. 8.26)}$$

where:

D_c = outer diameter of the concrete plug (mm)
μ = Coulomb friction coefficient (-)

and:

$$n = \frac{L}{\Delta z} \qquad \text{(Eq. 8.27)}$$

L = length of the concrete plug (mm)
Δz = size of the mesh in vertical direction (mm)

and:

$$m = \frac{2\pi}{\Delta\theta} \qquad \text{(Eq. 8.28)}$$

$\Delta\theta$ = size of the mesh in circumferential direction (radians)

and:

$$\sigma_{cont}(z_i, \theta_j) = \sigma_{norm}(z_i) + \sigma_{bend}(z, \theta) \quad \text{(Eq. 8.29)}$$

$$\sigma_{bend}(z_i, \theta_j) = \begin{cases} (\sigma_{bend,max} - \sigma_{bend,max} \cdot \frac{2 \cdot z_i}{L}) \cdot \sin(\theta_j)^2 & \text{if } 0 \leq \theta_j \leq \pi \\ (-\sigma_{bend,max} + \sigma_{bend,max} \cdot \frac{2 \cdot z_i}{L}) \cdot \sin(\theta_j)^2 & \text{if } \pi < \theta_j \leq 2\pi \end{cases} \quad \text{(Eq. 8.30)}$$

$$\sigma_{bend,max} = \frac{24 \cdot M}{\pi \cdot D_c \cdot L^2} \quad \text{(Eq. 8.31)}$$

M = bending moment acting on the concrete plug (kNm)

and:

$$H(\sigma_{cont}(z_i, \theta_j)) = \begin{cases} 0 & \text{if } \sigma(z_i, \theta_j) \leq 0 \\ 1 & \text{if } \sigma(z_i, \theta_j) > 0 \end{cases} \quad \text{(Eq. 8.32)}$$

In this formula, the resulting contact stress, $\sigma_{cont}(z_i, \theta_j)$, may not exceed the maximum contact stress, which is equal to the design compressive strength of concrete, f_{cd}. This condition is therefore as follows.

$$\sigma_{cont}(z_i, \theta_j) \leq f_{cd} \quad \text{(Eq. 8.33)}$$

8.5.4. Results of interaction between normal force and bending moment

This subsection discusses the influence of the bending moment on the normal force resistance using the proposed interaction model. To this end, it was analyzed what the normal force resistance is when a bending moment also acts on the connection. This analysis was again carried out for different diameters of the concrete plug.

To determine the contact stress due to the normal force, as detailed in Chapter 4, various input parameters are required in addition to the varied diameter. These input parameters are primarily assumed to be the same as those used in the example from Section 6.1. The only differences are that for a realistic comparison of different situations with varying diameters, the thickness of the pipe pile and the length of the concrete plug must also vary with the diameter. Therefore, a constant ratio, $D_p/t_p = 50$, is maintained for the ratio between the pile diameter and thickness, and a constant ratio, $L/D_p = 10$, is maintained for the ratio between the plug length and pile diameter. These ratios are practical, as an increase in pile diameter also leads to an increase in the thickness of the pile and the length of the plug.

The contact stress caused by the bending moment can be determined, as in Section 8.1, using the geometry of the concrete plug and the magnitude of the bending moment. The geometry is defined by the pile diameter and the constant ratios between the diameter, pile thickness, and plug length. The magnitude of the bending moment is assumed to equal the bending moment resistance of the reinforced cross-section, using a fixed percentage of reinforcement as specified in Section 8.3.4. In practice, this resistance depends on the design bending moment, as the plug reinforcement is dimensioned to transfer this moment. Consequently, the plug will not always have a fixed reinforcement percentage. To account for this, the influence of the bending moment is determined for several reinforcement ratios, representing different design bending moments. The magnitude of these bending moments can be seen in Figure 8.6.

Figure 8.21 shows the results of the analysis, presenting the normal force resistance for different diameters and bending moments. This resistance was determined using the proposed interaction model. The figure shows resistance for three cases: without a bending moment and with two different bending moments. The bending moments are taken to be equal to the cross-section capacity with two different reinforcement ratios, representing the maximum reinforcement ratio and a lower ratio. The maximum ratio scenario corresponds to the maximum bending moment resistance for each diameter plug, leading

to the largest increase in normal force resistance. However, in practical design situations, the actual bending moment is often lower, resulting in less reinforcement. Therefore, the influence is also shown for a scenario where the bending moment matches the resistance with a lower reinforcement ratio, providing a smaller increase in normal force capacity but representing a more realistic design situation.

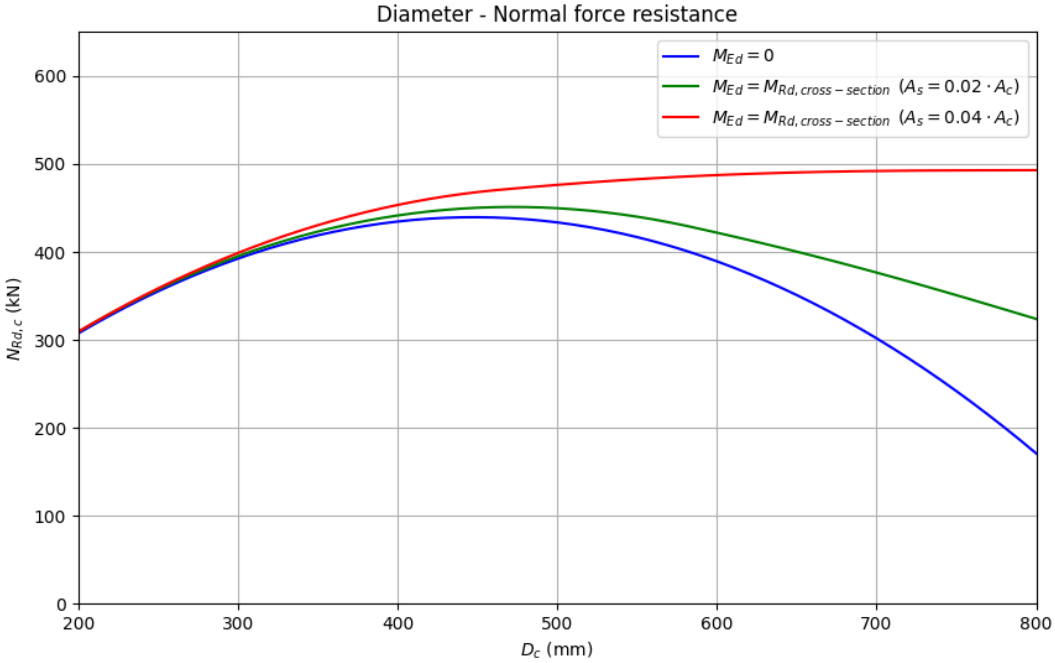

Figure 8.21: Diameter - Normal force resistance.

Figure 8.21 indicates that, as expected with the proposed interaction between normal force and bending moment, the presence of a bending moment leads to additional normal force resistance. This increase is particularly noticeable for larger diameters. This can be explained by the fact that the contact stress caused by the normal force alone decreases with larger diameters, as discussed in subsection 6.2.2. Less contact stress results in lower normal force resistance, and thus a decrease in this resistance is observed for larger diameters in the absence of a bending moment. For larger diameters, the resulting contact stress is mainly influenced by the presence of a bending moment, causing a significant difference in resistance between scenarios with and without a bending moment. For smaller diameters the increase in normal force resistance is smaller, because here the contact stress originating from the normal force is relatively larger, so that the stresses originating from the bending moment have less influence. Another factor that plays a role with smaller diameters is that the bending moment resistance of the cross-section is so lower that it has less influence on the resulting contact stress.

One of the main reasons for the relatively small increase in normal force resistance due to the bending moment is the conservative assumption of transferring the moment over the entire length of the plug. This assumption leads to relatively low additional contact stresses, which in turn result in only a slight increase in normal force resistance. If further research were to be conducted to determine the actual length over which the moment is transferred, the model could be refined to reflect this more accurately. Should this research reveal that the actual length is significantly shorter, the model could predict a higher normal force resistance due to increased contact stresses over the shorter transfer length.

8.6. Conclusion interaction between normal force and bending moment

In the previous section, a model was proposed to estimate the interaction between normal force and bending moment, producing a resulting contact stress distribution. The model assumes that contact stresses originating from the bending moment can lead to additional normal force resistance. Contact stresses from the normal force, determined using Chapter 4, are combined with those from the bending moment's wrenching mechanism. This results in a final stress distribution for the contact stresses between the concrete plug and the steel pipe pile, which can be converted into a normal force resistance using the Coulomb friction principle.

The results of the model showed that practical values for the bending moment could indeed lead to additional normal force resistance. This additional force is mainly observed at larger diameters, while for smaller diameters, the increase is minimal. The difference arises because contact stresses due to the normal force, combined with Poisson's effect, have less influence on the resulting stress distribution for larger pipe pile diameters. As a result, the bending moment has a relatively greater impact on the stress distribution, leading to a more significant difference between scenarios with and without the bending moment.

To use the model in practice, several verifications are necessary. It must be investigated whether the assumed interaction between contact stresses from the normal force and bending moment can indeed be combined as proposed. Additionally, research should focus on the length over which the bending moment is transferred via the concrete plug, as this length significantly influences the level of contact stresses arising from the bending moment and the assumed additional normal force resistance.

9

Discussion

This chapter provides an evaluation of the findings from the previous chapters, focusing on the practical applicability of the proposed theoretical models for the force transfer due to friction. This chapter aims to connect the theoretical research with engineering applications, assessing how the developed model performs in a practical context.

9.1. Applicability of proposed friction model

This section explores the applicability of the friction-based normal force transfer model proposed in Chapter 4. The first part focuses on evaluating the model through a case study involving the design of a concrete plug connection for pipe piles. This analysis assesses whether the normal force resistance predicted by the model is adequate for transferring the loads in the given case study scenario.

The second part of the section expands the discussion to a broader context. It examines the general applicability of the model by analyzing whether the friction-based normal force transfer is proportional to the practical load-bearing requirements of pipe piles in various engineering applications. The study covers different pipe pile diameters to assess the model's effectiveness across a range of scenarios.

9.1.1. Case study analysis

This subsection examines the applicability of the proposed model for normal force transfer through friction. The analysis is based on a practical case study involving connections between open-ended pipe piles and a concrete pile cap using a concrete plug connection. Specifically, the case study pertains to the ”PHS Oostertoegangbruggen” project in Amsterdam. This project entails the replacement of five existing railway bridges on the east side of Amsterdam Central Station, situated between the Prins Hendrikkade and the Ruijterkade, as depicted in Figure 9.1.

As Figure 9.1 shows, the project amounts to five bridges in total. This involves four steel bridges including intermediate and end supports and one concrete bridge including the intermediate supports. The most interesting for this discussion are the steel bridges because both the end and intermediate supports will be completely replaced by new pile-based structures. The design of these new structures is shown in Figure 9.2. In the design of these supports, it was decided to transfer the horizontal loads resulting from the variable loads to the foundation via the intermediate supports. Due to this choice, the governing loads acting on the intermediate supports are the largest, which is why these supports are mainly analyzed in this discussion.

Figure 9.1: Location of ”PHS Oostertoegangbruggen” project.

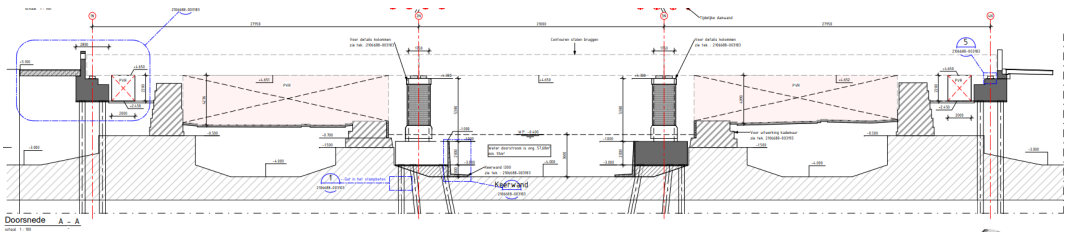

Figure 9.2: Design for the new situation of the steel bridge end and intermediate supports.

9.1.1.1. Design loads combinations intermediate supports

On the intermediate supports a distinction can be made between two different load combinations. The first load combination consists of only a normal force and a negligible bending moment. This load combination is representative of a situation in which only the permanent loads act on the structure. The second load combination arises from a combination of these permanent loads and the variable loads acting on the structure. As a result, in addition to a higher normal force, this combination also has an additional bending moment that must be taken into account.

Table 9.1 shows the governing loads for both load combinations. This shows both the maximum normal force and the maximum bending moment that must be transferred to each pile from the concrete cap. This therefore equals the load acting on each concrete plug connection.

Table 9.1: Design load combinations intermediate supports.

Load combination	N_{Ed} (kN/pile)	M_{Ed} (kNm/pile)
Permanent load	900	0
Permanent load + Variable load	2400	350

The governing combination for assessing normal force resistance is the load case that includes both permanent and variable loads. This combination is critical because it results in a significantly higher design normal force compared to the situation with only permanent loads. Additionally, the positive effect of the bending moment on friction, as discussed in Section 8.4, is not considered in this assessment due to the lack of model verification and the relatively small magnitude of the bending moment compared to the normal force to be transferred.

9.1.1.2. Normal force resistance through friction

Initially, it will be analyzed whether the normal force can be transferred by friction, so that no mechanical connections need to be installed in the pipe pile. This could have the advantage of preventing additional costs and labor-intensive work. To determine the normal force resistance due to friction, the proposed model from Chapter 4 will be used.

To determine the normal force resistance using the model from Chapter 4, firstly the geometry of the steel pipe pile and the concrete plug from the case study are required. The dimensions associated with this geometry are shown in Table 9.2. The dimensions of the pipe pile are a result of a calculation for the geotechnical pile bearing capacity. With these pipe pile dimensions, the total geotechnical pile bearing capacity is approximately equal to the design normal force.

Table 9.2: Element geometry case study.

Element geometry		
Outer diameter steel pipe pile	D_p	= 600 mm
Wall thickness steel pipe pile	t_p	= 10 mm
Outer diameter concrete plug	$D_c = D_p - 2 \cdot t_p$	= 580 mm
Length of the concrete plug	L	= 6000 mm

In addition to the geometry of the connection, the material properties of both the concrete and steel are also required to determine the normal force resistance using the proposed model. In the case study, strength class C30/37 was used for the concrete. The concrete properties of this strength class are shown in figure 9.3.

Table 9.3: Concrete material properties case study (NEN EN 1992-1-1).

Concrete property		
Characteristic cylinder compressive strength	f_{ck}	= 30 MPa
Mean compressive strength	$f_{cm} = f_{ck} + \Delta f$, $\Delta f = 8$	= 38 MPa
Design compressive strength	$f_{cd} = f_{ck}/\gamma_c$, $\gamma_c = 1.5$	= 20 MPa
Young's modulus after 28 days	$E_{cm} = 22000 \cdot (0.1 \cdot f_{cm})^{0.3}$	≈ 30589 MPa
(Initial) Poisson ratio	ν_c	= 0.20

The properties of the steel of the pipe pile have been determined using steel class S235. The required steel properties for the model are shown in table 9.4.

Table 9.4: Steel material properties case study.

Steel property		
Design yield strength	f_{yd}	= 235 MPa
Young's modulus	E_s	= 210 GPa
Poisson ratio	ν_s	= 0.30

In addition to the geometry of the connection and the material properties, the input values are also required for the Coulomb friction coefficient and the factor for the surface irregularities. These two values have been entered as respectively 0.512 and 0.036 as determined in section 6.3.2.2, whereby the model parameters have been updated. Furthermore, the value for the concrete shrinkage has been determined for a period of 100 years, which is equal to the design life time of the bridge from the case study.

After entering all these input parameters in the model, the normal force resistance due to friction, $N_{Rd,c}$, was equal to 318 kN. With this resistance the unity check can then be determined for the governing load situation. This governing situation is the situation in which both permanent and variable loads act on the structure. The unity check with the resistance due to friction is as follows:

$$UC = \frac{N_{Ed}}{N_{Rd,c}} = \frac{2400}{318} = 7.55 > 1.0 \rightarrow not\ ok \quad \text{(Eq. 9.1)}$$

It can be concluded that the unity check for the normal force with the resistance due to friction is well above 1.0, which means that this resistance is not sufficient. As a result, it is not sufficient to transfer the normal force through friction, so mechanical connections are required to transfer the normal force.

9.1.1.3. Normal force resistance through shear rings

As shown in the previous paragraph, the normal force cannot be transferred by friction in the case study. mechanical connections are therefore required for transferring the normal force as an alternative to this friction. The use of shear rings was chosen for these mechanical connections. This resistance per shear ring can be determined as explained in Chapter 7.

To determine the capacity of these shear rings, in addition to the already given geometry of the pipe pile and concrete properties (Table 9.2 and 9.3), the geometry of the rings is required. For this geometry of the rings, the minimum dimensions given in CUR Recommendation 77 have been adopted. The resulting dimensions for the geometry are included in table 9.5.

Table 9.5: Geometry of shear rings.

Ring geometry		
Height of shear ring	h	= 25 mm
Width of shear ring	w	= 25 mm
Spacing of the shear rings	s	= 85 mm

Using the geometry of the shear rings, the normal force resistance, $N_{Rd,ring}$, can be determined per shear ring according to Chapter 7. This resistance per shear ring is equal to 639 kN. The number of rings required to transfer the governing normal force can then be determined by dividing this load by the resistance per ring. This is shown below.

$$n = \frac{N_{Ed}}{N_{Rd,ring}} = \frac{2400}{639} = 3.76 \rightarrow 4\ shear\ rings\ required \quad \text{(Eq. 9.2)}$$

As can be concluded from the above calculation, at least 4 shear rings are required to transfer the normal force.

9.1.2. General evaluation of applicability

In addition to the situation of the case study, it is also interesting to analyze the general applicability of the model, so that it can be determined for more situations whether it is interesting to realize the transfer of force with friction. Whether this is interesting depends on whether the normal force resistance due to friction between the plug and the pipe pile is comparable to the design normal forces that occur in practice. A first benchmark would be to compare the normal force resistance of the steel pipe pile itself with the normal force resistance that can be achieved with friction. If the resistance due to friction comes close to the resistance of the steel pipe itself, it could be concluded that the steel pipe pile can be fully utilized and it is therefore attractive to transfer the force through friction. The normal force resistance of the steel pipe pile can be determined using the expression below. The resistance is given as the surface area of the steel pipe pile multiplied by the design yield strength of the steel.

$$N_{Rd,pile} = A_{pile} \cdot f_{yd} \quad \text{(Eq. 9.3)}$$

where:

$$A_{pile} = \frac{(D_p^2 - D_c^2) \cdot \pi}{4} \quad \text{(Eq. 9.4)}$$

D_p = outer diameter of pile (mm)
D_c = outer diameter of concrete plug (mm)

and:

f_{yd} = design yield strength (MPa)

To compare these resistances for multiple situations, different diameters of the pipe pile are examined. This was chosen because in practice the diameter of the pipe pile is often adjusted based on the design load that must be transferred per pile. This is due to the fact that with a larger pile diameter the geotechnical load-bearing capacity increases, meaning that more normal force can be transferred per pile. When the diameter is adjusted in practice, the thickness of the pipe pile and the length of the concrete plug often change accordingly. For this purpose, firstly, a constant ratio, $D_p/t_p = 50$, has been maintained for the ratio between the diameter and thickness of the pipe pile. Secondly, a constant ratio, $L/D_p = 10$, was used for the ratio between the length of the concrete plug and the diameter of the pipe pile. These ratios are required to determine the geometry of the concrete plug connection and therefore the normal force resistance. In addition to this geometry, the material properties are also required. These properties are assumed to be the same as in the case study from section 9.1.1.2. Figure 9.3 shows the final comparison between the normal force resistance of the pipe pile and the normal force resistance due to friction for several diameters.

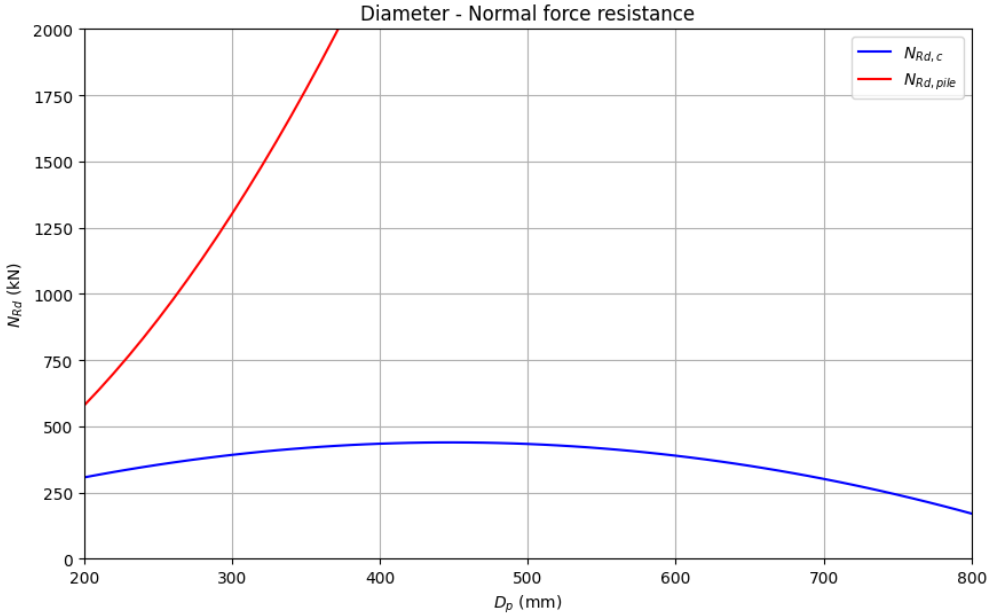

Figure 9.3: Diameter - Normal force resistance.

From Figure 9.3, it can be concluded that the difference between the normal force resistance of the pipe pile and the normal force resistance that can be transferred by friction is relatively large, especially for larger diameters. The difference is so significant that transferring the forces via friction does not come close to utilizing the normal force capacity of the pipe pile. However, in practice, the normal

force resistance of the pipe pile itself is rarely decisive for the ultimate normal force resistance that can be transferred per pipe pile. This is because the geotechnical load-bearing capacity of the pipe pile is typically lower than its normal force resistance. Determining the geotechnical load-bearing capacity per pipe pile diameter is not feasible for this comparison and varies greatly with factors such as soil layer composition. Therefore, an assumption must be made to roughly estimate the geotechnical bearing capacity for different diameters.

This assumption will be based on a fixed relationship between the normal force resistance of the pipe pile and the geotechnical load-bearing capacity. Therefore, the normal force resistance of the pipe pile will be reduced to reflect its geotechnical load-bearing capacity. The factor used for this reduction is derived from the case study, which provided a ratio between the normal force resistance of the pipe pile and its geotechnical bearing capacity. In the case study, this factor was 0.55, meaning the geotechnical bearing capacity was only 55% of the normal force resistance of the pipe pile.

The utilization of the geotechnical load-bearing capacity can then be determined using this assumption. This can be obtained by dividing the normal force resistance due to friction by the reduced normal force capacity of the steel pipe pile, which represents the geotechnical load-bearing capacity. This is shown in the expression below.

$$\eta = \frac{N_{Rd,c}}{0.55 \cdot N_{Rd,pile}} \tag{Eq. 9.5}$$

where:

$N_{Rd,c}$ = normal force resistance due to friction (kN)
$N_{Rd,pile}$ = normal force resistance of the steel pipe pile (kN)

Figure 9.4 shows the results of the utilization ratio between the assumed geotechnical load-bearing capacity and the normal force resistance due to friction. It can be concluded that the utilization is relatively low, especially for larger diameter piles. As a result, if the load is transferred via friction, a significant portion of the geotechnical load-bearing capacity will remain unused, leading to capacity loss and potentially requiring more piles to transfer the total load.

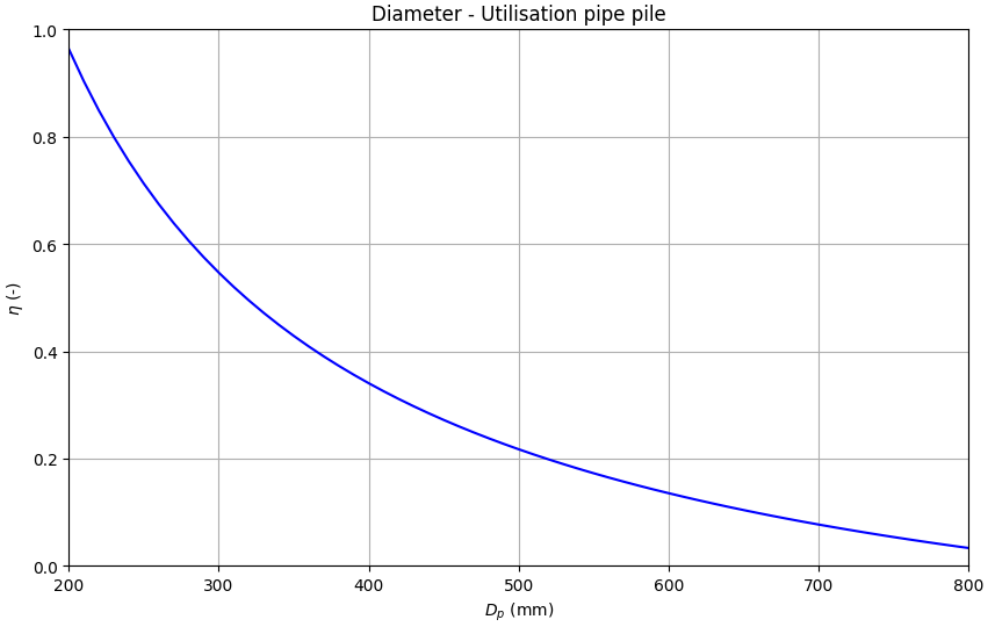

Figure 9.4: Diameter - Utilisation pipe pile.

An alternative to transferring the normal force via friction is the use of mechanical connections, such as shear rings, as previously discussed. Figure 9.5 illustrates a comparison between the normal force resistance achieved through friction and the total normal force resistance achieved with an increasing number of shear rings. The geometry of these rings is the same as specified in Table 9.5. The figure demonstrates that using rings can achieve a significantly higher normal force capacity compared to friction. Therefore, the use of rings can help better utilize the geotechnical load-bearing capacity of the pipe piles, which may reduce the number of piles needed to carry the total load.

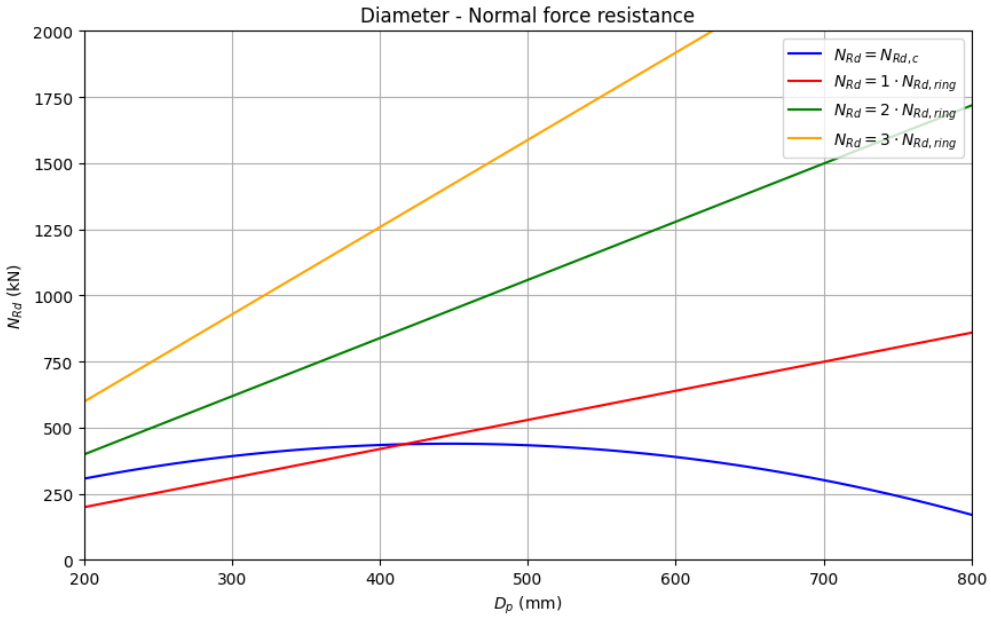

Figure 9.5: Diameter - Normal force resistance.

9.1.3. Conclusion of discussion on applicability of proposed friction model

The analysis concludes that the normal force resistance provided by the proposed friction model is generally insufficient for practical design applications. Specifically, in the case study, this frictional resistance falls short of transferring the design loads from the concrete cap to the steel pipe pile, necessitating the use of mechanical connections for effective load transfer. Furthermore, a broader examination of various pipe pile diameters revealed that the friction model's capacity is not proportional to the geotechnical load-bearing capacity, especially for larger diameters.

This discrepancy implies that relying solely on friction for normal force transfer results in a lower effective resistance compared to the geotechnical bearing capacity, which could require the use of additional piles to achieve the desired load transfer. Given practical constraints, such as limited space for additional piles and increased costs associated with additional piles and larger concrete caps, alternative mechanical connections, such as shear rings, offer a more viable solution. Shear rings provide significantly higher normal force resistance compared to friction, enabling a more efficient use of the geotechnical load-bearing capacity and potentially reducing the need for additional piles.

9.2. Inclusion of normal force and bending moment interaction

In Chapter 8 a model was proposed in which the influence of the bending moment on the normal force resistance was included. In this model, the contact stresses caused by the bending moment are combined with the contact stresses caused by the normal force originating from the Poisson's effect. The contact stresses caused by the normal force can be obtained from the model in Chapter 4, where the normal force resistance by friction can be determined.

Due to the additional contact stresses originating from the bending moment, an additional normal force resistance can be achieved with the proposed model. How significant this additional normal force resistance will be and whether it will have a major influence on the total normal force capacity must be analyzed. If this has relatively little influence on the total normal force capacity and therefore gives little additional resistance, taking this moment into account will have little influence on the choice of using mechanical connections for the purpose of transferring the normal force.

The influence of the bending moment on the normal force capacity depends on several factors, including the value of the bending moment acting on the connection and the geometry of the connection. The value of the bending moment is a fixed design value for the design of the concrete plug connection, which is determined by the forces acting on the entire structure and the overall design of the structure. This value cannot therefore be adjusted to achieve a higher normal force resistance. However, this value is limited by the maximum bending moment resistance of the concrete plug connection. This maximum resistance is, as determined in Chapter 8, dependent on the bending moment resistance of the cross-section of the plug. The maximum bending moment resistance of the cross-section can be determined, with the maximum allowable reinforcement ratio being applied in the cross-section. This maximum allowable reinforcement ratio according to Eurocode 2 is equal to 0.04. The geometry of the connection differs per situation and depends on the diameter of the pipe pile. In practice, this diameter is chosen based on the required geotechnical load-bearing capacity per pipe pile. The thickness of the pipe pile and the length of the plug are also often proportional to this diameter.

To analyze the influence of the bending moment on the normal force resistance, the normal force resistance is plotted in Figure 9.6. The resistance is shown for both a situation without a bending moment and with a bending moment. For the situation with a bending moment, a bending moment has been used that is equal to the maximum moment resistance of the cross-section. This therefore means the resistance of a cross-section provided with maximum reinforcement. This is an extreme situation that is very unlikely in practice, but it does allow for a good look at the maximum additional normal force resistance and thus the strength of the model. In addition, the resistance is plotted for different diameters of the pipe pile, which are often used in practice. It was also necessary to maintain realistic values for the thickness of the pile and the length of the plug for these different diameters. For this purpose, firstly, a constant ratio, $D_p/t_p = 50$, has been maintained for the ratio between the diameter and thickness of the pipe pile. Secondly, a constant ratio, $L/D_p = 10$, was used for the ratio between the length of the concrete plug and the diameter of the pipe pile. Other input parameters, such as the material properties, are again assumed to be the same as in the case study from section 9.1.1.2.

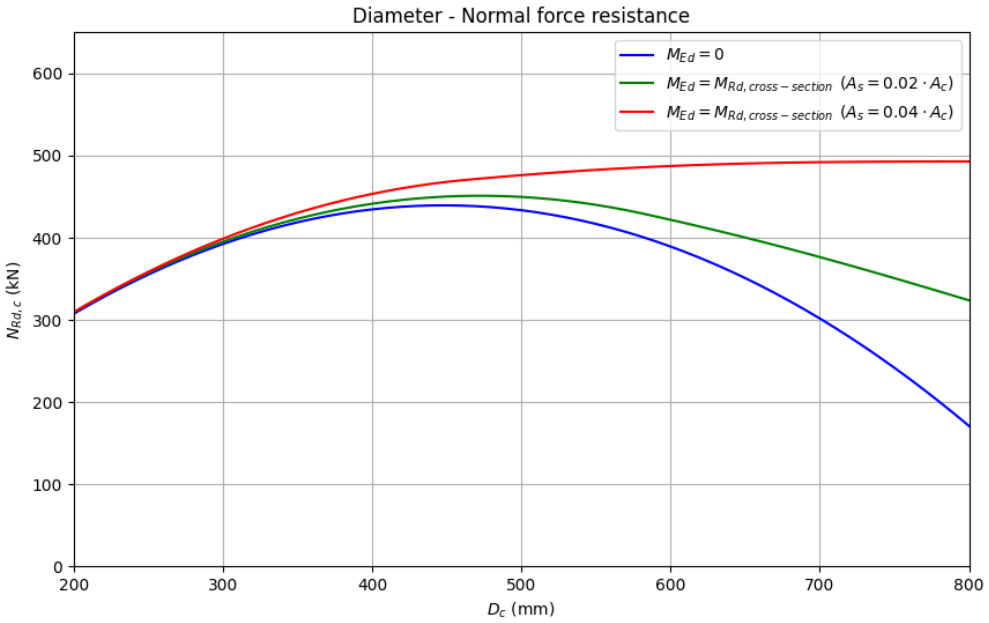

Figure 9.6: Diameter - Normal force resistance with and without bending moment.

From Figure 9.6 it can be concluded that with a maximum bending moment, as expected, the normal force capacity increases compared to a situation without bending moment. This increase is especially noticeable for larger diameters, where the normal force resistance without bending moment starts to decrease again. This is because the contact stresses originating from the normal force decrease with larger diameters. For smaller diameters the increase in normal force resistance is smaller, because here the contact stress originating from the normal force is relatively larger, so that the stresses originating from the bending moment have less influence. Another factor that plays a role with smaller diameters is that the bending moment resistance of the cross-section is significant lower and therefore has less influence on the resulting contact stress.

Although Figure 9.6 indicates an increase in normal force resistance due to the bending moment, it does not conclusively determine whether this increase is sufficient to eliminate the need for mechanical connections. A comparison with the assumed geotechnical load-bearing capacity of the pipe pile, as in subsection 9.1.2, is necessary. This subsection analyzed the extent to which the geotechnical load-bearing capacity could be utilized without mechanical connections. The geotechnical bearing capacity was assumed to be 55% of the pipe pile's normal force resistance. Figure 9.7 shows the utilization of the assumed geotechnical load-bearing capacity for different diameters, with and without bending moment.

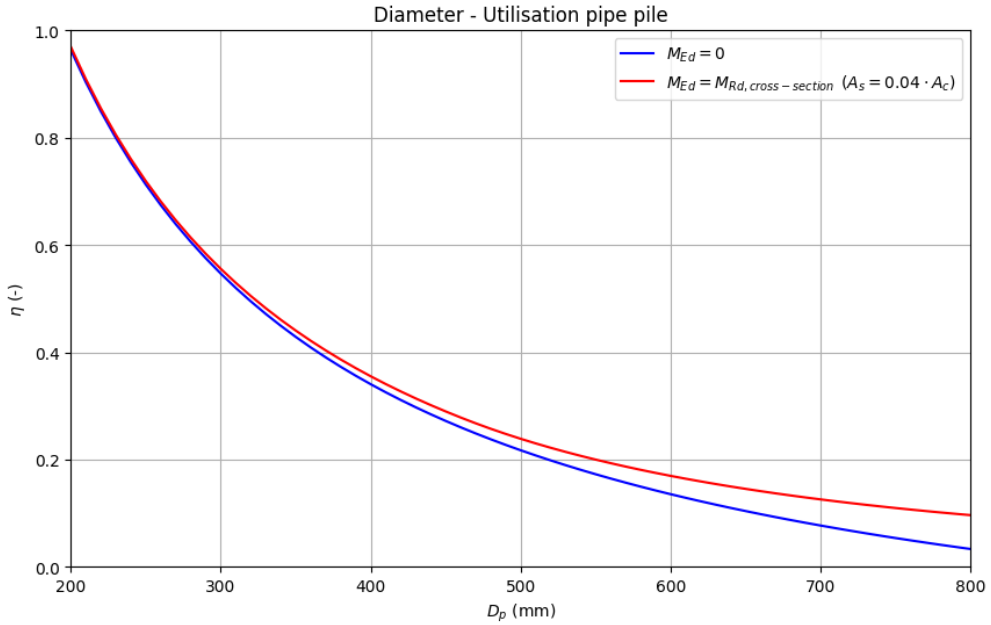

Figure 9.7: Diameter - Utilisation pipe pile with and without bending moment.

Figure 9.7 indicates that while the bending moment increases the utilization of the steel pipe pile, this increase is small. For smaller diameters, the increase is negligible, making the interaction between normal force and bending moment in the model practically insignificant. For larger diameters, the increase is relatively more substantial, but the overall utilization remains low, limiting its practical application. It should also be noted that this comparison has been made for a situation where the present bending moment is equal to the maximum moment resistance of the cross-section where a maximum amount of reinforcement has been applied. In practice, the design bending moment will usually be lower than this bending moment resistance, so that the influence of the bending moment on the utilization will be even more minimal.

9.2.1. Conclusion of discussion on inclusion of normal force and bending moment interaction

The proposed model incorporating the interaction between normal force and bending moment shows that while the presence of a bending moment can indeed increase normal force resistance, this increase is relatively small. For smaller diameters, the effect is minimal, making the interaction's impact negligible. Although the increase is more significant for larger diameters, it remains insufficient to fully utilize the geotechnical load-bearing capacity of the pipe pile. Consequently, despite some additional resistance from the bending moment, mechanical connections such as shear rings are still necessary to achieve the required normal force resistance.

10

Conclusions and Recommendations

This chapter provides the most important conclusions that can be drawn from the results of this thesis. In addition, a main conclusion is given to the main question from the introduction and recommendations are given for further research into this topic.

10.1. Conclusions

In this thesis, research was conducted into the force transfer between concrete substructures and steel pipe piles. Specific research has been conducted into a situation in which a connection is made between these two elements using a concrete plug in the steel pipe pile. The load cases that must be transferred and which have been included in the research consist of a situation in which a normal force acts on the concrete plug and a situation in which a normal force in combination with a bending moment acts on the concrete plug. These forces can be transferred through the concrete plug by two different methods. These methods consists of friction, also referred to as bond, and welded elements such as shear rings or studs, also referred to as mechanical connections. In practice, force transfer through friction is preferred, because the installation of mechanical connections is often both labor and cost-intensive.

However, the transfer of forces through friction is not always fully permitted in practice. For example, Rijkswaterstaat demands, through the requirements of the ROK V2.0, that when forces have to be transferred from the concrete part in the pile to the steel pile, this force transfer is not permitted to be fully realized via friction between the concrete and steel. However, the requirement provides little clarification as to why this is not permitted and what proportion of the forces may be transferred through friction. A literature study was carried out into other sources that describe something about the transfer of force through friction.

In this study it was found that existing design codes and recommendations for this specific application are very limited and again do not provide a clear answer to what part of the forces can be transferred by friction. For example, Eurocode 4 and The British Standard (BSI) only describe a standard value that can be applied for the bond strength between steel and concrete. These values that are described differ substantially and are not dependent on parameters found from the parameter study, such as the geometry of the connection and the concrete shrinkage. Using a standard value for the bond strength, while in practice this strength depends on several parameters, can lead to the bond strength being over- or underestimated in certain situations. This makes using this standard value less desirable.

Furthermore, there are design models for the bond strength of grouted sleeve connections, which according to Nezamian et al. (2002) could be applied for the bond strength of concrete plug connections. However, the applicability of these models to a different type of application, and therefore a situation for which they have not been validated, is uncertain.

As a result of the literature study, it was decided to set up a new analytical model for determining the bond strength between concrete and steel for plugged connections. This new model uses the geometry of the connection, the material properties of both concrete and steel and other factors such as concrete shrinkage, surface irregularities and Coulomb friction coefficient as input for determining the bond strength. The most uncertain parameters in the model are the surface irregularities and the Coulomb friction coefficient. At the same time, these factors also have a relatively large influence on the output of the model. It was therefore decided to update these factors based on the results of various push-out tests. This update showed that the model provides relatively conservative values for the bond strength with a value for the surface irregularities of 0.036 millimeters and a value of 0.5 for the Coulomb friction coefficient. The predictions of the updated model for the bond strength do have a relatively large Mean Average Error (MAE) of 0.589 MPa, which is mainly due to the large sizes of scatter in certain test sets, which were used for the update. However, for test results with a lower degree of scatter, for which it was decided to give more weight to the update, this MAE is relatively small.

It was also analysed, using the model, what the most important influencing factors were on the bond strength between steel and concrete for plugged connections. When analysing specifically for the geometry of the connection, it appears that the diameter in particular has a very significant influence on the bond strength. This shows that for smaller diameters the bond strength is relatively high and could possibly be used to transfer the normal force, while for larger diameters this is less possible because the bond strength is significantly lower. This can be explained by the fact that with a larger diameter of the pipe pile, the effect of confinement on the concrete plug decreases. Another factor that also plays a role in lower bond strength with larger diameter piles is that the effect of concrete shrinkage increases. This shrinkage also has a major influence on the bond strength in the model, because with more shrinkage less contact pressure is created between the steel and concrete. In final design situations it may therefore be recommended to use concrete with less shrinkage, so that the bond strength is less reduced.

Figure 10.1 shows the bond strength results for different diameters piles using this model. These results were determined once with the shrinkage determined as the Model Code prescribes and once the results were determined without shrinkage. Furthermore, the other parameters such as the thickness of the pipe pile and the length of the concrete plug in the model have also been adjusted to realistic values that correspond to the diameter for which the result is shown.

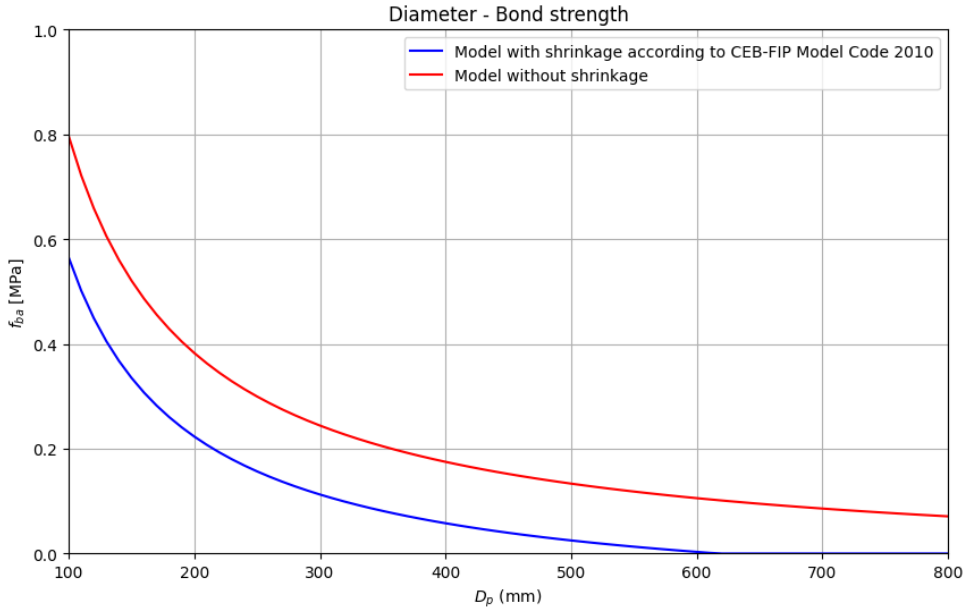

Figure 10.1: Bond strength versus different diameters of the steel pile.

When it is not possible to transfer the normal force through friction, for example with larger diameter piles, mechanical connections can be applied. Shear rings can be used for these mechanical connections on the inside of the steel pipe pile to transfer the normal force. These mechanical connections can be verified using the calculation recommendations and requirements from both Eurocode 4 and CUR Recommendation 77. The shear rings can be then verified as a block dowel when it is assumed that the shear connection fails due to the failure of the concrete in compression.

In addition to a normal force, in many cases a bending moment must also be transferred from the substructure to the steel pipe pile. This moment can be transferred by the wrenching mechanism of the concrete plug in the steel pipe pile, which arises as a result of the bending moment. The stress distribution that can be assumed, due to wrenching, is linear across the height of the plug and sinusoidal around the circumference of the plug. This assumption can be made when the contact stresses remain within the allowable concrete compressive stress. The length of the plug must be determined in such a way that the contact pressures that arise between the concrete and steel do not exceed both the maximum allowable concrete compressive stress and the maximum allowable hoop stress in the steel pipe pile.

Furthermore, research has also been carried out into the interaction between the bending moment and the normal force. A model has been proposed for this purpose, in which the contact stresses that arise as a result of the bending moment are combined with the contact stresses that arise as a result of the normal force to obtain a resulting contact stress distribution. Due to this interaction, it has been assumed that in the event of a dominant bending moment, additional normal force resistance can be obtained because more contact stresses arise between the concrete and steel. However, for the application of this model, a number of verifications must be made regarding the assumed resulting stress distribution and the length over which the moment is introduced in the concrete plug.

10.2. Final conclusion

All these conclusions ultimately lead to a final conclusion on the main research question from the introduction. This question was as follows:

"To what extent can the force transfer in concrete plug connections within open-ended steel pipe piles be achieved without mechanical connections, and how does this compare to a situation with mechanical connections?"

In this thesis, research was carried out into the force transfer in concrete plug connections in steel pipe piles, specifically studying the possibility to realise the transfer of forces without relying on mechanical connections. The forces investigated include normal force and bending moment. In practice, these two types of forces are often critical in applications such as bridges, which is the specific focus of this research.

First, research was conducted into the possibility of transferring the normal force without mechanical connections. In the absence of mechanical connections, the normal force must be transferred by another mechanism. This mechanism, which has been the subject of research in this thesis, is the friction between the steel pipe pile and the concrete plug. This friction which is commonly referred to as 'bond' in the literature and will be referred to as such hereafter. To determine the normal force resistance due to friction, a model has been proposed in this thesis in Chapter 4. With this model, the normal force resistance can be determined as well as the average bond strength between the concrete plug and the steel pipe pile, based on the various design parameters of the connection.

The results of the model show that it is indeed possible to transfer normal force via friction with concrete plug connections. However, this frictional resistance is relatively small, particularly for larger diameters, when compared to the practical loads that need to be transferred. As already discussed in the Discussion chapter, the geotechnical load bearing capacity for which a certain diameter pile is used often cannot be utilized with the resistance through friction. This means that if the resistance due to friction is taken as the governing normal force resistance, more piles are required to transfer the total load from the substructure to the ground.

Given practical constraints, using additional piles is often undesirable due to the increased costs associated with both the extra piles and a larger concrete cap. Consequently, in the Discussion chapter an analysis was conducted to compare the normal force resistance achievable with mechanical connections against that provided by friction. The mechanical connection explored in this comparison consists of shear rings installed on the inside of the steel pipe pile, which have been evaluated using the calculation recommendations and requirements from Eurocode 4 and CUR Recommendation 77. This analysis demonstrated that shear rings can achieve significantly higher normal force resistance compared to friction. As a result, the geotechnical load-bearing capacity of the pipe pile can be utilized more effectively, eliminating the need for additional piles and making mechanical connections a more efficient solution than relying on friction.

Regarding the transfer of the bending moment, it was found that this bending moment could be transferred via the wrenching mechanism between the concrete plug and the steel pipe pile. As a result of the bending moment, the concrete plug starts to wrench in the steel pipe pile, causing contact stresses across the height of the interface between these two elements. The bending moment is transferred through these contact stresses, which can be represented by a linear distribution along the height and a sinusoidal distribution around the circumference of the plug, provided that the stresses do not exceed the allowable concrete compressive strength. The structural verification of the bending moment can thus be performed by evaluating the allowable stresses for a given design moment or by calculating the bending moment resistance from the maximum allowable stress. However, it has been found that the wrenching mechanism is not governing the maximum allowable bending moment resistance of the plug, but that bending moment resistance of the cross-section of the plug itself is governing because this resistance is lower. This resistance will therefore determine the final allowable bending moment of the connection.

To summarize, this research highlights that friction alone can achieve normal force transfer in concrete plug connections, but it is often insufficient for larger piles where mechanical connections like shear rings offer a more effective solution. While the wrenching mechanism can manage bending moments, the ultimate bending moment resistance is dictated by the concrete plug's cross-sectional strength. Overall, the study shows that mechanical connections are a more efficient way to transfer normal force and should therefore often be applied in effective design.

10.3. Recommendations

Various recommendations follow from the research that can be used for further research into force transfer using a concrete plug. These recommendations are as follows:

1. **Update model parameters with help of longitudinal stress distributions**
   In the current model update, two parameters have been updated; the surface irregularities and the Coulomb friction coefficient. However, from test results, only the bond strength was available to perform this update. In theory, multiple variations of these updated parameters could lead to a good estimation of the test results via the model, because the parameters have a similar effect on the bond strength in the model. A solution to this could be to obtain longitudinal stress distributions over the height of the plug via push-out tests. These distributions can be used as a second factor in the cost function of the update. This is possible because the Coulomb friction coefficient has a different influence than the surface irregularities on this longitudinal stress distribution and therefore the parameters can be better distinguished from each other in the update.

2. **Bending moment stress distribution around the circumference**
   To transfer the bending moment via wrenching, a stress distribution must be assumed over both the height and circumference of the plug, which arises due to the bending moment. For the circumferential stress distribution, it has been determined that either a sinusoidal or quadratic sinusoidal distribution can be assumed. Comparing these two, the sinusoidal distribution results in a lower bending moment resistance and is recommended for design purposes, as it is more conservative when there is uncertainty about the actual stress distribution. Future research could verify which distribution actually occurs in practice. If it is found that a quadratic sinusoidal distribution is more accurate, this would result in a higher wrenching bending moment resistance.

3. **Safety factor for proposed model with normal force through friction**
   For the new model in which the normal force capacity can be determined by friction, a safety factor must be applied so that a design value for the bond strength can be determined. This safety factor was initially determined in accordance with Appendix D from Eurocode 0. However, the safety factor from this determination is very conservative, which means that test results for bond strength are relatively underestimated by the model. This has several causes, such as the large amounts of scatter in the test results used to determine the safety factor and the lack of available results. This leads to a more conservative safety factor with the Eurocode determination. In addition, the model parameters have also been updated relatively conservatively, because they have mainly been updated based on the test data that was overestimated in the first place. In addition to the conservative safety factor, this also leads to a more conservative model. It is therefore recommended to collect more test results or to collect test results that contain less scatter, so that the safety factor can be determined on more reliable data. Another option is to have a safety factor determined using a method other than the one from Appendix D from Eurocode 0.

4. **Interaction between normal force and bending moment**
   There is limited literature on the interaction between the normal force and bending moment in the concrete plug. It is expected that a large bending moment will create additional contact pressures due to the deformation of the concrete plug within the steel pipe pile, potentially increasing the normal force capacity. This thesis proposes an interaction model for this purpose. However, to apply this model in practice, several verifications are necessary. It must be demonstrated that the assumed resulting contact stress distribution around the circumference of the concrete plug actually occurs. Additionally, research must be conducted into the length over which the bending moment is transferred from the concrete plug to the steel pipe pile.

5. **Estimation of concrete plug shrinkage**
   The concrete shrinkage has been found to be one of the most important influencing factors on the bond strength between the concrete plug and the steel pipe pile. This, therefore, has a major influence on the normal force resistance of the concrete plug connection. In this thesis, the amount of shrinkage for the input of the proposed model for the normal force resistance was determined using the shrinkage model from the CEB-FIP Model Code 2010. However, it is uncertain to what extent this model can accurately determine the concrete shrinkage of steel-concrete structures. This is because steel-concrete structures, such as the concrete plug, generally have lower shrinkage than normal concrete structures. As a result, there is a possibility that the model of the CEB-FIP Model Code 2010 overestimates the shrinkage values of the concrete plug.

   Research by Chen et al. (2023) confirms this possibility. The researcher conducted research into the shrinkage in concrete-filled steel tube (CFST) columns and concluded that the shrinkage in this type of column is overestimated by the shrinkage model of the Model Code. This was explained by the fact that the Model Code mainly overestimates the drying shrinkage of the concrete, the type of shrinkage that is partly prevented by the confinement of the surrounding steel tube. A solution, according to the researcher, was to assume a higher value for the relative humidity in the Model Code model than prescribed in the standard. This will lead to a reduction in the drying shrinkage resulting from the model.

   However, in practice, it is still uncertain what the exact shrinkage of the concrete plug will be and which factors exactly contribute to this. This uncertainty is due to a lack of literature on the shrinkage determination for concrete plug connections. It is therefore recommended that further research be conducted into the shrinkage for this application. If it can be demonstrated that the shrinkage can indeed be assumed to be lower than in the Model Code model, this will result in higher bond strength and, therefore, higher normal force resistance.

References

[1] T. Aly et al. “Incremental collapse threshold for pushout resistance of circular concrete filled steel tubular columns”. In: *Journal of constructional steel research* (2009), pp. 11–18.

[2] British Standards Institution. *BS 5400: Steel, concrete and composite bridges - Part 4: Code of practice for design of concrete bridges*. Tech. rep. BS 5400-4. London, UK: British Standards Institution, 2005.

[3] Z. Chen et al. “Creep and shrinkage monitoring and modelling of CFST columns in a super high-rise under-construction building”. In: *Journal of buidling engineering* (2023).

[4] CUR. *CUR-Aanbeveling 77:2014 Rekenregels voor ongewapende onderwaterbetonvloeren*. Tech. rep. 77. CROW, 2014.

[5] Det Norske Veritas AS. *DNV-OS-J101: Design of Offshore Wind Turbine Structures*. Tech. rep. DNV-OS-J101. Høvik, Norway: Det Norske Veritas AS, 2013.

[6] European Committee for Standardization. *Eurocode 0: Basis of Structural Design*. Tech. rep. EN 1990. Brussels, Belgium: European Committee for Standardization, 2002.

[7] European Committee for Standardization. *Eurocode 1: Actions on Structures - Part 1-4: General Actions - Wind Actions*. Tech. rep. EN 1991-1-4. Brussels, Belgium: European Committee for Standardization, 2005.

[8] European Committee for Standardization. *Eurocode 2: Design of Concrete Structures - Part 1: General Rules and Rules for Buildings*. Tech. rep. EN 1992-1-1. Brussels, Belgium: European Committee for Standardization, 2004.

[9] European Committee for Standardization. *Eurocode 2: Design of Concrete Structures - Part 2: Concrete Bridges - Design and Detailing Rules*. Tech. rep. EN 1992-2. Brussels, Belgium: European Committee for Standardization, 2005.

[10] European Committee for Standardization. *Eurocode 3: Design of Steel Structures - Part 1-1: General Rules and Rules for Buildings*. Tech. rep. EN 1993-1-1. Brussels, Belgium: European Committee for Standardization, 2005.

[11] European Committee for Standardization. *Eurocode 4: Design of Composite Steel and Concrete Structures - Part 2: General Rules and Rules for Bridges*. Tech. rep. EN 1994-2. Brussels, Belgium: European Committee for Standardization, 2005.

[12] M.J. Gebman, S.A. Ashford, and J.I Restrepo. *Axial Force Transfer Mechanisms within Cast-In-Steel-Shell Piles*. Research Project. San Diego La Jolla, 2006.

[13] L. Menard. “The Menard Pressuremeter: Interpretation and Application of the Pressuremeter Test Results to Foundations Design”. In: *Sols-Soils* 26 (1975).

[14] A. Nezamian. “Bond strength of concrete plugs embedded in tubular steel piles”. PhD thesis. Monash University, 2003.

[15] NORSOK Standard. *NORSOK N-004: Design of Steel Structures*. Rev. 3. Norway: Standard Online AS for NTNU Universitetsbiblioteket, Feb. 2013.

[16] *OTC 4715: New API Equation for Grouted Pile-to-Structure Connections*. Offshore Technology Conference. 1984.

[17] Rijkswaterstaat. *Guidelines for Nonlinear Finite Element Analysis of Concrete Structures*. Tech. rep. RTD 1016-1. Version 2.3. Rijkswaterstaat, 2022.

[18] C.W. Roeder, B. Cameron, and C.B. Brown. “Bond strength in concrete filled steel tubes”. In: *Journal of structural engineering* (1999), pp. 477–484.

[19] ROK. *Richtlijnen Ontwerp Kunstwerken*. Tech. rep. Rijkswaterstaat GPO, 2017.

[20] H. Shakir-Khalil. “Pushout strength of concrete-filled steel hollow sections”. In: *The structural engineer* (1993).

[21] M.T. Stephens, D.E. Lehman, and C.W. Roeder. “Verbinding tussen buispalen en landhoofden bij integraalviaducten”. In: *Engineering Structures* 122 (2016), pp. 323–337.

[22] M. Steunenberg, R.G. Sexsmith, and S.F. Stiemer. “Seismic behavior of steel pile to precast concrete cap beam connections”. In: *Journal of Bridge Engineering* 3.4 (1998), pp. 177–185.

[23] Delft University of Technology. *CIEM0000: Interdisciplinary Mechanics and Design for Civil Engineering*. 2022.

[24] United Kingdom Department of Energy. *Guidance on Design, Construction and Certification of Offshore Installations*. Tech. rep. London, UK: United Kingdom Department of Energy, 1992.

[25] K.S. Virdi and P.J. Dowling. “Bond strength in cocnrete filled steel tubes”. In: *IABSE proceedings* (1980), pp. 125–139.

[26] Lin Wan-Wendner, Ioan Pop, and Werner Vits. “Optimized Structural Design of Concrete Pile Plug in Steel Pipe Piles”. In: *ACI Structural Journal* 119.6 (Nov. 2022), p. 154. DOI: 10.14359/51734802.

[27] K. Wiersma and E. Bosman. “Verbinding tussen buispalen en landhoofden bij integraalviaducten”. In: *Cement* (2023).

[28] L. Zhao et al. “The Connection Design Study Between Superstructure and Pile”. In: *ISOPE International Ocean and Polar Engineering Conference* (2020).

A

Test results

A.1. Push-out test

The push-out test is a widely used method for evaluating the bond strength between steel and concrete in composite columns, particularly those involving concrete-filled steel tubes. This test helps determine how well the steel and concrete work together under load, which is critical for the structural integrity of composite columns. This section outlines the preparation of test specimens, the testing setup and instrumentation, the testing procedure, and the measurements and analysis involved.

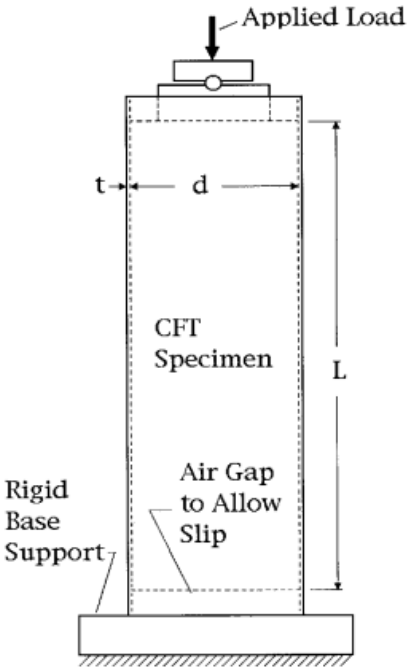

Figure A.1: Push-out test (Roeder et al. (1999))

A.1.1. Test specimen preparation

The push-out test specimens are meticulously prepared to ensure accuracy and consistency in testing. Steel tubes are first cut and machined to the required lengths, ensuring the ends are parallel and perpendicular to the sides. The internal surfaces are cleaned using wire brushes to remove any rust, loose scale, grease, and oil, which could affect the bond strength between the steel and concrete.

After cleaning, polystyrene plugs are fitted at the bottom of the tubes to facilitate the movement of the concrete core during testing. The tubes are then filled with concrete and allowed to cure for approximately four weeks, though some specimens may have different curing times for comparative analysis. To prepare the surface for uniform load application, the tops of the specimens are ground to be level with the steel rim.

A.1.2. Testing setup and instrumentation

The testing is conducted using a universal compression testing machine, typically with a capacity of 300 tons or 500 tons for larger specimens. Steel loading pads, which are slightly smaller in diameter than the internal diameter of the steel tubes, are placed at both ends of the specimen to ensure even distribution of the applied load.

To measure the movement of the concrete core relative to the steel tube, deflection transducers are positioned around the periphery of the tube. Usually, three transducers are used, and the average of their readings provides an accurate measurement of the core's deflection.

A.1.3. Testing procedure

The testing begins with the application of an initial load to eliminate any effects of irregularities on the concrete surface. This load is then released, and zero readings are recorded to serve as a baseline for subsequent measurements.

The load is then incrementally increased at a controlled rate, generally about 1.5 tons per minute. Deflections are recorded at regular intervals initially, and more frequently as significant changes in the load-deflection curve are observed. This incremental loading continues until the concrete core moves out of the tube or the travel limit of the testing machine is reached.

A.1.4. Measurements and analysis

During the test, the bond stress capacity is evaluated by calculating the average interface stress at the initial slip of the concrete core relative to the steel tube. This is determined using the formula:

$$f_{ba} = \frac{N_{slip}}{D_c \cdot L \cdot \pi} \qquad \text{(Eq. A.1)}$$

where:

N_{slip} = load at initial slip (N)
D_c = outer diameter of the concrete plug (mm)
L = length of the concrete plug (mm)

The load-deflection response is plotted to analyse the bond behavior, identify the point of initial slip, and determine the ultimate load capacity. By comparing the results from different specimens, the effect of various parameters, such as the surface roughness of the steel, the length of the steel-concrete interface, and the concrete strength, can be systematically studied.

A.2. Test results Roeder et al. (1999)

Roeder et al. (1999) used a push-out test to investigate the influence of the length of the concrete plug on the bond strength between steel and concrete. The test specimens used, together with the results of the test, are shown in the table below.

Table A.1: Test specimens and results Roeder et al. (1999)

Specimen	D_p (mm)	t_p (mm)	L (mm)	f_{ck} (MPa)	Concrete age (days)	f_{ba} (MPa)
II-1	247.6	13.46	810	47.2	23	0.773
II-2	247.6	13.46	810	46.6	28	0.786
II-3	247.6	13.46	810	46.6	24	0.775
II-5	341.4	7.11	1064	47.3	28	0.282
II-6	341.4	7.11	1064	47.3	24	0.355
II-7	341.4	7.11	1775	43.9	29	0.175
II-8	341.4	7.11	1775	43.9	29	0.187
II-9	598.4	5.59	1927	44.9	25	0.145
II-10	598.4	5.59	1927	47.2	25	0.176

A.3. Test results Nezamian et al. (2002)

Nezamian et al. (2002) used a push-out test to investigate the influence of the length of the concrete plug on the bond strength between steel and concrete. The test specimens used, together with the results of the test, are shown in the table below.

Table A.2: Test specimens and results Nezamian et al. (2002)

Specimen	D_p (mm)	t_p (mm)	L (mm)	f_{ck} (MPa)	Concrete age (days)	f_{ba} (MPa)
S1000-1	237	11.5	1000	50	28	2.02
S1000-2	237	11.5	1000	50	28	2.00
S750-1	237	11.5	750	50	28	4.96
S500-1	237	11.5	500	50	28	2.06
S500-2	237	11.5	500	50	28	2.02
S1.25D	244.10	11	305.10	40	38	2.38
S1.75D	244.10	11	427.20	40	38	1.45
S2.0D	248.10	13	488.20	40	38	3.27

A.4. Test results Aly et al. (2009)

Aly et al. (2009) used a push-out test to investigate the influence of the concrete compressive strength on the bond strength between steel and concrete. The test specimens used, together with the results of the test, are shown in the table below.

Table A.3: Test specimens and results Aly et al. (2009)

Specimen	D_p (mm)	t_p (mm)	L (mm)	f_{ck} (MPa)	Concrete age (days)	f_{ba} (MPa)
A1	114.3	3.2	522	71	66	1.03
B1	114.3	3.2	522	41	64	1.19
C1	114.3	3.2	522	69	32	0.92
D1	114.3	3.2	522	64	56	1.18
F1	114.3	3.2	522	41	33	1.23
H1	114.3	3.2	522	70	98	1.00

A.5. Test results Virdi and Dowling et al. (1980)

Virdi and Dowling et al. (1980) used push-out tests to investigate the influence of several parameters on the bond strength between steel and concrete. The table below shows the specimen (Group MA) and test results for the test where the influence of the shrinkage was examined.

Table A.4: Test specimens and results Virdi and Dowling et al. (1980) for Group MA

Specimen	D_p (mm)	t_p (mm)	L (mm)	f_{ck} (MPa)	Concrete age (days)	f_{ba} (MPa)
MA 1	154.58	6.35	342.9	25.65	7	2.16
MA 4	155.27	6.35	342.9	35.78	7	3.52
MA 5	154.66	6.35	342.9	25.67	7	2.59
MA 9	155.04	6.35	342.9	30.46	10	2.90
MA 2	155.30	6.35	342.9	35.78	14	2.90
MA 7	154.71	6.35	342.9	35.78	14	3.12
MA 8	154.66	6.35	342.9	35.78	14	3.21
MA 10	155.04	6.35	342.9	37.23	21	3.65
MA 3	155.17	6.35	342.9	40.33	28	3.45
MA 6	154.58	6.35	342.9	40.33	28	2.96

The table below shows the specimen (Group CS) and test results for the test where the influence of the concrete compressive strength was examined.

Table A.5: Test specimens and results Virdi and Dowling et al. (1980) for Group CS

Specimen	D_p (mm)	t_p (mm)	L (mm)	f_{ck} (MPa)	Concrete age (days)	f_{ba} (MPa)
CS14	155.68	6.35	342.9	21.99	28	1.94
CS21	154.97	6.35	342.9	21.99	28	1.88
CS28	155.32	6.35	342.9	21.99	28	1.30
CS19	155.19	6.35	342.9	27.35	28	2.24
CS22	155.40	6.35	342.9	27.35	28	1.38
CS25	156.16	6.35	342.9	27.35	28	2.11
CS12	156.24	6.35	342.9	28.10	28	1.43
CS24	155.88	6.35	342.9	28.10	28	1.56
CS27	156.49	6.35	342.9	28.10	28	1.85
CS12	156.57	6.35	342.9	30.06	28	1.77
CS18	155.17	6.35	342.9	30.06	28	1.89
CS26	156.26	6.35	342.9	30.06	28	1.60
CS11	156.08	6.35	342.9	36.58	28	1.91
CS16	155.68	6.35	342.9	36.58	28	1.87
CS20	156.16	6.35	342.9	36.58	28	2.11
CS15	155.50	6.35	342.9	41.73	28	2.34
CS17	156.46	6.35	342.9	41.73	28	1.51
CS23	156.36	6.35	342.9	41.73	28	1.54

The table below shows the specimen (Group LN) and test results for the test where the influence of the length of the concrete plug was examined.

Table A.6: Test specimens and results Virdi and Dowling et al. (1980) for Group LN

Specimen	D_p (mm)	t_p (mm)	L (mm)	f_{ck} (MPa)	Concrete age (days)	f_{ba} (MPa)
LN41	150.32	9.53	149.35	40.32	28	1.97
LN42	149.58	9.53	149.35	40.32	28	2.19
LN43	149.25	9.53	149.35	40.32	28	2.15
LN29	148.49	9.53	223.77	40.32	28	1.63
LN30	148.67	9.53	223.77	40.32	28	2.01
LN31	148.89	9.53	223.77	40.32	28	2.03
LN32	148.59	9.53	298.45	40.32	28	2.10
LN33	149.73	9.53	298.45	40.32	28	2.26
LN34	150.90	9.53	298.45	40.32	28	2.37
LN35	149.02	9.53	373.13	40.32	28	2.46
LN36	150.67	9.53	373.13	40.32	28	2.56
LN37	150.52	9.53	373.13	40.32	28	2.37
LN38	149.15	9.53	447.80	40.32	28	2.90
LN39	149.58	9.53	447.80	40.32	28	2.82
LN40	149.78	9.53	447.80	40.32	28	2.73

The table below shows the specimen (Group SZ) and test results for the test where the influence of the size of the diameter and wall thickness of the pipe pile was examined.

Table A.7: Test specimens and results Virdi and Dowling et al. (1980) for Group SZ

Specimen	D_p (mm)	t_p (mm)	L (mm)	f_{ck} (MPa)	Concrete age (days)	f_{ba} (MPa)
SZ50	149.20	9.68	463.55	46.33	47	2.42
SZ51	150.06	9.73	463.55	46.33	47	1.79
SZ52	149.28	9.63	463.55	46.33	47	2.38
SZ53	156.39	6.53	463.55	46.33	47	1.10
SZ54	156.29	6.55	463.55	46.33	47	1.30
SZ55	156.79	6.63	463.55	46.33	47	1.01
SZ56	158.90	5.74	463.55	46.33	47	1.47
SZ57	157.84	5.69	463.55	46.33	47	1.25
SZ58	158.78	5.61	463.55	46.33	47	1.45
SZ59	206.98	6.50	463.55	46.33	47	1.90
SZ60	207.67	6.63	463.55	46.33	47	1.94
SZ61	206.63	6.81	463.55	46.33	47	1.76
SZ62	231.57	7.34	463.55	46.33	47	0.63
SZ63	231.27	7.34	463.55	46.33	47	0.52
SZ64	231.95	7.19	463.55	46.33	47	0.58
SZ65	305.82	9.55	463.55	46.33	47	2.01
SZ66	305.36	9.58	463.55	46.33	47	1.99
SZ67	305.99	9.53	463.55	46.33	47	2.00

The table below shows the specimen (Group ST) and test results for the test where the influence of the surface treatment was examined.

Table A.8: Test specimens and results Virdi and Dowling et al. (1980) for Group ST

Specimen	D_p (mm)	t_p (mm)	L (mm)	f_{ck} (MPa)	Concrete age (days)	f_{ba} (MPa)
ST44	157.43	7.19	342.9	46.28	28	0.42
ST45	156.72	7.19	342.9	46.28	28	0.31
ST46	156.92	7.19	342.9	46.28	28	0.27
PH47	155.19	6.60	342.9	46.28	28	0.75
PH48	155.42	6.86	342.9	46.28	28	1.13
PH49	155.35	6.86	342.9	46.28	28	0.72
CS15	155.50	6.35	342.9	41.73	28	2.34
CS17	156.46	6.35	342.9	41.73	28	1.51
CS23	156.36	6.35	342.9	41.73	28	1.54

The table below shows the specimen (Group CC) and test results for the test where the influence of the the compaction of the concrete was examined.

Table A.9: Test specimens and results Virdi and Dowling et al. (1980) for Group CC

Specimen	D_p (mm)	t_p (mm)	L (mm)	f_{ck} (MPa)	Concrete age (days)	f_{ba} (MPa)
CC70	149.76	9.73	342.9	30.73	28	2.63
CC71	148.84	9.93	342.9	30.73	28	2.55
CC72	148.89	9.88	342.9	30.73	28	2.48
CC73	149.40	9.78	342.9	37.27	28	2.02
CC74	148.84	9.70	342.9	37.27	28	2.11
CC75	149.86	9.70	342.9	37.27	28	2.14
CC76	150.29	9.80	342.9	35.39	28	2.13
CC77	148.89	9.80	342.9	35.39	28	2.27
CC78	149.30	9.75	342.9	35.39	28	2.14
CC79	150.29	9.68	342.9	35.39	28	1.85
CC80	150.14	9.68	342.9	35.39	28	2.21
CC81	149.66	9.83	342.9	35.39	28	1.49
CC82	148.79	9.68	342.9	35.39	28	1.80
CC83	148.39	9.70	342.9	35.39	28	1.54
CC84	148.79	9.70	342.9	35.39	28	1.50
CC85	148.95	9.70	342.9	35.39	28	1.16
CC86	149.94	9.68	342.9	35.39	28	1.47
CC87	149.48	10.08	342.9	35.39	28	1.66

A.6. Test results Shakir-Khalil et al. (1993)

Shakir-Khalil et al. (1993) used a push-out test to investigate the influence of the length of the concrete plug on the bond strength between steel and concrete. The test specimens used, together with the results of the test, are shown in the table below.

Table A.10: Test specimens and results Shakir-Khalil et al. (1993)

Specimen	D_p (mm)	t_p (mm)	L (mm)	f_{ck} (MPa)	Concrete age (days)	f_{ba} (MPa)
Y4a	168.3	5	202	71	28	0.88
Y4b	168.3	5	203	41	28	0.93
Y5a	168.3	5	399	69	28	0.79
Y5b	168.3	5	400	64	28	0.80
Y6a	168.3	5	600	41	28	0.72
Y6b	168.3	5	599	70	28	0.65

B

Python code

In this thesis, several methods have been numerically developed, including, for example, the model for the transfer of normal force through friction and the model in which normal force is combined with the bending moment. These numerical methods were developed using a Python script, so that they could easily be used to obtain results. These Python scripts are shown in this appendix.

B.1. Model transfer of normal force through friction

The first Python script used was the Python script for determining the transfer of normal force by friction. The first formula entered in Python for this purpose is the formula for the contact force per strip of the concrete plug, $\sigma_{i,rr,i}$. This formula is determined as follows:

$$\sigma_{i,rr,i} = \frac{2E_s t_p(((4E_c\epsilon_s+4v_c\sigma_{c,z,i})D_c-8E_c u_{irr,rr})E_s-4v_s\sigma_{s,z,i}D_pE_c)t_p+K_s((E_c\epsilon_s+v_c\sigma_{c,z,i})D_c-2E_c u_{irr,rr})D_p^2}{\left(8D_cE_s^2t_p^2(v_c-1)+2t_p(-4E_c+(v_c-1)K_sD_c)E_sD_p^2-D_p^4E_cK_s\right)} \quad \text{(Eq. B.1)}$$

The Python implementation of the formula for this contact stress is shown in the code cell below.

```
def sigma_i_rr_i_func(D_p, D_c, t_p, E_s, E_c, v_s, v_c, e_s, sigma_s_z, sigma_c_z, u_r, K_s)
                                                    :
    numerator = 4 * (((D_c * e_s - 2 * u_r) * E_c + D_c * v_c * sigma_c_z) * K_s * D_p ** 2 -
                                                     4 * D_p * E_c * t_p * v_s * sigma_s_z + 4
                                                     * ((D_c * e_s - 2 * u_r) * E_c + D_c *
                                                    v_c * sigma_c_z) * E_s * t_p) * E_s * t_p
    denominator = (((-8 * E_s * t_p / D_p ** 2 - 2 * K_s) * E_c + 4 * D_c * E_s * t_p * K_s *
                                                     (v_c - 1) / D_p ** 2) * D_p ** 2 + 4 *
                                                    E_s * (-2 * E_c + 4 * D_c * E_s * t_p * (
                                                    v_c - 1) / D_p ** 2) * t_p) * D_p ** 2

    sigma_i_rr_i = numerator / denominator

    return sigma_i_rr_i
```

The second formula is the formula for the total normal force capacity of the concrete plug, $N_{Rd,c}$. This formula is as follows:

$$N_{Rd,c} = \sum_{i=0}^{i=n} \Delta F_{zz,i} = D_c \cdot \pi \cdot \Delta z \cdot \mu \sum_{i=0}^{i=n} \sigma_{i,rr,i} \tag{Eq. B.2}$$

The Python implementation of the formula for this normal force capacity is shown in the code cell below.

```
def N_Rd_func(D_p, D_c, t_p, E_s, E_c, v_s, v_c, e_s, u_r, mu, K_s, L, N_s, N_c, delta_z):
    sigma_c_z = [-N_c / (D_c ** 2 * np.pi / 4)]
    sigma_s_z = [-4 * N_s / ((D_p ** 2 - D_c ** 2) * np.pi)]
    sigma_i_rr = []

    L_array = np.arange(0, int(L+delta_z), delta_z)

    f_ba_array = []

    for i in range(len(L_array)):
        sigma_i_rr_i = (sigma_i_rr_i_func(D_p, D_c, t_p, E_s, E_c, v_s, v_c, e_s, sigma_s_z[-
                                                    1], sigma_c_z[-1], u_r, K_s))
        if sigma_i_rr_i < 0:
            sigma_i_rr_i = 0

        f_ba_i = sigma_i_rr_i * mu

        sigma_i_rr.append(sigma_i_rr_i)
        f_ba_array.append(f_ba_i)
        sigma_c_z.append(sigma_c_z[-1]+((f_ba_array[-1] * delta_z * D_c * np.pi)/((D_c ** 2 *
                                                    np.pi / 4))))
        sigma_s_z.append(sigma_s_z[-1]-((4 * f_ba_array[-1] * delta_z * D_c)/((D_p ** 2 - D_c
                                                    ** 2))))

    f_ba = np.mean(f_ba_array)
    N_Rd = np.sum(f_ba_array) * D_c * np.pi * delta_z

    return sigma_c_z, sigma_s_z, sigma_i_rr, L_array, f_ba_array, f_ba, N_Rd
```

The last code cell is for the iterative method to determine the total normal force capacity. The iterative process begins by comparing the calculated normal force capacity, $N_{Rd,c}^{(i)}$, with the initial guess for the normal force acting on the concrete plug, $N_c^{(i)}$. If the absolute difference between these values is within a predefined tolerance, convergence is achieved.

$$|N_{Rd,c}^{(i)} - N_c^{(i)}| < \text{tolerance} \tag{Eq. B.3}$$

If convergence is not achieved, the normal force is adjusted using a damping factor, α, to control the step size of the update. The adjusted normal force for the next iteration, $N_c^{(i+1)}$, is calculated as follows:

$$N_c^{(i+1)} = N_c^{(i)} + \alpha \cdot (N_{Rd,c}^{(i)} - N_c^{(i)}) \tag{Eq. B.4}$$

where:

α = damping factor to control the step size of the update (-)

This process is repeated iteratively until the calculated normal force capacity closely matches the normal force acting on the concrete plug, indicating convergence. When convergence is achieved, the normal force capacity value determined at that time can be taken as the final capacity.

The Python implementation of this method for iterative procedure is shown in the code cell below.

```
def solve_N_Rd(D_p, D_c, t_p, E_s, E_c, v_s, v_c, e_s, u_r, mu, K_s, L, N_s, N_c_initial,
                                                delta_z=10, tolerance=0.01, alpha=0.1,
                                                max_iter=10000):
    for i in range(max_iter):
        sigma_c_z, sigma_s_z, sigma_i_rr, L_array, f_ba_array, f_ba, N_Rd = N_Rd_func(D_p,
                                                        D_c, t_p, E_s, E_c, v_s, v_c, e_s, u_r
                                                        , mu, K_s, L, N_s, N_c_initial,
                                                        delta_z)

        if abs(N_Rd - N_c_initial) < tolerance:
            return N_c_initial, sigma_c_z, sigma_s_z,  sigma_i_rr, L_array, f_ba_array, f_ba,
                                                                N_Rd

        N_c_initial += (N_Rd - N_c_initial) * alpha

    return None, None, None, None, None, None, None, None
```

B.2. Model transfer of normal force and bending moment

The second Python script used was the Python script for determining the transfer of normal and bending moment due to interaction. The first formula entered in Python for this purpose is the formula for determining the assumed contact stresses, $\sigma_{bend}(z_i, \theta_j)$, that arise as a result of the bending moment over the height and circumference of the concrete plug. This formula is as follows:

$$\sigma_{bend}(z_i, \theta_j) = \begin{cases} (\sigma_{bend,max} - \sigma_{bend,max} \cdot \frac{2 \cdot z_i}{L}) \cdot \sin(\theta_j)^2 & \text{if } 0 \leq \theta_j \leq \pi \\ (-\sigma_{bend,max} + \sigma_{bend,max} \cdot \frac{2 \cdot z_i}{L}) \cdot \sin(\theta_j)^2 & \text{if } \pi < \theta_j \leq 2\pi \end{cases} \quad \text{(Eq. B.5)}$$

where:

$$\sigma_{bend,max} = \frac{24 \cdot M}{\pi \cdot D_c \cdot L^2} \quad \text{(Eq. B.6)}$$

M = bending moment acting on the concrete plug (kNm)

The Python implementation of the formula for this contact pressure is shown in the code cell below.

```
def sigma_bend_func(M_Ed, D_c, L, delta_theta=0.01, delta_z=10):
    theta_array = np.arange(0, np.pi + delta_theta, delta_theta)
    z_array = np.arange(L/2, -(L + 2 * delta_z) / 2, -delta_z)

    sigma_bend_max = M_Ed * 24 / (np.pi * D_c * L ** 2)

    sigma_bend_0_pi = np.zeros((len(z_array), len(theta_array)))
    sigma_bend_pi_2pi = np.zeros((len(z_array), len(theta_array)))

    for i, z in enumerate(z_array):
        for j, theta in enumerate(theta_array):
            sigma_bend_0_pi[i, j] = sigma_bend_max * np.sin(theta)**2 * (2 * z / L)
            sigma_bend_pi_2pi[i, j] = -sigma_bend_max * np.sin(theta)**2 * (2 * z / L)

    return z_array, theta_array, sigma_bend_0_pi, sigma_bend_pi_2pi
```

The second formula put in Python for this model is the formula for the normal force capacity, $N_{Rd,c}$. This combines the contact stresses arising due to the normal force, $\sigma_{norm}(z_i)$, with the contact stresses arising due to the bending moment, $\sigma_{bend}(z, \theta)$, in order to to achieve a total normal force capacity with the Coulomb friction coefficient. This formula is as follows:

$$N_{Rd,c} = \sum_{j=0}^{n} \sum_{i=0}^{m} \sigma(z_i, \theta_j) \cdot \mu \cdot H(\sigma(z_i, \theta_j)) \cdot \frac{D_c}{2} \cdot \Delta\theta \cdot \Delta z \qquad \text{(Eq. B.7)}$$

where:

D_c = outer diameter of the concrete plug (mm)
μ = Coulomb friction coefficient (-)

and:

$$n = \frac{L}{\Delta z} \qquad \text{(Eq. B.8)}$$

L = length of the concrete plug (mm)
Δz = size of the mesh in vertical direction (mm)

and:

$$m = \frac{2\pi}{\Delta\theta} \qquad \text{(Eq. B.9)}$$

$\Delta\theta$ = size of the mesh in circumferential direction (radians)

and:

$$\sigma(z_i, \theta_j) = \sigma_{norm}(z_i) + \sigma_{bend}(z, \theta) \qquad \text{(Eq. B.10)}$$

and:

$$H(\sigma(z_i, \theta_j)) = \begin{cases} 0 & \text{if } \sigma(z_i, \theta_j) \leq 0 \\ 1 & \text{if } \sigma(z_i, \theta_j) > 0 \end{cases} \qquad \text{(Eq. B.11)}$$

The Python implementation of the formula for this normal force capacity is shown in the code cell below.

```
def sigma_norm_bend_func(sigma_i_rr, sigma_bend_0_pi, sigma_bend_pi_2pi, D_c, mu, delta_theta
                                                =0.01, delta_z=10):
    sigma_norm_bend_0_pi = np.empty_like(sigma_bend_0_pi)
    sigma_norm_bend_pi_2pi = np.empty_like(sigma_bend_pi_2pi)


    for i in range(len(sigma_bend_0_pi)):
        for j in range(len(sigma_bend_0_pi[i])):
            sigma_norm_bend_0_pi[i][j] = sigma_bend_0_pi[i][j] + sigma_i_rr[i]
            if sigma_norm_bend_0_pi[i][j] < 0:
                sigma_norm_bend_0_pi[i][j] = 0

    for i in range(len(sigma_bend_pi_2pi)):
        for j in range(len(sigma_bend_pi_2pi[i])):
            sigma_norm_bend_pi_2pi[i][j] = sigma_bend_pi_2pi[i][j] + sigma_i_rr[i]
            if sigma_norm_bend_pi_2pi[i][j] < 0:
                sigma_norm_bend_pi_2pi[i][j] = 0

    N_Rd = (np.sum(sigma_norm_bend_0_pi) + np.sum(sigma_norm_bend_pi_2pi)) * D_c / 2 * mu  *
                                                    delta_z * delta_theta

    return sigma_norm_bend_0_pi, sigma_norm_bend_pi_2pi, N_Rd
```

B.3. Shrinkage model

The concrete shrinkage model of the Model Code, which was used to determine the shrinkage, was also put into Python, so that it could be used in the previous models to determine the concrete shrinkage. This Python code is shown in the code cell below.

```python
def shrinkage_fib(t, L, f_cm, a_as, a_ds1, a_ds2, RH):
    h = 2 * L

    beta_as = 1 - np.exp(-0.2 * t ** (1 / 2))
    e_cas0 = -a_as * ((0.1 * f_cm)/(6 + 0.1 * f_cm)) ** 2.5 / (10 ** 6)
    e_cas = beta_as * e_cas0

    e_cds0 = ((220 + 110 * a_ds1) * np.exp(-a_ds2 * f_cm)) / (10 ** 6)
    beta_RH = -1.55 * (1 - (RH / 100) ** 3)
    beta_ds = (t / (0.035 * (h ** 2) + t)) ** (1 / 2)
    e_cds = e_cds0  * beta_RH * beta_ds

    e_cs = e_cas + e_cds

    return e_cs
```

C

Determination of safety factor model normal according to Eurocode 0

In this thesis, a model has been set up to determine the normal force that can be transmitted by friction between steel and concrete for concrete plug connections. If this model is applied in a design, it must be provided with a safety factor so that the design bond strength can be determined. This can be done using appendix D from Eurocode 0, as implemented in this appendix.

C.1. Determination of characteristic bond strength

First the characteristic value for the bond strength can be determined using Eurocode 0. This characteristic value can be determined as shown in this section.

C.1.1. Estimate of the correction factor b

The first step is to determine an estimate of the correction factor b. This b is the best least squares approximation for the slope between the experimental value and the theoretical value of the model. This factor is determined in the following formula.

$$b = \frac{\sum r_e \cdot r_t}{\sum r_t^2} = \frac{\sum \overline{f}_{ba} \cdot f_{ba}}{\sum f_{ba}^2} \approx 1.295 \quad \text{(Eq. C.1)}$$

C.1.2. Estimation of the coefficients of variation

The second step in the process is to determine the coefficient of variation of the deviations. The natural algorithm of the deviation term, Δ_i, must be calculated for each experimental value r_{ei} using the following formula.

$$\Delta_i = \ln(\frac{r_{ei}}{b \cdot r_{ti}}) = \ln(\frac{\overline{f}_{ba}^{(i)}}{b \cdot f_{ba}^{(i)}}) \quad \text{(Eq. C.2)}$$

The estimated value $\overline{\Delta}$ can then be determined using the following formula, where the average values of Δ_i is determined.

$$\overline{\Delta} = \frac{1}{n} \cdot \sum_{i=1}^{n} \Delta_i \approx 0.066 \quad \text{(Eq. C.3)}$$

The standard deviation s_{Δ}^2 can then be determined using the formula below.

$$s_{\Delta}^2 = \frac{1}{n-1} \cdot \sum_{i=1}^{n} (\Delta_i - \overline{\Delta})^2 \approx 0.493 \quad \text{(Eq. C.4)}$$

The coefficient of variation V_{δ} can then be determined from the deviation terms using the following formula.

$$V_{\delta} = \sqrt{\exp(s_{\Delta}^2) - 1} \approx 0.525 \quad \text{(Eq. C.5)}$$

The coefficients of variation V_{Xi} of the basic variables are assumed to be equal to 0, as shown below. This is not realistic for the actual situation, but determining the coefficients of variation of all basic variables of the model is beyond the scope of this thesis.

$$V_{rt}^2 = \sum_{i=1}^{j} V_{Xi}^2 = 0 \quad \text{(Eq. C.6)}$$

With the coefficient of variation V_{δ} and V_{Xi}, the coefficient of variation V_r^2 can then be found using the product function.

$$V_r^2 = (V_{\delta}^2 + 1) \cdot \left[\prod_{i=1}^{j} (V_{Xi}^2 + 1) \right] - 1 \approx 0.276 \quad \text{(Eq. C.7)}$$

C.1.3. Determination of the characteristic value of the resistance

After obtaining all the coefficients of variation, the characteristic value for the bond strength, $f_{ba,k}$, can be obtained using the following formula.

$$f_{ba,k} = b \cdot f_{ba}(x) \cdot \exp(-k_{\infty} \cdot \alpha_{rt} \cdot Q_{rt} - k_n \cdot \alpha_{\delta} \cdot Q_{\delta} - 0.5 \cdot Q^2) \rightarrow f_{ba,k} = 0.510 \cdot f_{ba}(x) \quad \text{(Eq. C.8)}$$

where:

k_n = characteristic fractional factor = 1.64
k_{∞} = value of k_n when $n \rightarrow \infty$ = 1.64

and:

$$Q_{rt} = \sqrt{\ln(V_{rt}^2 + 1)} = 0 \quad \text{(Eq. C.9)}$$

and:

$$Q_{\delta} = \sqrt{\ln(V_{\delta}^2 + 1)} \approx 0.493 \quad \text{(Eq. C.10)}$$

and:

$$Q = \sqrt{\ln(V_r^2 + 1)} \approx 0.493 \quad \text{(Eq. C.11)}$$

and:

$$\alpha_{rt} = \frac{Q_{rt}}{Q} = 0 \quad \text{(Eq. C.12)}$$

and:

$$\alpha_{\delta} = \frac{Q_{\delta}}{Q} = 1 \quad \text{(Eq. C.13)}$$

C.2. Determination of design bond strength

Secondly, the design value for the bond strength can be determined using Eurocode 0. This design value can be determined as shown in this section.

C.2.1. Determination of the design value of the resistance

When the design value for the bond strength must be determined according to Eurocode 0, almost all steps remain the same as in C.1. The only difference is that the characteristic fractional factor k_n is replaced by fractional factor $k_{d,n}$. The design bond strength, $f_{ba,d}$, can then be determined with the following formula.

$$f_{ba,d} = b \cdot f_{ba}(x) \cdot \exp(-k_{d,\infty} \cdot \alpha_{rt} \cdot Q_{rt} - k_{d,n} \cdot \alpha_{\delta} \cdot Q_{\delta} - 0.5 \cdot Q^2) \rightarrow f_{ba,d} = 0.256 \cdot f_{ba}(x) \quad \text{(Eq. C.14)}$$

where:

$k_{d,n}$ = design fractional factor = 3.04
$k_{d,\infty}$ = value of $k_{d,n}$ when $n \rightarrow \infty$ = 3.04

and:

$$Q_{rt} = \sqrt{\ln(V_{rt}^2 + 1)} = 0 \quad \text{(Eq. C.15)}$$

and:

$$Q_{\delta} = \sqrt{\ln(V_{\delta}^2 + 1)} \approx 0.493 \quad \text{(Eq. C.16)}$$

and:

$$Q = \sqrt{\ln(V_r^2 + 1)} \approx 0.493 \quad \text{(Eq. C.17)}$$

and:

$$\alpha_{rt} = \frac{Q_{rt}}{Q} = 0 \quad \text{(Eq. C.18)}$$

and:

$$\alpha_{\delta} = \frac{Q_{\delta}}{Q} = 1 \quad \text{(Eq. C.19)}$$

D

Wrenching stress distributions around the circumference of the plug

In this appendix the determination of the capacity of each wrenching stress distribution around the circumference of the concrete plug is determined.

D.1. Linear distribution

The first stress distribution that can be assumed for the contact stress around the concrete plug is a linear distribution. This distribution is shown in Figure D.1.

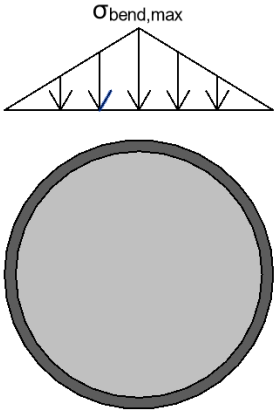

Figure D.1: Linear stress distribution.

This linear distribution for the stress over both the height and along the circumference of the concrete plug can be described using the following formula:

$$\sigma_{bend}(z,x) = \sigma_{bend,max} \cdot \frac{4 \cdot x \cdot z}{L \cdot D_c} \quad \text{(Eq. D.1)}$$

where:

$\sigma_{bend,max}$= maximum wrenching stress on top and bottom of the concrete plug (MPa)
D_c = outer diameter of the concrete plug (mm)
L = length of the concrete plug (mm)

To determine the wrenching force, F_{wrench}, using the linear stress distribution, the integral equation below must be solved. The contact stress is integrated over half the height of the plug, L, and because of the linear progression, integrated over half the outer diameter of the concrete plug, D_c, after which it is multiplied by a factor of 2 , to arrive at the force over the entire diameter.

$$F_{wrench} = 2 \cdot \int_0^{\frac{D_c}{2}} \int_0^{\frac{L}{2}} \sigma_{bend}(z,x)\, dz\, dx = \frac{\sigma_{bend,max} \cdot D_c \cdot L}{8} \quad \text{(Eq. D.2)}$$

To arrive at the wrenching moment from the wrenching force, M_{wrench}, the wrenching force must be multiplied by the internal lever arm between the pressure diagonals over the height of the concrete plug. This is shown in the formula below:

$$M_{wrench} = F_{wrench} \cdot \frac{2 \cdot L}{3} = \frac{\sigma_{bend,max} \cdot D_c \cdot L^2}{12} \quad \text{(Eq. D.3)}$$

D.2. Sinusoidal distribution

The second stress distribution that can be assumed for the contact stress around the concrete plug is a sinusoidal distribution. This distribution is shown in Figure D.2.

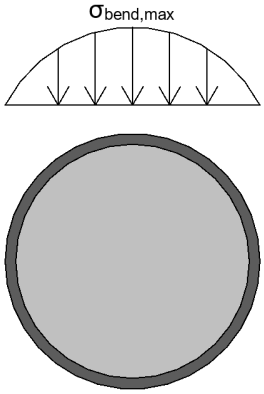

Figure D.2: Sinusoidal stress distribution.

This sinusoidal distribution for the stress over both the height and along the circumference of the concrete plug can be described using the following formula:

$$\sigma_{bend}(z,x) = \sigma_{bend,max} \cdot \sin(\frac{x \cdot \pi}{D_c}) \cdot \frac{2 \cdot z}{L} \quad \text{(Eq. D.4)}$$

where:

$\sigma_{bend,max}$= maximum wrenching stress on top and bottom of the concrete plug (MPa)
D_c = outer diameter of the concrete plug (mm)
L = length of the concrete plug (mm)

To determine the wrenching force, F_{wrench}, using the linear stress distribution, the integral equation below must be solved. The contact stress is integrated over half the height of the plug, L and integrated over the outer diameter of the concrete plug, D_c.

$$F_{wrench} = \int_0^{D_c} \int_0^{\frac{L}{2}} \sigma_{bend}(z,x)\, dz\, dx = \frac{\sigma_{bend,max} \cdot D_c \cdot L}{2 \cdot \pi} \quad \text{(Eq. D.5)}$$

To arrive at the wrenching moment from the wrenching force, M_{wrench}, the wrenching force must be multiplied by the internal lever arm between the pressure diagonals over the height of the concrete plug. This is shown in the formula below:

$$M_{wrench} = F_{wrench} \cdot \frac{2 \cdot L}{3} = \frac{\sigma_{bend,max} \cdot D_c \cdot L^2}{3 \cdot \pi} \quad \text{(Eq. D.6)}$$

D.3. Quadratic sinusoidal distribution

The third stress distribution that can be assumed for the contact stress around the concrete plug is a quadratic sinusoidal distribution. This distribution is shown in Figure D.3.

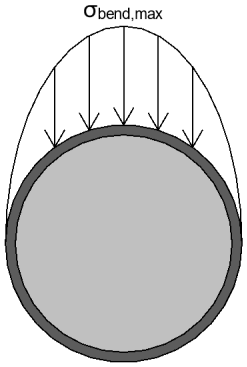

Figure D.3: Quadratic sinusoidal stress distribution.

This quadratic sinusoidal distribution for the stress over both the height and along the circumference of the concrete plug can be described using formula below:

$$\sigma_{bend}(z,\theta) = \sigma_{bend,max} \cdot \sin(\theta)^2 \cdot \frac{2 \cdot z}{L} \quad \text{(Eq. D.7)}$$

where:

$\sigma_{bend,max}$= maximum wrenching stress on top and bottom of the concrete plug (MPa)
D_c = outer diameter of the concrete plug (mm)
L = length of the concrete plug (mm)

To determine the wrenching force, F_{wrench}, using the linear stress distribution, the integral equation below must be solved. The contact stress is integrated over half the height of the plug, L and integrated over half the outer radius of the concrete plug, θ.

$$F_{wrench} = \int_0^{\pi} \int_0^{\frac{L}{2}} \sigma_{bend}(z,\theta) \cdot \frac{D_c}{2}\, dz\, d\theta = \frac{\pi \cdot \sigma_{bend,max} \cdot D_c \cdot L}{16} \quad \text{(Eq. D.8)}$$

To arrive at the wrenching moment from the wrenching force, M_{wrench}, the wrenching force must be multiplied by the internal lever arm between the pressure diagonals over the height of the concrete plug. This is shown in the formula below:

$$M_{wrench} = F_{wrench} \cdot \frac{2 \cdot L}{3} = \frac{\pi \cdot \sigma_{bend,max} \cdot D_c \cdot L^2}{24} \quad \text{(Eq. D.9)}$$

D.4. Uniform distribution

The fourth stress distribution that can be assumed for the contact stress around the concrete plug is a uniform distribution. This distribution is shown in Figure D.4.

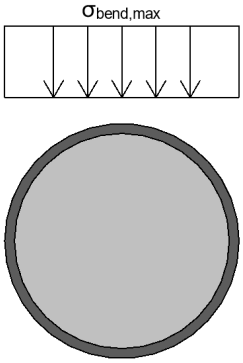

Figure D.4: Uniform stress distribution.

This sinusoidal distribution for the stress over both the height and along the circumference of the concrete plug can be described using the following formula:

$$\sigma_{bend}(z, x) = \sigma_{bend,max} \cdot \frac{2 \cdot z}{L} \quad \text{(Eq. D.10)}$$

where:

$\sigma_{bend,max}$= maximum wrenching stress on top and bottom of the concrete plug (MPa)
D_c = outer diameter of the concrete plug (mm)
L = length of the concrete plug (mm)

To determine the wrenching force, F_{wrench}, using the linear stress distribution, the integral equation below must be solved. The contact stress is integrated over half the height of the plug, L and integrated over the outer diameter of the concrete plug, D_c.

$$F_{wrench} = \int_0^{D_c} \int_0^{\frac{L}{2}} \sigma_{bend}(z, x)\, dz\, dx = \frac{\sigma_{bend,max} \cdot D_c \cdot L}{4} \quad \text{(Eq. D.11)}$$

To arrive at the wrenching moment from the wrenching force, M_{wrench}, the wrenching force must be multiplied by the internal lever arm between the pressure diagonals over the height of the concrete plug. This is shown in the formula below:

$$M_{wrench} = F_{wrench} \cdot \frac{2 \cdot L}{3} = \frac{\sigma_{bend,max} \cdot D_c \cdot L^2}{6} \quad \text{(Eq. D.12)}$$

E

Bending moment resistance cross-section

This chapter presents an example calculation for the bending moment resistance of the cross-section of a concrete plug. The bending moment resistance is determined according to the method outlined in Eurocode 2 (NEN-EN 1992-1-1), specifically described in subsection 8.2.1. In this method, the bending moment resistance is calculated assuming a rectangular stress block for the portion of the concrete that is in compression, as illustrated in Figure E.1.

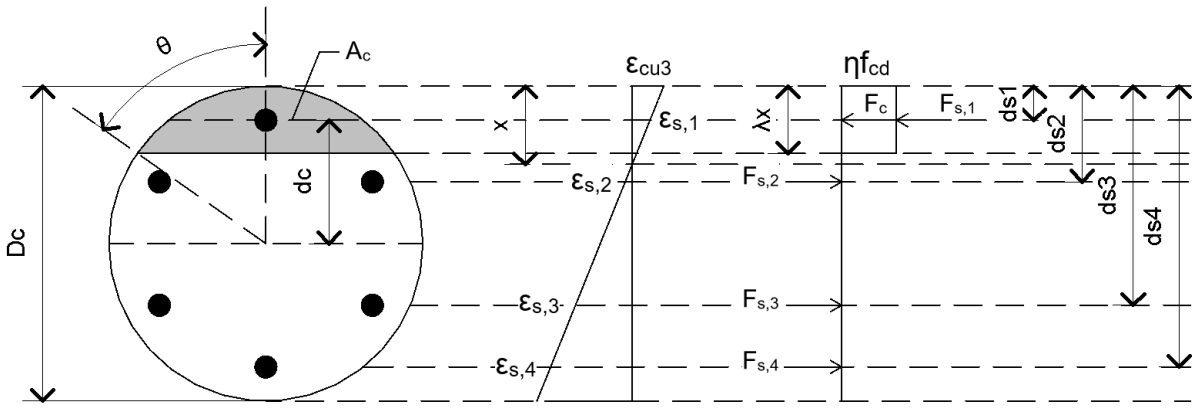

Figure E.1: Strains, Forces and Moment arms.

E.1. Input parameters

Several input parameters are required to calculate the bending moment resistance. The first set of parameters consists of the geometry of the concrete plug, detailed in Table E.1.

Table E.1: Concrete plug geometry.

Element geometry		
Outer diameter steel pipe pile	D_p	= 600 mm
Wall thickness steel pipe pile	t_p	= 10 mm
Outer diameter concrete plug	$D_c = D_p - 2 \cdot t_p$	= 580 mm

In addition to the geometry of the concrete plug, the layout of the reinforcement applied in the plug is also required. For the reinforcement layout it was decided to use an amount of reinforcement steel that almost achieves the maximum reinforcement ratio of 0.04. This reinforcement layout is shown in table E.2.

Table E.2: Reinforcement lay-out.

Element geometry		
Number of reinforcement bars	n	= 10 mm
Diameter of reinforcement bar	ϕ	= 36 mm
Concrete cover	c	= 40 mm

The required material properties of the concrete are based on a strength class of C30/37. Table E.3 contains the required material properties of these strength classes.

Table E.3: Concrete material properties.

Concrete property		
Characteristic cylinder compressive strength	f_{ck}	= 30 MPa
Design compressive strength	$f_{cd} = f_{ck}/\gamma_c$, $\gamma_c = 1.5$	= 20 MPa
Ultimate compressive strain concrete	ϵ_{cu3}	= 0.0035

The material properties of the reinforcing steel are based on type B500B. The required material properties of this type are shown in table E.4.

Table E.4: Reinforcement steel material properties.

Reinforcement steel property		
Yield strength reinforcement steel	f_y	= 500 MPa
Design yield strength reinforcement steel	$f_{yd} = f_y/\gamma_s$, $\gamma_s = 1.15$	= 435 MPa
Young's modulus	E_s	= 210 GPa

E.2. Results of calculation for bending moment resistance

Using the given input parameters, the bending moment resistance, M_{Rd}, of the cross-section was then determined. This resistance is shown in table E.5. The bending moment resistance is calculated without a favorable compressive normal force, so that the sum of the internal forces in the cross-section, F_{int}, is equal to zero.

Table E.5: Bending moment resistance and resulting internal force.

F_{int} (kN)	M_{Rd} (kNm)
0.0	793.6

Table E.6 shows the results of the calculation for the part of the concrete that is in compression as a result of the bending moment. The table shows, among other things, the internal force that acts in this part of the concrete.

Table E.6: Concrete part in compression cross-section.

Concrete nr.	D_c (mm)	x_u (mm)	d_c (mm)	A_c (mm^2)	$\epsilon_{cu3} \cdot 10^3$ (-)	f_{cd} (N/mm^2)	F_c (kN)
1	580	200	196	59108	3.50	20	1182

Table E.7 shows the results of the calculation for the reinforcement steel in the cross-section. This shows the stresses and forces acting in each reinforcement bar, which are caused by the bending moment.

Table E.7: Reinforcement steel cross-section.

Rebar nr.	x (mm)	y (mm)	d_s (mm)	ϕ (mm)	A_s (mm^2)	$\epsilon_s \cdot 10^3$ (-)	σ_s (N/mm^2)	F_s (kN)
1	0	232	58	36	1018	2.48	435	443
2	-136	188	102	36	1018	1.71	358	364
3	-221	72	218	36	1018	-0.33	-69	-70
4	-221	-72	362	36	1018	-2.85	-435	-443
5	-136	-188	478	36	1018	-4.88	-435	-443
6	0	-232	522	36	1018	-5.66	-435	-443
7	136	-188	478	36	1018	-4.88	-435	-443
8	221	-72	362	36	1018	-2.85	-435	-443
9	221	72	218	36	1018	-0.33	-69	- 70
10	136	188	102	36	1018	1.71	358	364

Figure E.2 shows the steel stresses and the part of the concrete that is in compression as a result of the bending moment.

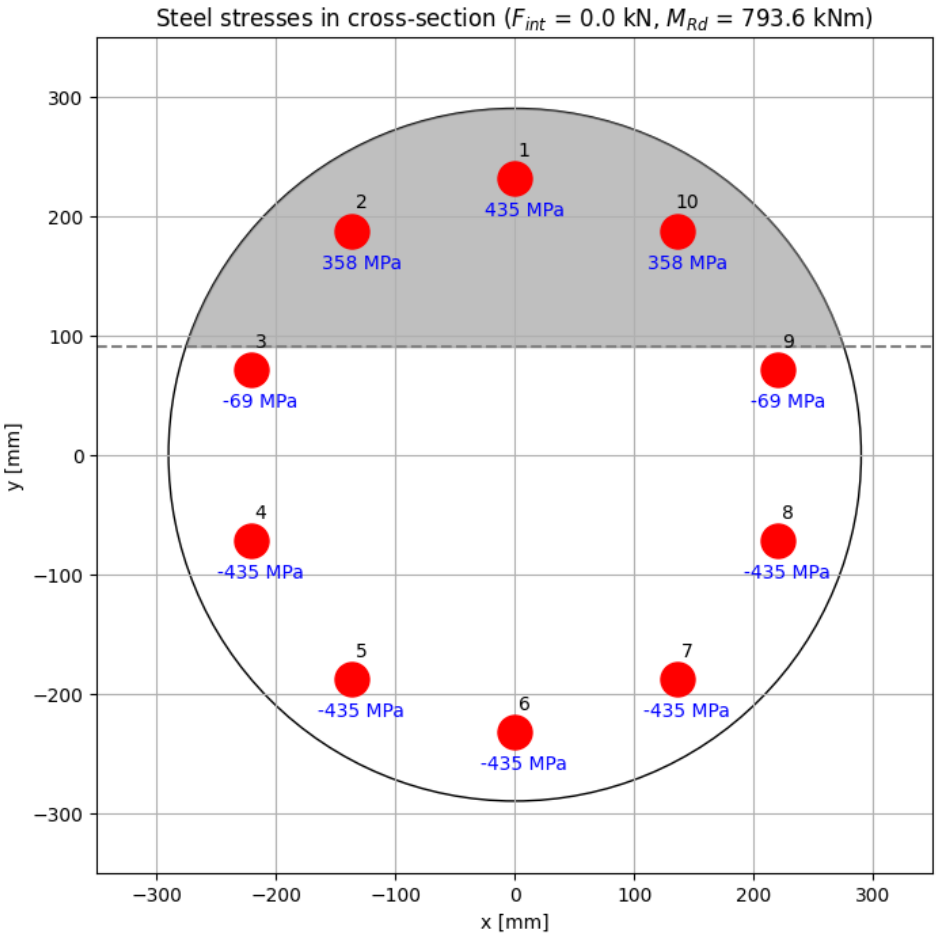

Figure E.2: Steel stresses in cross-section.

Figure E.3 shows the internal forces in the reinforcing bars and the part of the concrete that is in compression as a result of the bending moment.

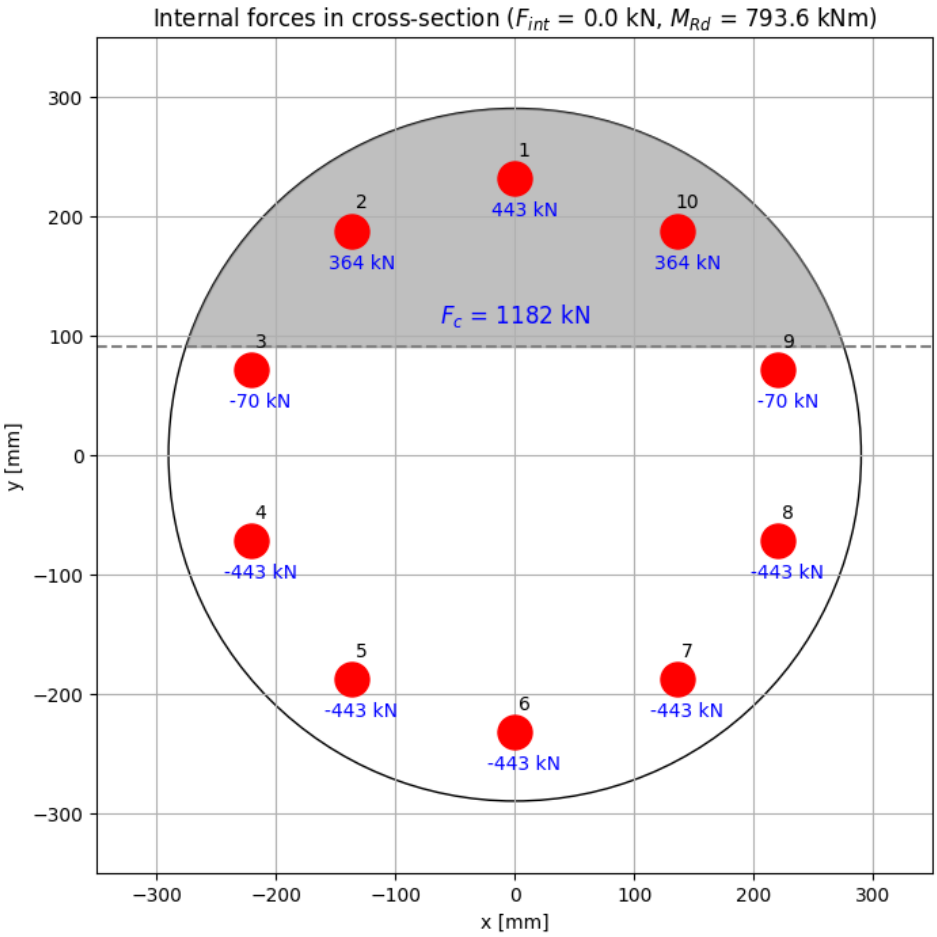

Figure E.3: Internal forces in cross-section.